Effects of Rotor Tip Clearance on an Embedded Compressor Stage Performance

by

Sitanun Sakulkaew

B.S. Mechanical Engineering
California Institute of Technology (2010)

Submitted to the Department of Mechanical Engineering
in partial fulfillment of the requirements for the degree of

Master of Science in Mechanical Engineering

at the

MASSACHUSETTS INSTITUTE OF TECHNOLOGY

June 2012

Author .....
Department of Mechanical Engineering
May 11, 2012

Certified by .....
Choon S. Tan
Senior Research Engineer
Department of Aeronautics and Astronautics
Thesis Supervisor

Read by .....
John G. Brisson
Professor, Department of Mechanical Engineering
Thesis reader

Accepted by .....
David E. Hardt
Chairman, Department Committee on Graduate Students

Effects of Rotor Tip Clearance on an Embedded Compressor Stage Performance

by

Sitanun Sakulkaew

Submitted to the Department of Mechanical Engineering
on May 11, 2012, in partial fulfillment of the
requirements for the degree of
Master of Science in Mechanical Engineering

Abstract

Compressor efficiency variation with rotor tip gap is assessed using numerical simulations on an embedded stage representative of that in a large industrial gas turbine with Reynolds number being approximately 2×10^6 to 7×10^6. The results reveal three distinct behaviors of efficiency variation with tip gap. For relatively small tip gap (less than 0.8% span), the change in efficiency with tip gap is non-monotonic with an optimum tip gap for maximum efficiency. The optimum tip gap is set by two competing flow processes: decreasing tip leakage mixing loss and increasing viscous shear loss at the casing with decreasing tip gap. An optimum tip gap scaling is established and shown to satisfactorily quantify the optimal gap value. For medium tip gap (0.8% - 3.4% span), the efficiency decreases approximately on a linear basis with increasing tip clearance. However, for tip gap beyond a threshold value (3.4% span for this rotor), the efficiency becomes less sensitive to tip gap as the blade tip becomes more aft-loaded thus reducing tip flow mixing loss in the rotor passage. The threshold value is set by the competing effects between increasing tip leakage flow and decreasing tip flow induced mixing loss with increasing tip gap. Thus, to desensitize compressor performance variation with blade gap, rotor should be tip aft-loaded and hub fore-loaded while stator should be tip fore-loaded and hub aft-loaded as much as feasible. This reduces the opportunity for clearance flow mixing loss and maximizes the benefits of reversible work from unsteady effects in attenuating the clearance flow through the downstream blade-row. The net effect can be an overall compressor performance enhancement in terms of efficiency, pressure rise capability, robustness to end gap variation and potentially useful operable range broadening. Preliminary assessment of a stage redesign with a 4% chord more tip aft-loaded blade design for 1.7 % span tip clearance yields 0.2 point stage efficiency benefit.

Thesis Supervisor: Choon S. Tan
Title: Senior Research Engineer
Department of Aeronautics and Astronautics

Acknowledgments

The work presented in this thesis was carried out over a course of two-year with the support of MITEI Sustaining Member Siemens CKI, agreement dated 09/30/2008. This work would not have been possible without the collaboration and support from many people to whom I would like to express my gratitude here.

First, I would like to thank my adviser, Dr. Choon Tan for his guidance. I really appreciate his support throughout my graduate study at MIT. He cheerfully encouraged me and gave me constructive suggestions whenever I ran into difficulties with my research, patiently listened to my presentation practices over and over again, and let me think and convince myself whenever I am skeptical.

I would like to express my gratitude to several engineers at Siemens Energy for their continuous and intensive support. I thank Dr. Paul Spedaler and Dr. Christoph Starke for all the advice and support. I am grateful to Dr. Christian Cornelius for his helpful comments and suggestions from his extensive experience in CFD and compressor technology as well as his help in blade designing. I am also grateful to Dr. Matthew Montgomery who coordinated the collaboration between MIT and Siemens. His thoughtful suggestions and comments as well as his effective paraphrasing were invaluable in our research meetings. Especially, I would like to thank Dr. Eric Donahoo, to whom I cannot say how much I am indebted for his support. This work would not have been accomplished without his countless advice, innumerable computational meshes, various vital inputs as well as management of this research project.

Also, I would like to thank my research collaborators at NASA GRC, Dr. John Adamczyk, Dr. M. Celestina of NASA GRC and Mr. S. Kulkarni of Case Western Reserve University. They have provided me numerous constructive comments and suggestions as well as crucial inputs from APNASA simulations for my computation setup and assessment. Likewise, I am grateful to Professor N.A. Cumpsty for helpful comments and discussions. I also would like to thank Professor John Brisson for reading my master's thesis.

My fellow labmates at GTL have also been a great support and source of knowledge. A special thanks to Metodi Zlatinov, my benevolent officemate, for enlightening discussions, advice and help on CFX, CFD and aerodynamics. I am also very grateful to Andreas Peters and Jeff Defoe for all their help on NUMECA, CFD and computational setup.

Finally, I want to thank my friends and family for their support throughout the years. My sister always brightens up my mood with her cheerful attitude. I am deeply grateful to my father and my mother for their unconditional love. It is their encouragement and support which kept me going.

Contents

List of Figures

List of Tables

Nomenclature

A	Area
C_d	Discharge coefficient
P	Pressure
Pr_t	Turbulence Prandtl number
R	Radius
Re	Reynolds number $= \frac{Vc}{\nu}$
S	Entropy
T	Temperature
U	Blade rotational speed
V	Velocity
W_{lost}	Lost work
c	Chord
g	Tip gap
h	Enthalpy
k	Thermal conductivity
m	Mass flow rate
p	Pitch
s	Entropy
s	Span
v	Velocity
u	Velocity
x_i	Coordinate x_i
β	Relative flow angle

γ	Stagger angle
η	Efficiency
μ	Dynamic viscosity
ν	Kinematic viscosity
ρ	Fluid density
σ	Solidity $= \frac{c}{p}$
τ	shear stress
ϕ	Flow coefficient $= \frac{V_x}{U}$
ψ	Stage loading coefficient $= \frac{\Delta h_t}{U^2}$

Subscripts

c	circumferential direction
casing	at the casing
eff	effective
gen	generated
hub	at the hub
inlet	at inlet to stage
irrev	irreversible
outlet	at exit from stage
p	pressure side
rotoroutlet	at downstream mixing plane or sliding plane
s	suction side
t	stagnation conditions
therm	due to viscous effects
tip	at the tip
x	axial direction
visc	due to viscous effects
1	at stage or rotor inlet

2	at rotor exit

Superscripts

$()''$	per unit area
$()'''$	per unit volume
$\dot{()}$	per unit time

Abbreviation

IGT	Industrial gas turbine
LE	Leading edge
PS	Pressure side
SS	Suction side
TE	Trailing edge

Chapter 1

Introduction

Compressor rotor has a small clearance between the tip of rotating blade and stationary casing, referred to as tip clearance or tip gap. Tip clearance allows the working fluid to leak through the gap from pressure side to suction side. This leakage jet, driven by the pressure difference between the blade pressure surface and suction surface, has a velocity of the similar magnitude but of a different direction as the flow on the pressure side. As shown in Figure 1-1, tip leakage flow appears as a shear layer which rolls up into a vortex core. This is thus a source of increased flow blockage (reducing pressure rise capability) and entropy generation (decreasing efficiency).

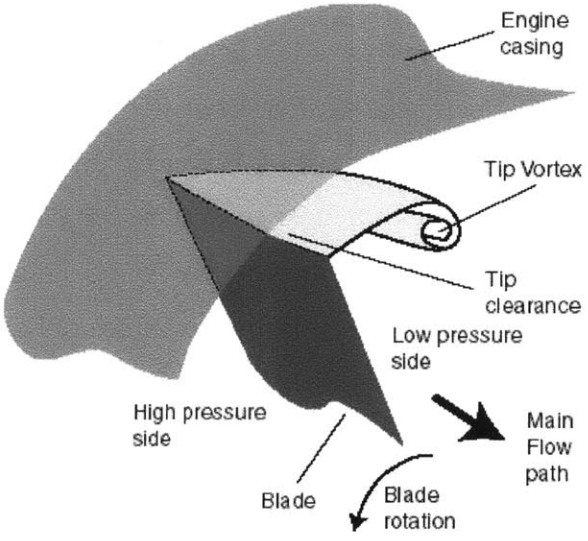

Figure 1-1: A sketch illustrating formation of compressor tip leakage flow

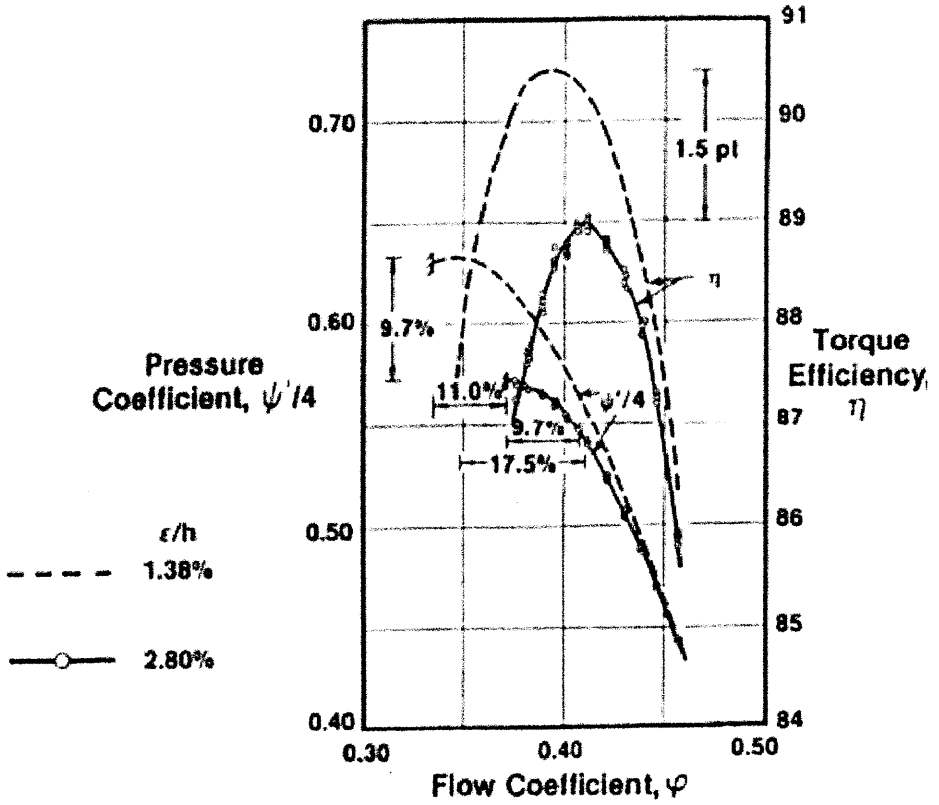

Figure 1-2: The effect of tip clearance on the performance of a low-speed 4-stage compressor (Wisler, 1985 [28])

The effect of the change in tip clearance (within a typical tip clearance range in aerospace compressor) on compressor efficiency, pressure rise capability and stall margin for a low speed 4-stage compressor is shown in Figure 1-2 and for a high-speed six-stage compressor in Figure 1-3. Based on Wisler [28], an increase in tip clearance of low speed 4-stage compressor from 1.38 percent to 2.8 percent span reduces the peak efficiency by 1.5 points, the peak pressure rise by 9.7 points and the flow range by 11 points. As for the high speed six-stage compressor, Freeman found that an increase in tip clearance (from 1 percent to 3 percent span for all rotors) not only causes a drop in pressure rise and efficiency but also moves the surge line considerably to the right. These thus show that the impact of the change in tip gap on compressor performance (both high-speed and low-speed compressors) can be significant.

There are two aspects of flow response to the generation of tip leakage flow. The

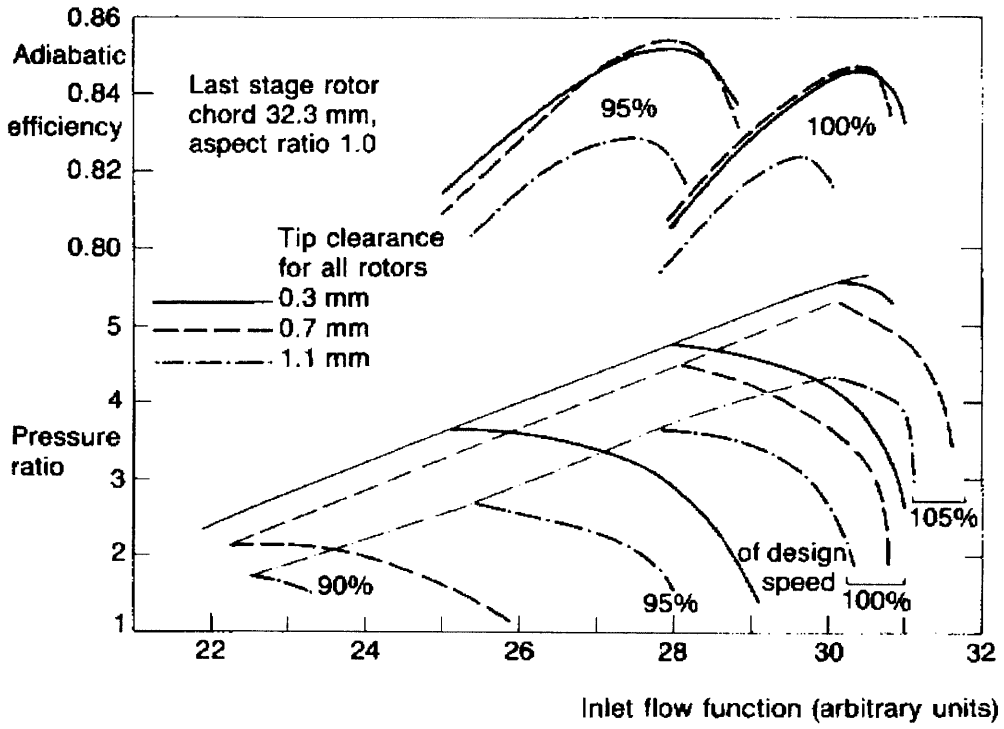

Figure 1-3: The effect of tip clearance on the performance of a high-speed six-stage compressor (Freeman, 1985 [10])

first aspect is fluid dynamic blockage (local effect) that effectively reduces the flow area and thus results in a decrease in pressure rise, work capability and stable flow range. The second aspect is a thermodynamic effect due to additional entropy generation (in other words, loss which is a global effect), resulting in an efficiency drop. Hence, it is important to address both aspects of flow response associated with tip clearance flow. An overall goal of this thesis is then to provide a quantitative understanding of loss and flow blockage generation in an embedded compressor stage with rotor tip clearance varying from vanishing value to large value ($\sim$ 5% span). This range of variation is representative of that found in large industrial gas turbine compressor

1.1 Research background

As alluded in the above, rotor tip and stator hub clearance flow is known to have a strong impact on compressor performance, as measured in terms of pressure rise

capability, efficiency, useful operating range, and its sensitivity to clearance variation (Koch and Smith [13], Cumpsty [6]). Considerable research programs carried out in the past several decades have been directed at understanding the compressor endwall flow, which is dominated by clearance flow, to a level adequate for design and performance assessment on a quantitative basis. The status of compressor tip clearance flows based on the outcomes of these various useful research efforts can be concisely summarized as follows:

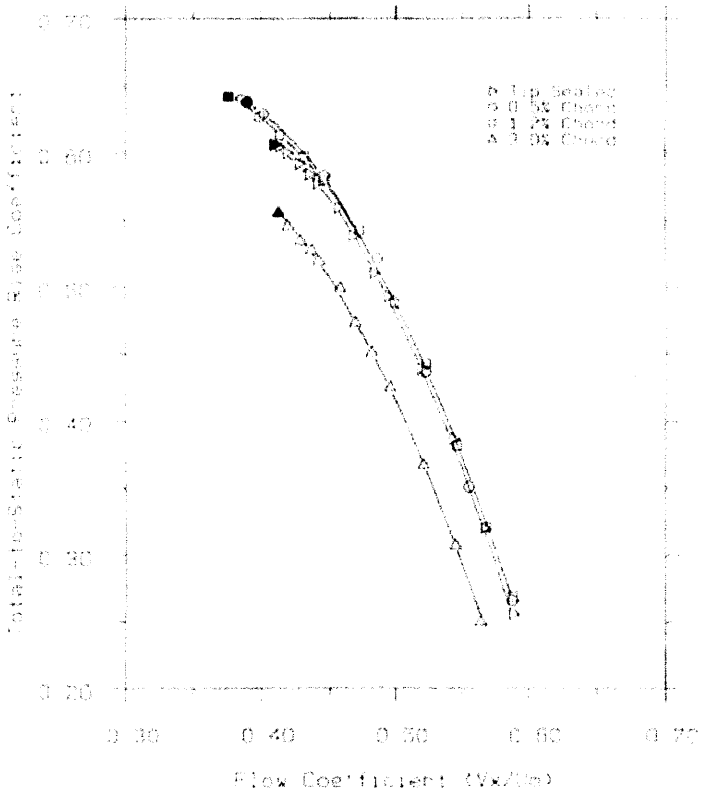

Figure 1-4: McDougall and Cumpsty's tip clearance effects on Deverson's compressor performance. [18, 6]

1. Over a limited range of non-dimensional tip clearances, endwall flows are qualitatively understood.

2. Some aspects, namely those having to do with loss, can also be quantitatively captured over this limited range.

3. Other aspects, namely those having to do with the specific phenomena that set the limits on peak pressure rise, are still dealt with empirically.

4. The existing general picture of endwall flow does not apply all the way to vanishing clearance. At vanishing clearance, the structure of the fluid motion is qualitatively different than at a clearance of, say, 1% chord, at which the endwall flow region is dominated by the clearance flow and the roll-up of the shear layer into a vortex.

5. The behavior of efficiency versus tip clearance is non-monotonic (Cumpsty [6], Wennerstrom [26]), presumably because of this change in flow structure so that there exists an optimum tip gap for maximum efficiency. Figure 1-4 shows that for Deverson compressor at design, the pressure rise of the rotor with 1.2 % chord tip clearance is higher than that of 0.5 % chord and 3 % chord tip clearance, implying that the optimum tip gap at design is approximately 1.2% chord. Similarly, Wennerstrom (Figure 1-5) found that the efficiency of a high-speed transonic compressor with a rotor tip gap of 0.5% span is higher than that with a tip gap of 0.3 % span and 0.7 % span. Thus, the optimum tip gap for maximum efficiency in Wennerstrom's transonic compressor is between 0.3-0.7% span. However, even though both experiments showed the existence of the optimum tip clearance, thus far its value has not yet been satisfactorily quantified and the parameters that mark the change in the behavior are not known in any depth.

6. While there have been computations and experiments implemented to demonstrate large clearance (relative to tip gap in a compressor representative of that in modern design) effects in a linear cascade (Williams et al. [27]), there is a lack of understanding as to why and how there can be a qualitative change in the observed behavior.

7. The time-averaged effect of rotor tip flow interacting with downstream stator (Valkov and Tan [24, 25]) and with upstream stator wakes (Sirakov and Tan

[20]) have been assessed and the associated fluid dynamic aspects are understood.

8. While controlling tip clearance flow through its unsteady excitation (Bae et al.[3]) has demonstrated the feasibility of reducing compressor performance sensitivity to tip flow, there is still a lack of understanding on the how-to of mitigating compressor performance sensitivity to tip gap variation.

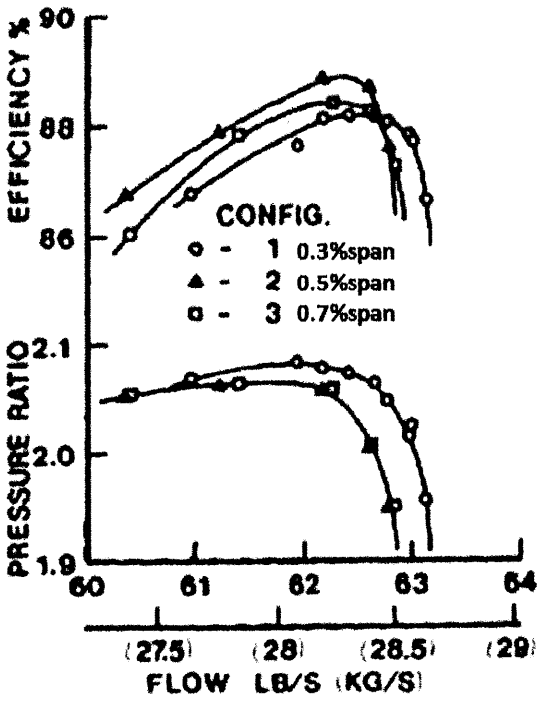

Figure 1-5: Wennerstrom's tip clearance effects on compressor performance at design speed. [26]

1.2 Aerospace gas turbine compressor versus large industrial gas turbine compressor for power generation

Even though flow physics underlying the flow behaviors in aerospace gas turbine compressor and industrial gas turbine (IGT) compressor are similar, there are several

significant differences in design and flow parameters as follows:

1. Due to the relatively large blade span in front stages and relatively short blade span in rear stages, blade clearance in large industrial gas turbine compressor can be as small as 0.5% span in front stages and as large as 5% span in rear stages. Thus, the range of tip clearance in large industrial gas turbine compressor has a much broader variation than that in aerospace gas turbine compressor.

2. Taking into account manufacturing cost, industrial gas turbine compressor uses cantilevered stator instead of shrouded stator. As a result, in addition to tip clearance, compressor also has hub clearance, a gap between stationary stator and rotating hub, which results in additional loss related to hub leakage flow. However, aerospace gas turbine compressor generally has shrouded stator to reduce aeromechanical difficulties.

3. Multi-stage large IGT compressor operates at high Reynolds number e.g. between 2 $\times 10^6$ to 7 $\times 10^6$, while aerospace gas turbine compressor typically operates at Reynolds number less than 0.5×10^6.

The main focus of the thesis is on the flow physics in a representative stage of a large industrial gas turbine compressor for power generation. However, the concepts and the understandings based on the results in this thesis are equally applicable to aerospace gas turbine compressor as well.

1.3 Research motivation

As noted in the research background section, there exists a non-zero optimum blade gap for maximum efficiency. However, thus far flow processes as well as design parameters that set the optimal blade gap are not yet known. Thus, a goal of this thesis is to quantify the value of the optimum blade end gap and to determine flow processes that set this optimum value. This is to be followed by an establishment of a scaling

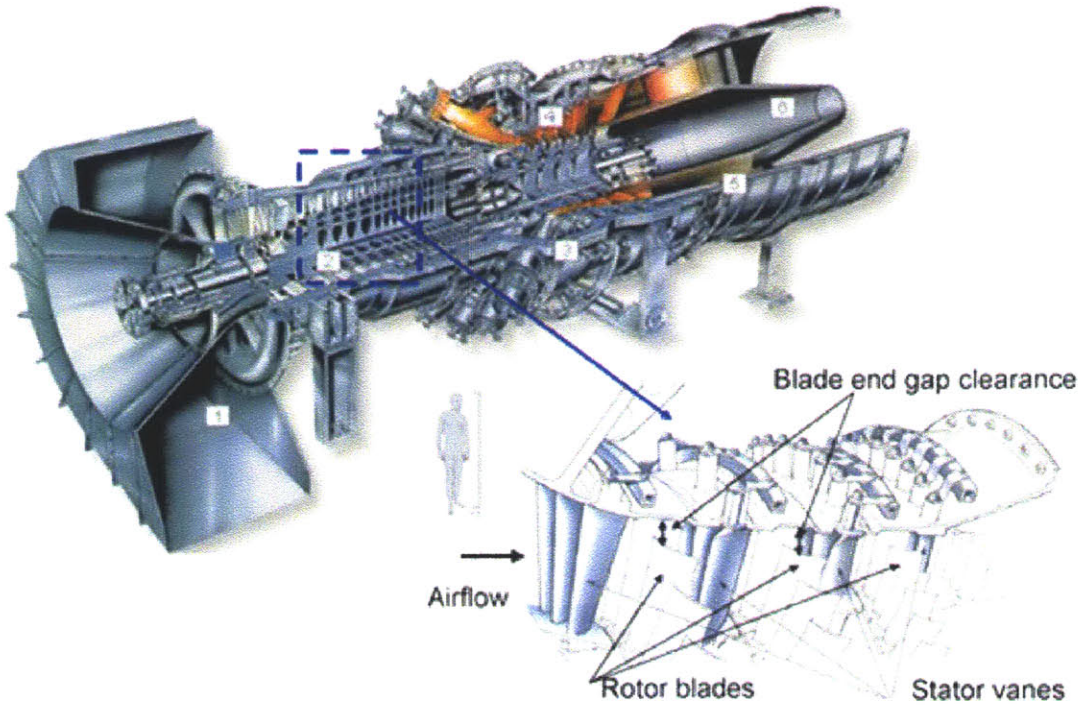

Figure 1-6: Representative compressor in large industrial gas turbine for power generation.

for optimum blade end gap estimation. This scaling would allow one to determine the engineering feasibility (as limitted by manufacturability and mechanical layout) of an optimum blade gap implementation for maximum compressor efficiency. Furthermore the scaling rule would also enable one to estimate how far a compressor of given blade end gap distribution is from the optimum.

In the past, industrial gas turbine compressor for power generation has been designed for high efficiency at a selected operating point. The efficiency would drop off (often steeply) as the operating point departs away from the design value. Thus, another goal is to define a design strategy for high efficiency retention at off-design and broadened island of peak efficiency.

In summary, this research focuses on two important aspects of compressor technology. The first aspect seeks to quantify the efficiency variation as blade clearance approaches zero and establish a physical rationale behind the existence of the optimum blade end gap for maximum efficiency. The second aspect aims to address

loss and flow blockage generation in multistage axial compressor for establishing a design guideline for compressor performance enhancement both at design and at off-design. In order to address these two aspects, several research questions are posed as delineated in the next section.

1.4 Research questions

The research questions to be addressed are:

1. What are the flow processes that set the optimum blade end gap, i.e. rotor tip clearance and cantilevered stator hub clearance? How does the optimum blade gap vary with different parameters, e.g. operating point, design characteristics, etc?

2. What are the flow processes that determine the sensitivity of compressor efficiency to blade end-gap variation?

3. How does the rotor endwall flow (essentially the rotor tip leakage flow) respond to changes in operating conditions?

4. Based upon the answers to question 2 and 3, what are the most effective ways to control the physical features of the endwall flow and how does one connect the geometry to the desired fluid dynamics? In other words, what is the suggested strategy to: (i) significantly reduce the opportunity for blade end clearance flow induced loss and flow blockage generation thus improving compressor performance, and (ii) reduce compressor performance sensitivity to blade end gap variation?

The answers to above research questions would be utilized to address the implication of blade clearance flow on multi-stage compressor performance.

1.5 Contributions

The key findings of this research includes new understandings of the flow physics underlying the efficiency response to blade end gap variation as well as a hypothesis on a design strategy to improve compressor performance. These are summarized below:

1. There are three distinct regimes of rotor efficiency variation with tip gap size: small tip gap (less than 0.8% span for the stage analyzed), medium tip gap (0.8% to 3.4% span) and large tip gap (larger than 3.4% span). The distinguishing features of each region are as follows:

   (a) For small tip gap, there exists an optimum tip gap for maximum efficiency, which is set by the competing effects for loss generation associated with casing/hub shear (which increases with decreasing gap-to-span ratio) and mixing out of clearance flow (which decreases with decreasing gap-to-span ratio). A scaling for optimum tip gap has been established and shown to be able to satisfactorily quantify the value of the optimal gap. The scaling delineates the parameter values (e.g. Reynolds number, operating points, stage aerodynamic and geometrical characteristics) that mark the change in behavior of efficiency variation with gap-to-span ratio and compressor operating points.

   (b) For medium tip gap, the efficiency variation with tip clearance is found to be in accord with Denton's tip leakage mixing model [8]. The efficiency increases approximately on a linear basis when tip clearance decreases and the dominant flow process responsible for the change in efficiency in this tip gap range is tip leakage mixing. For the embedded compressor stage assessed here, there is approximately 1 point efficiency benefit for every 1% span decrease in tip gap size.

   (c) For large tip gap, the efficiency sensitivity to tip gap is reduced. When tip clearance increases, the blade tip peak loading and thus the tip leak-

age flow formation are aft-shifted toward trailing edge. This reduces the opportunity for the mixing out of the tip flow in rotor passage (and the tip flow induced flow blockage and loss production as well) so that the tip leakage flow can remain relatively unmixed at the rotor exit. As such the rotor efficiency would become less sensitive to tip clearance variation beyond a critical gap value set by two competing effects in loss generation: an increase in tip leakage mass flow rate associated with increasing tip gap and a decrease in tip flow mixing loss due to blade tip being aft-loaded as tip gap increases.

2. For rotor design with its tip peak loading located in the immediate blade leading edge region, the assumption that the mixing-out of tip flow is complete within the rotor passage is a good approximation; for this situation Denton's tip leakage mixing model is applicable. However, for rotor design with aft-loaded tip, there is less opportunity for the tip flow to realize its mixing-out loss generation potential, therefore Denton's model is not applicable here because of its inherent assumption of instantaneous mixing of tip leakage flow with main flow.

3. For large industrial gas turbine compressor with Reynolds number 2×10^6 to 7×10^6, the blade surface boundary layer is relatively thin and robust. So, the dominant source of flow blockage and loss generation is the leakage flow. Therefore, to reduce compressor performance sensitivity to clearance gap variation, rotor should be tip aft-loaded and hub fore-loaded while stator should then be tip fore-loaded and hub aft-loaded as much as it is feasible so as to reduce the opportunity for blade clearance flow induced loss and flow blockage generation. This would also create an environment for maximizing the benefits of reversible work from unsteady effects through the downstream blade-row in attenuating the wake-like clearance flow. It is hypothesized that the overall performance benefit can include compressor performance enhancement as measured in terms of efficiency, stage loading, broadening of useful operating range and of island of peak efficiency.

4. Preliminary assessment of the design strategy defined in (3) above shows that with tip aft-loaded rotor blade design, the tip leakage flow formation and mixing out process are delayed; however, it has been observed that flow begins to separate on the rotor trailing edge suction side.

   (a) There should thus be an optimum blade loading design that minimizes the total loss from mixing-out of leakage flow (which decreases with aft-loading rotor tip/stator hub) and flow separation on the suction side of the rotor tip/stator hub trailing edge (which increases with aft-loading rotor tip/stator hub).

   (b) There is a 0.2 point efficiency benefit when aft-load the rotor blade tip by 4% chord for the stage with rotor of 1.7% span tip clearance.

1.6 Organization of thesis

The thesis is organized as follows. Chapter 2 first describes the conceptual framework of approach and the design of computations aiming at defining rotor efficiency variation with tip gap and answering the research questions posed. This is then followed by the presentation and the discussion of key results to elucidate the three distinct behaviors of efficiency variation with tip clearance in chapter 3. The formulation of analysis to establish the optimum tip gap scaling for maximum efficiency is described and the physical rationales as to why the efficiency is desensitized to tip gap beyond a threshold value are given. Subsequently, Chapter 4 presents computed results based on unsteady embedded stage simulations to elucidate the benefit of rotor-stator unsteady interaction. Based upon all the results, a hypothesis on a design strategy to improve compressor performance in terms of efficiency, sensitivity to blade end gap as well as operating range is formulated. Chapter 5 then describes preliminary findings on the effects of the change in the blade tip loading distribution on the compressor performance changes. Finally, chapter 6 summarizes the key new findings and proposes recommendations for future work.

Chapter 2

Framework of approach

To address the research questions posed in the previous chapter, a systematic research approach was developed. A series of computations was designed and implemented. The computed results were then post-processed to investigate flow physics and develop physical rationales to explain the observed flow behaviors. This chapter will describe the computational set up and the conceptual framework used to establish causality between flow features of interest and their effects on compressor performance.

2.1 Computational setup

A series of computations for a representative embedded rotor-stator stage shown in Figure 2-1 (stage 9 of a 13-stage large IGT (industrial gas turbine) compressor representative of that in Siemens high-performance gas turbine SGT-8000H at a pressure ratio of 19:1 as presented in Eulitz, et al. [9]) is designed and implemented. The operating Reynolds number is approximately 2×10^6 and the compressor stage design characteristics are representative of trend for current and next generation large industrial gas turbine compressors. For example, representative values for hub-to-tip ratio is $\sim$ 0.9, aspect ratio in the range of $\sim$ 1 to 2, solidity $\sim$1 to 1.3, and blade passage pressure rise coefficient $\sim$ 0.3 to 0.5, etc. Thus, the results to be presented in this thesis are generic to compressor design space of engineering interest.

A commercial CFD program, CFX V12.0, is utilized to calculate the flow fields

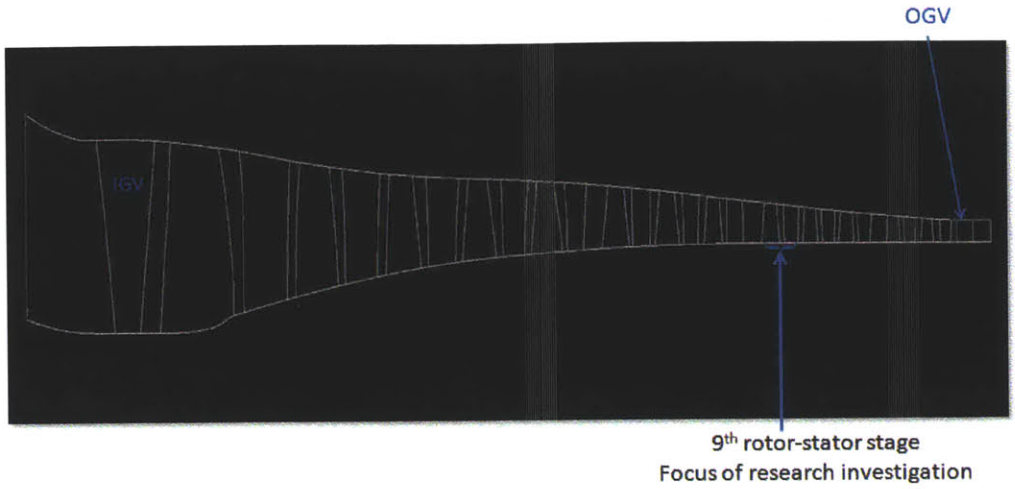

Figure 2-1: A representative 13-stage compressor (not to scale). Stage 9 is the focus of this research investigation.

at second-order accuracy in the selected compressor stage and CFX-Post, a post-processing program, is employed for interrogating the computed flow fields. Steady calculations, with a mixing plane appropriately located in the intra rotor-stator gap, have been carried out for 12 different tip clearances ranging from 0.04% up to 5% span, all of which with a 1.9% span stator hub clearance. Unsteady calculations, with a sliding plane located in the intra rotor-stator gap, have also been carried out for tip gap of 1.7% span and 5% span, as well as a modified stage design with a rotor tip gap of 1.7% span tip clearance. For CFX V12.0, phase-lag sliding plane option is not available, thus unsteady calculation in CFX is performed with an assumption of a unity rotor-stator blade ratio, despite the non-unity blade ratio of the stage. Therefore, the unsteady results presented here will provide correct trend for unsteady flow effects in compressor stage but the numerical values will be different from those expected in the actual ninth stage.

The grid used in the rotor-stator calculations (Figure 2-2) consists of approximately 5 million nodes, with 2.5 million nodes in rotor domain and 2.5 million nodes in stator domain. The grid resolution in the endwall regions and on the blade surfaces is high; there are at least 31 to 61 grid points spanning the radial tip gap. For all the computations the k-ω Shear Stress Transport turbulence model was used with y+

value being approximately 20 on the blade surfaces.

Boundary conditions specified at the stage inlet and stage outlet are taken from APNASA (Adamczyk [1]) computed flow for the entire 13-stage compressor (Kulkarni [14]). The APNASA computation has been assessed against test rig data for its adequacy. Radial distribution of stagnation pressure, stagnation temperature as well as absolute flow angle (based on stage 9 rotor inlet conditions from APNASA computed flow) is specified at the stage inlet. At the stage outlet, radial distribution of static pressure (based on stage 9 outlet flow from APNASA computations) is specified but is adjusted appropriately for each tip clearance to maintain the same corrected mass flow. Computations have been carried out at three operating points: at design, at 0.94 and 1.16 design mass flow.

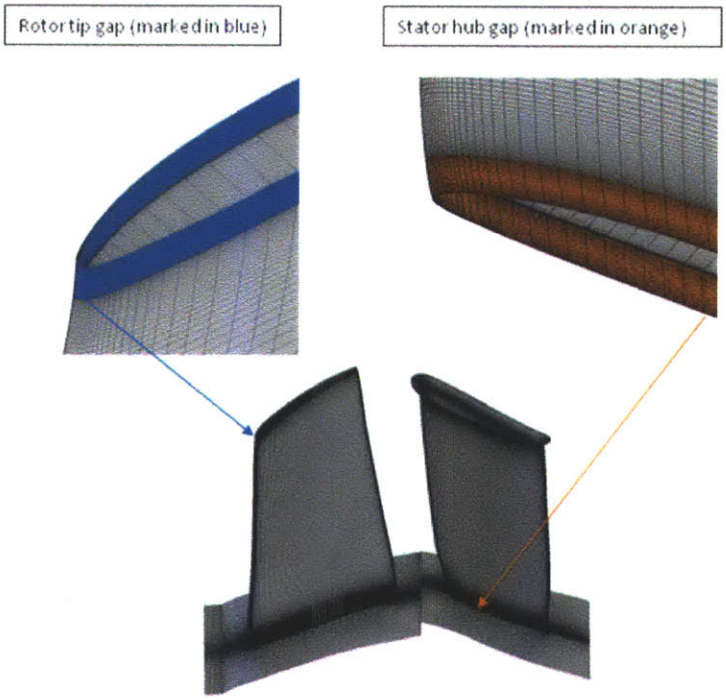

Figure 2-2: embedded compressor stage representative of that in large IGT compressor.

While there exists experimental data from a Siemens test rig for this representative compressor, the blade clearances as well as some stage configurations in the test rig are different from the models used in this study; thus the flow fields cannot be

directly compared between the available experimental data and the numerical data presented in this paper. However, Siemens has implemented detailed validation of CFX computed results against cascade data (subsonic and transonic), advanced high performance compressor rig data, and overall full-scale compressor test data including stability evaluation.

While these detailed assessments and validations have not been published, the work reported by Belamri et al. [4, 5] described representative assessments and validations of CFX computed flow, both mixing-plane approximation and time-accurate transient simulations, against experimental data for multistage axial compressor. In Belamri et al. [4], the results suggested that second order accurate advection model is recommended for higher accuracy. The overall flow assessment is satisfactory even with coarse mesh (21 thousands nodes per passage), though a finer mesh (e.g. 220 thousands nodes per passage) is required for an accurate assessment of secondary flow features with the use of SST turbulence model. A convergence of 6 orders of magnitude reduction is shown to be adequate for the overall mass flow and outlet total pressure to reach a constant value. Both the computed steady and transient flow fields based on second order accurate advection scheme and k-ω turbulence model with coarse mesh as well as fine mesh were compared against experimental data [5]. The CFX computed flow fields and experimental data show a good agreement in the local flow profiles (Figure 6.1 and 6.2 in [13]) as well as the relevant details of flow features (such as the location and the size of hub flow separation (Figure 7 in[5])). Thus CFX is an adequate tool for computing flow in compressor stages.

As previously noted, the computations presented in this paper use second order accurate advection scheme and SST turbulence model on fine meshes (2.5 million nodes per passage) with a convergence criteria of 6 orders of magnitude reduction. Hence the CFX computational setup is adequate for computing the flow fields in this representative compressor stage (Belamri et al.[4, 5]). Further assessments and validations of CFX computed flow fields performed by Mentor and Langtry et al [19, 15] were also found to agree with the experimental data from several compressor designs.

The flow profile based on CFX computations of compressor stage investigated has also been compared to that computed with APNASA by Kulkarni [14] for the same stage with similar nominal blade clearances. The results for the flow profiles at the stator inlet (downstream of the rotor) and the efficiency are in good agreement. In summary, the necessary background work has been carried out to ensure that the computed flows based on CFX solver are adequate for addressing the research issues/questions posed in the above.

2.2 Post-processing of computed results

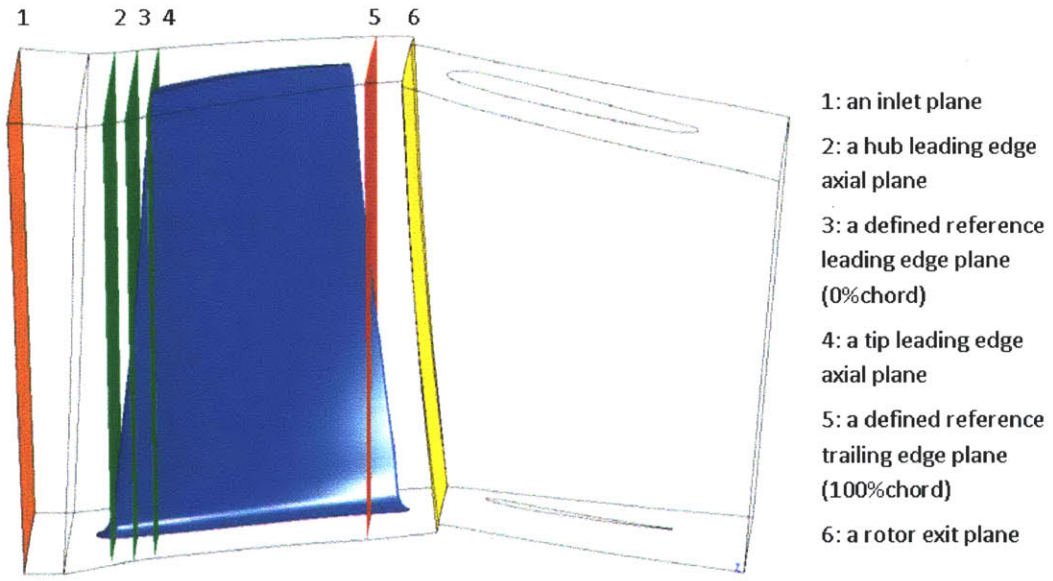

Figure 2-3: Stage 9 domain and rotor blade (blue) with reference planes as shown.

CFX-Post, a post-processing program, is employed for interrogating the computed flow fields. Before elaborating further the methodology to calculate loss (entropy generation) and flow blockage, it must be noted that the leaning of the rotor blade leading edge and trailing edge necessitates defining the location of an axial plane in the blade leading edge and trailing edge region; this is done to facilitate presenting the axial variation in flow feature, such as the accumulative entropy generation, along the axial coordinate in rotor passage. As illustrated in figure 2-3, the analyses presented in

this thesis use axial planes intersecting the blade leading edge at mid-span and blade trailing edge at mid-span to serve as reference axial locations of leading edge (0% chord) and trailing edge (100% chord), respectively in the presentation of computed results. The hub leading edge axial plane is taken to be that intercepting the blade leading edge at the hub while the tip leading edge axial plane is taken to be that intercepting the blade leading edge at the tip. When the axial location presented in the figures are to be referenced to leading edge and trailing edge axial locations at rotor tip, it will be clearly indicated as % tip chord (i.e. 0 % tip chord at rotor tip leading edge and 100% tip chord at rotor tip trailing edge).

2.3 Entropy as a measure of loss

Instead of using stagnation pressure drop as a mean to measure loss in compressor passage, entropy generation will be employed for lost work quantification. A measure of loss can be cast in terms of entropy generation ΔS due to irreversible processes in compressor flow path through the expression for lost work:

$$W_{lost} = T\Delta S \tag{2.1}$$

, where T denotes an appropriate reference temperature and ΔS the entropy generated. For a given computed flow field, the local entropy generation rate can be estimated using the dissipation function per unit volume Φ given below in Equation (2.2):

$$\begin{aligned}\frac{Ds_{irrev}}{Dt} = \Phi = \dot{S}'''_{gen} &= (\dot{S}'''_{gen})_{therm} + (\dot{S}'''_{gen})_{visc} \\ &= \frac{k_{eff}}{T^2}\left(\frac{\partial T}{\partial x_i}\right)^2 + \frac{1}{T}\tau_{ij}\frac{\partial u_i}{\partial x_j} \\ &= \frac{k_{eff}}{T^2}\left(\frac{\partial T}{\partial x_i}\right)^2 + \frac{1}{T}\left(\mu_{eff}\left(\frac{\partial u_i}{\partial x_j} + \frac{\partial u_j}{\partial x_i}\right) + \lambda_{eff}\frac{\partial u_k}{\partial x_k}\delta_{ij}\right)\frac{\partial u_i}{\partial x_j}\end{aligned} \tag{2.2}$$

using

$$k_{eff} = k + \frac{c_p \mu_{eddy}}{Pr_t}$$

$$\mu_{eff} = \mu + \mu_{eddy}$$

$$\lambda_{eff} = -\frac{2}{3}\mu_{eff}$$

with $Pr_t = 0.9$ in CFX.

The local entropy generation calculated using the above expression can be used to identify the location where loss is generated and the changes in local entropy generation rate in flow path can serve as a mean to identify the responsible flow processes. By integrating this local entropy generation rate over a volume from inlet up to any axial locations in the rotor passage, accumulative entropy generation rate and thus lost work can be computed. This approach will be referred as the "entropy dissipation method".

An alternative method for calculating the accumulative entropy generation rate is simply based on the change in the entropy flux. This is referred to as the "entropy flux method." For this approach, accumulative entropy generation in a volume extended from an inlet up to any axial locations is estimated from the difference in entropy flux on the inlet plane and on the axial plane of interest. The trend of efficiency variation with tip gap computed using accumulative entropy generation based on both the entropy dissipation and entropy flux methods are similar to that based on the use of work-averaged stagnation pressure and mass-averaged stagnation temperature (Cumpsty and Horlock [7]; Zlatinov et al.[30]).

Entropy dissipation method tends to underestimate the accumulative entropy generated compared to that based on entropy flux method unless the grid resolution is high enough (Zlatinov [30]); however, the trend from either methods is similar. Figure 2-4 shows accumulative entropy generation of the investigated rotor with 1.7% span tip clearance for 3 different mesh resolution: 0.4 million, 0.7 million and 5 million nodes total. The trends of the accumulative entropy generation from entropy flux method and entropy dissipation method are in agreement; entropy generation

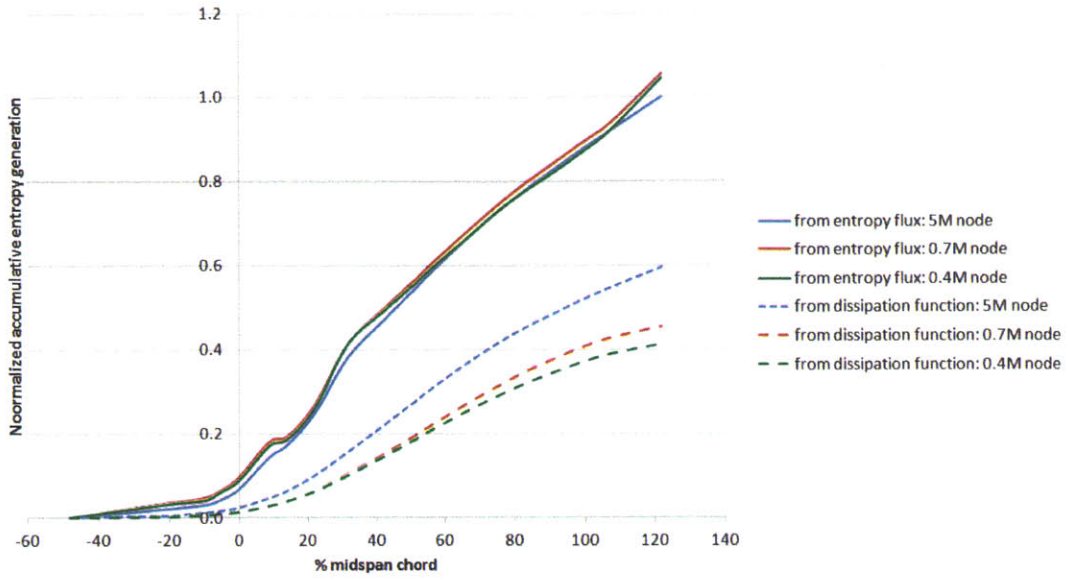

Figure 2-4: Comparison of accumulative entropy generation based on dissipation function and flux method for different mesh resolutions

increases inside the passage. The loss based on entropy dissipation is underestimated but the accuracy improves with the grid resolution (i.e. for higher grid resolution, the accumulative entropy generation based on entropy dissipation method approaches that based on entropy flux method). Nevertheless, the trend of the accumulative entropy generation based on entropy dissipation method agrees with that based on entropy flux method with high grid resolution of 5 million nodes. In other words, even though entropy dissipation method cannot quantify the accurate "absolute" value of loss for one specific case, the trend or the comparison of the qualitative change in loss between different cases (i.e. whether the loss will increase or decrease with tip gap for optimum tip gap identification) should be adequate.

2.4 Flow blockage as a measure of pressure rise capability

The second aspect of implementation details is identification of flow features that affect pressure rise capability and compressor useful operating range. This is reflected

in the generation of flow blockage, whose concept and implementation are far more challenging. Presently, there is a variety of flow blockage implementations, such as that by Smith (1969) [22], Khalid (1999) [12], Longley (2007) [17], etc. However, only Khalid's method will be utilized in the work presented in this thesis. For Khalid's method, the flow blockage definition is the "blocked area" A_b defined as

$$A_b = \int_d (1 - \frac{\rho v_m}{\rho_e V_e}) \, \mathrm{d}A \tag{2.3}$$

,where v_m denotes the velocity component in the core flow direction, V_e the velocity at the defect region edge, d the defect region, ρ the density and ρ_e the density at the defect region edge.

The defect region is defined by the region in the flow path where the non-dimensional gradient variable

$$\frac{|\nabla(\rho v_m)|_{r,\theta}}{\rho_{av} \frac{C_x}{c}} \geq 2 \tag{2.4}$$

In this expression, C_x denotes the inlet axial velocity, ρ_{av} the average inlet density and c the chord length. For a blockage evaluated on axial plane, the gradient of velocity in axial direction (i.e. normal to the axial plane) are irrelevant. Thus, only the radial and tangential components of the gradient are used to obtain the gradient magnitude.

Khalid used a cut-off value of 2 for the non-dimensional gradient $|\nabla(\rho v_m)|_{r,\theta}$ to identify defect area. Therefore, to assess the choice of the value of 2, a span-wise distribution of the non-dimensional gradient is assessed at midchord. Based on the result in Figure 2-5, one can infer that the value of 2 is a reasonable choice as it satisfactorily distinguishes the region of tip flow and the region of end wall boundary layers from the mainstream region. A value of 2.1 and 2.2 have been tested and the blockage results do not significantly change.

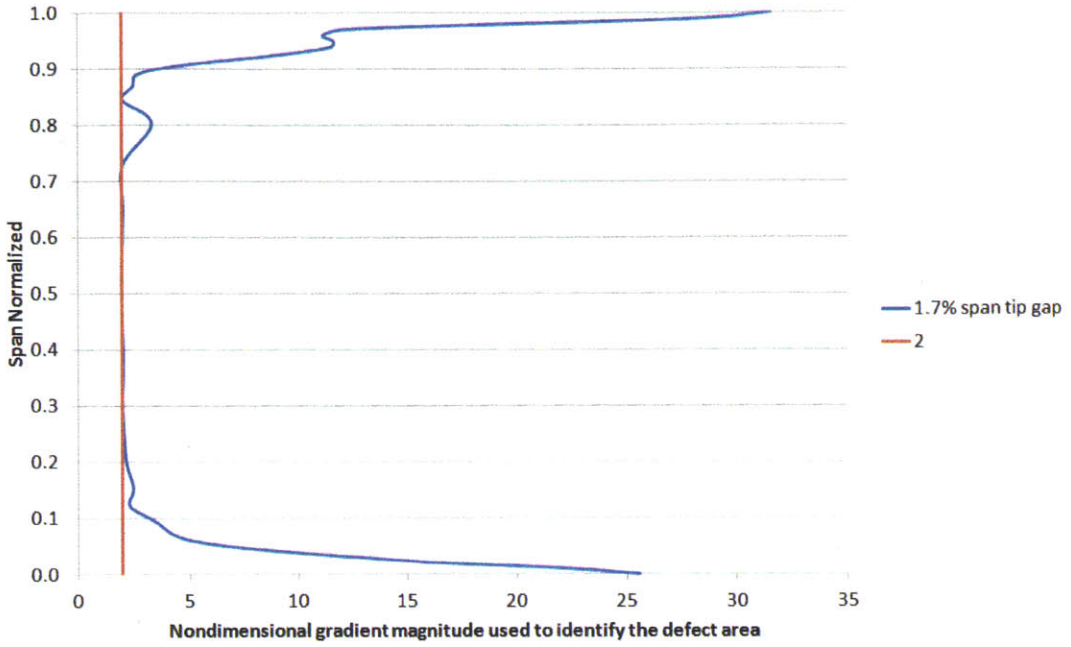

Figure 2-5: Validation of Khalid's cut-off gradient value for defected region identification.

The procedure to calculate flow blockage is as follows:

1. Calculate relative flow angle at midpitch from hub to shroud from tangential velocity and axial velocity at different axial locations.

2. Determine the main flow region away from the endwalls based upon the relative flow angle profile obtained. A linear curve is then fit on the relative flow angle in the main flow region to identify the mainflow direction in the defect regions (e.g. the end wall regions).

3. Calculate the gradient $\frac{|\nabla(\rho v_m)|_{r,\theta}}{\rho_{av}\frac{C_x}{c}}$ and define the defect regions and their edges based upon a cut off-value. There are islands of low gradient magnitude within the defect region, which must also be accounted for as defect region. Manually include these islands into the defect region.

4. Numerically integrate flow blockage using equation 2.3.

2.5 Summary

To address the research questions posed in the previous chapter, a systematic research approach was developed. A series of steady and unsteady computations was designed and implemented on an embedded compressor stage representative of that in high-performance large industrial gas turbine where the operational Reynolds number ranges from 2×10^6 to 7×10^6. A commercial CFD program, CFX V12.0, is utilized to calculate the flow fields at second-order accuracy in the selected compressor stage and CFX-Post, a post-processing program, is employed for interrogating the computed flow fields.

To establish the causality between flow features of interest and their effects on compressor performance, entropy generation is employed as a mean to measure loss in compressor passage. Flow blockage generation in the blade passage is used as a mean to identify flow features that affect pressure rise capability and compressor useful operating range. There are several flow blockage definition; however, only Khalid's method will be utilized in the work presented in this thesis. In the next chapters, the analysis of the computed results based upon the above conceptual framework will be discussed.

Chapter 3

Effects of tip clearance on compressor performance in steady flow

Steady state computational results have been obtained and post-processed to determine the effects of tip clearance on compressor stage performance. Flow fields in 12 different rotor tip clearances ranging from 0.04% span up to 5% span are investigated at three operating points: at design, at 0.94 and 1.16 design mass flow. Figure 3-1 shows the computed rotor efficiency at design and at 0.94 design mass flow, calculated based upon the work-average stagnation pressure and the mass-average stagnation temperature. The efficiencies presented here are those relative to the rotor efficiencies at 1.7% span tip clearance at design. It is shown that there are three distinct behaviors of efficiency variation with tip gap. For relatively small tip gap (less than 0.8% span for the investigated rotor as shown in Figure 3-1), the change in efficiency with tip gap is found to be non-monotonic and there is an optimum tip gap for maximum efficiency. For medium tip gap (from 0.8% span to 3.4% span), the efficiency decreases approximately on a linear basis with increasing tip gap. However, for the tip gap beyond a threshold value (3.4 % span for this rotor), the efficiency becomes less sensitive to tip gap as depicted in Figure 3-1. In this chapter, the effects of tip clearance on compressor performance are assessed for the three distinct regions of

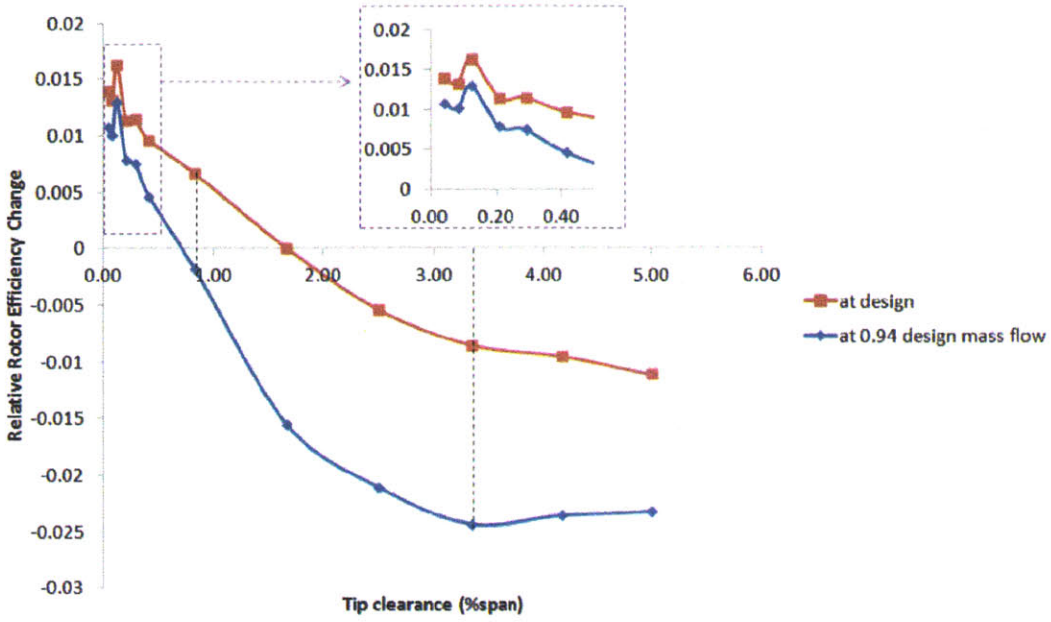

Figure 3-1: Rotor efficiency variation with tip clearance from vanishing to large value.

dependence on rotor tip gap. Since the results for rotor tip gap ranging from 0.8% to 3.4% span are in accord with previous published work on compressor tip flow, we will not dwell on the details for this range of rotor tip gap and a concise summary of key results will be provided. Following this, the results for tip gap less than 0.8% span and more than 3.4% span will be presented to bring out the distinguishing features of each region. These results and their implications are then used to formulate a hypothesis on the required attributes of compressor stage design for performance enhancement as measured in terms of efficiency, pressure rise capability and useful operable range as well as its sensitivity to tip gap variation. The formulation and assessment of the hypothesis will be presented in the following chapters.

3.1 Effects of medium tip clearance on compressor stage efficiency

Considerable research programs have been carried out in the past several decades to address the effects of the tip clearance size on the compressor performance. Wong

[29] found that for 2% chord increase in tip gap, the efficiency decreases roughly by 2%; in other words, in his experiments, there is a trade off of approximately 1% in efficiency per 1% chord increase in rotor tip gap. Similarly, the experimental results presented in Freeman [10] suggest that a 1% chord increase in tip clearance, produced by increasing the casing diameter, yields approximately 1.4% decrease in efficiency. These findings are in agreement with the results from Denton's leakage mixing model, where the loss is linearly proportional to the tip gap size.

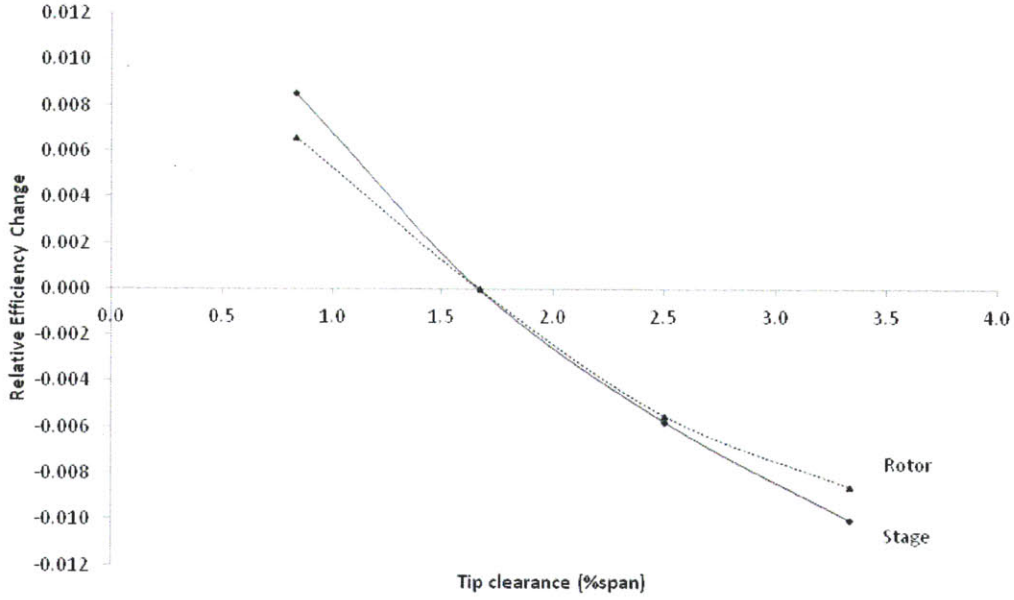

Figure 3-2: Efficiency variation with tip clearance for medium tip gap.

For the selected compressor stage, the computed rotor efficiency and stage efficiency variation with tip gap ranging from 0.8% span to 3.4% span at design are shown in Figure 3-2. The efficiencies presented here are those relative to the rotor and stage efficiency at 1.7% span tip clearance at design. The decrease in rotor efficiency and stage efficiency with an increase in tip clearance is found to be approximately linear with nearly 1 point drop in efficiency for each percent span increase in tip gap.

The net tip leakage mass flow is found to increase approximately linearly with tip gap as shown in Figure 3-3. According to Denton's leakage mixing model, the efficiency change should then be linearly proportional to tip gap size. In Figure 3-4,

the computed change in rotor efficiency (relative to the efficiency at 1.7% span) is assessed against the estimated rotor efficiency change from tip leakage mixing loss based on Denton's leakage mixing model. The agreement in the slopes of the two curves for the medium rotor tip gap ranging from 0.8% span to 3.4% span (up to the red line in the graph) demonstrates the applicability of Denton's leakage mixing model for this tip gap range. Since Denton's leakage mixing model assumes instantaneous mixing of the leakage flow with the main flow, the results also implies the near completion of mixing-out of the tip clearance flow within the rotor passage for this tip gap range. The computed results also show the existence of double leakage flow that constitutes an additional source of loss and flow blockage generation (Sirakov and Tan [20]) for this compressor stage (also see next section for small tip clearances).

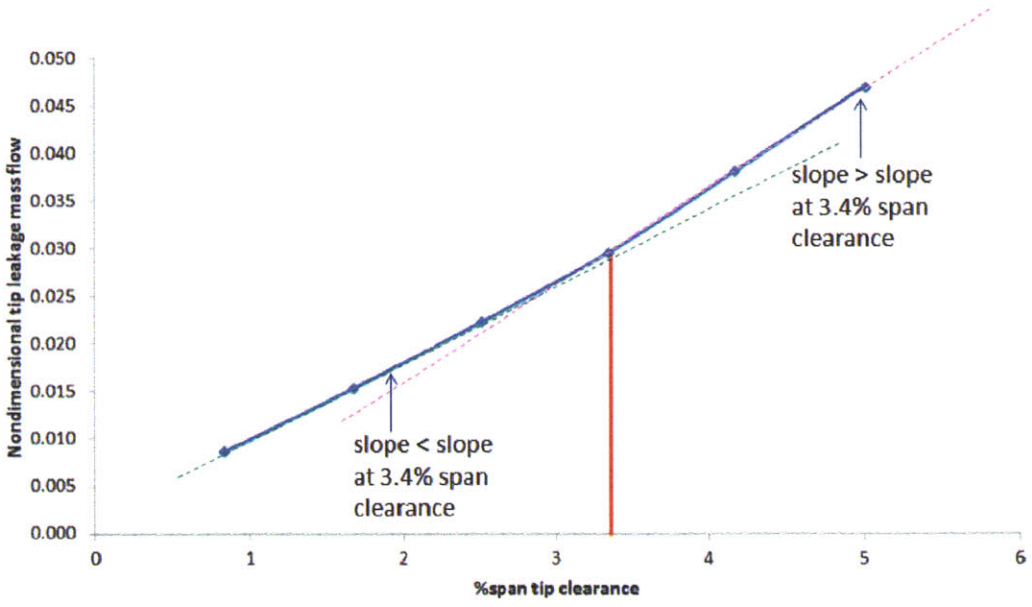

Figure 3-3: Nondimensional net tip leakage mass flow variation with tip clearance.

To summarize, both the qualitative and quantitative aspects of tip clearance flow are in agreement with published observations and results to-date. Denton's leakage mixing model has applicability in this compressor stage for rotor tip gap of 0.8% to 3.4% span. The results suggest approximately 1 point trade off in efficiency for each percent span increase in tip clearance.

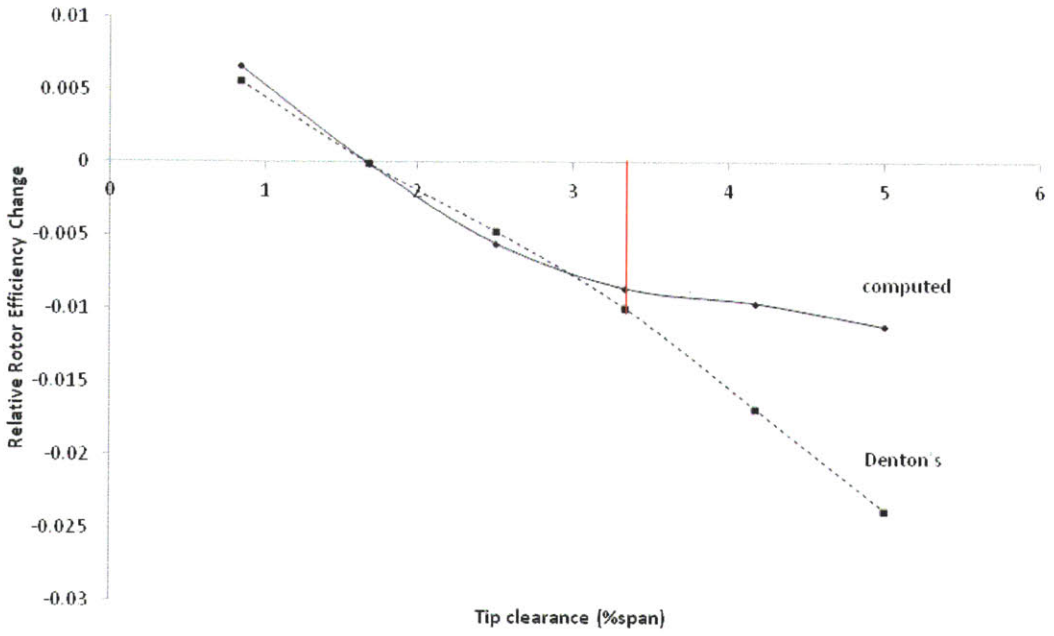

Figure 3-4: Loss variation with tip gap in rotor passage based on Denton's leakage mixing model with tip clearance for 0.8% to 5% span clearance.

3.2 Effects of small tip clearance on compressor stage performance

Several published work (e.g. Cumpsty [6], Wennerstrom [26]) have shown that as tip clearance approaches vanishing value, the change in efficiency with tip clearance variation becomes non-monotonic; there exists an optimum tip gap for maximum efficiency. McDougalls experimental results [18] on Deverson compressor, a low-speed single stage with aspect ratio of 0.8, shows that the optimum tip gap in Deverson compressor is approximately 1.2% chord; the peak pressure rise is higher with a tip clearance of 1.2% chord than the other tested clearances, 0.5% chord and 3% chord. Similarly, the experimental results on an Air Force Research Laboratory (AFRL) transonic compressor stage [26] shows that the efficiency increases when reducing the tip clearance from 0.94% chord to 0.68% chord but decreases when reducing the tip clearance from 0.68% chord to 0.42% chord. The measured efficiency trend with decreasing tip gap thus suggests an optimum tip clearance of approximately

0.68% chord. However, thus far the value of the optimum tip gap has not yet been satisfactorily quantified and the parameters marking the change in the behavior are not known in any depth.

For the selected compressor stage, when tip clearance is sufficiently small (which is less than 0.8% span for this stage), the efficiency variation with tip clearance is non-monotonic and there exists an optimum tip clearance for maximum efficiency as shown in Figure 3-1. In this section, we will determine the flow processes setting up the optimum tip clearance and establish an optimum blade end gap scaling.

For small tip clearance, viscous effect becomes significant and the endwall loss is no longer set by only the pressure-driven clearance flow and the roll-up of the shear layer into a vortex. When tip clearance decreases below the optimal, the total entropy generation in the rotor passage (i.e. the accumulative entropy generation at the rotor exit) begins to increase with decreasing tip gap. Figure 3-5 shows that at design loss generated in the rotor passage with tip clearance of 0.13% span is lower than that of both 0.08% span tip gap and 0.4% span tip gap. Thus, the tip gap of 0.08% span is below an optimum tip clearance value for minimum loss.

To determine what flow processes set up optimum tip gap, local entropy generation inside the rotor passage with small tip clearances is assessed. Figure 3-6 shows that for small tip clearance, even though local entropy generation near the leading edge of the rotor blade is lower with decreasing tip gap (which is in agreement with the common observation for medium tip gap due to the decrease in tip leakage mixing loss), the local entropy generation toward trailing edge becomes higher for smaller tip gap. Therefore, there must be at least one competing flow process whose loss increases with decreasing tip gap, as opposed to the decrease in mixing loss from tip leakage flow. The loss due to this competing flow process becomes more dominant toward trailing edge compared to tip leakage mixing loss.

In other words, when tip gap decreases, the loss due to tip leakage mixing decreases but the loss due to the competing flow process increases. Consequently, the optimum tip gap occurs when the total loss from the tip leakage mixing loss and the competing flow processes is at a minimum. From the computed flow fields at various tip gap

ranging from 0.04% to 0.8% span clearance, four specific flow processes are analyzed and assessed for their individual contribution to loss generation in rotor passage; these are tip clearance flow, double-leakage flow, flow corner separation at the tip, and viscous shear at the casing.

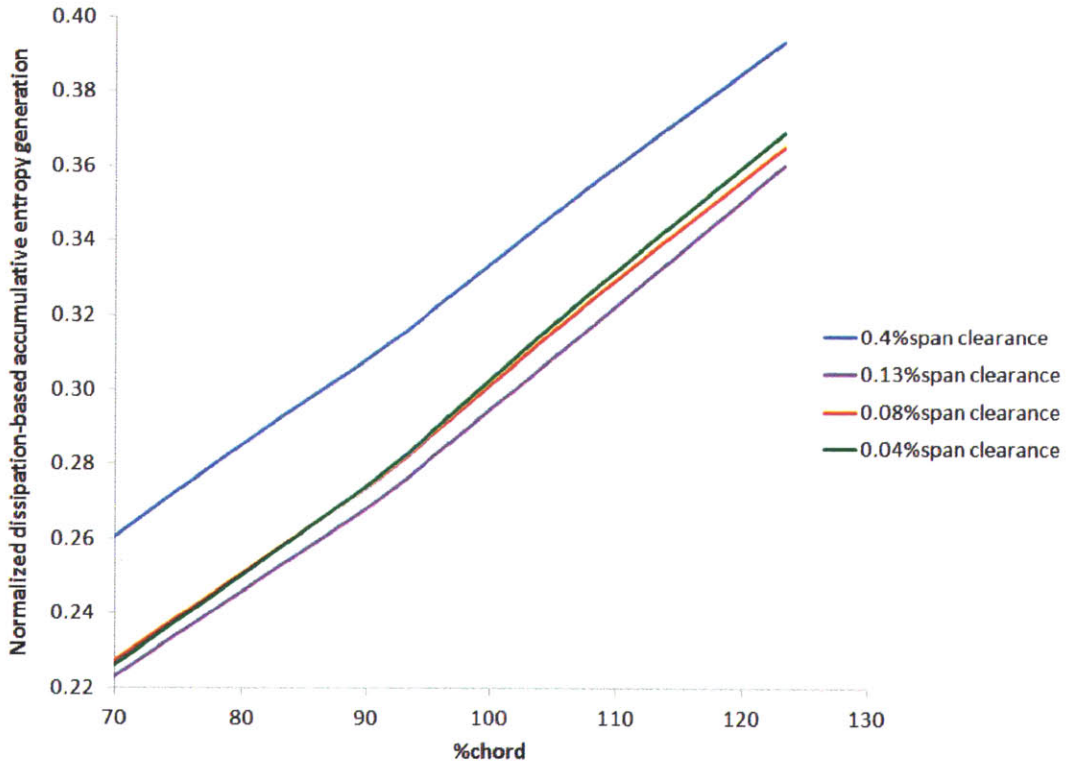

Figure 3-5: Distribution of accumulative entropy generation in rotor passage for small tip clearances near rotor trailing edge at design.

First, the tip leakage mass flow through the gap is determined to linearly decrease with tip gap size (Figure 3-7) and as a result, using Denton's leakage mixing model the tip leakage mixing loss decreases linearly as well (Figure 3-8). As for double tip leakage flow (alluded to in previous section), its flow path is elucidated in Figure 3-9 through releasing two particles in the tip gap near the leading edge. The tip leakage flow originated from leading edge to 15% axial chord intercepts the adjacent blade over a region extending from 35% axial chord to trailing edge. However, a reduction in tip gap to vanishing value is accompanied by a corresponding diminishing of double leakage flow. Thus double leakage flow is not a dominant contributor to efficiency

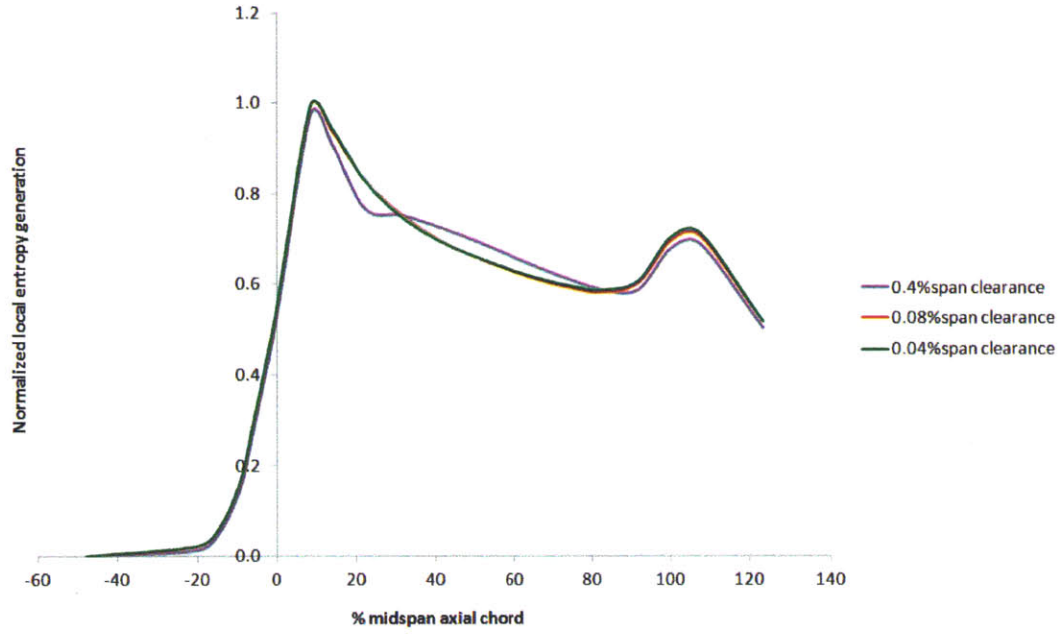

Figure 3-6: Distribution of local entropy genereation in rotor passage for small tip clearances at design.

variation with tip gap less than 0.8% span.

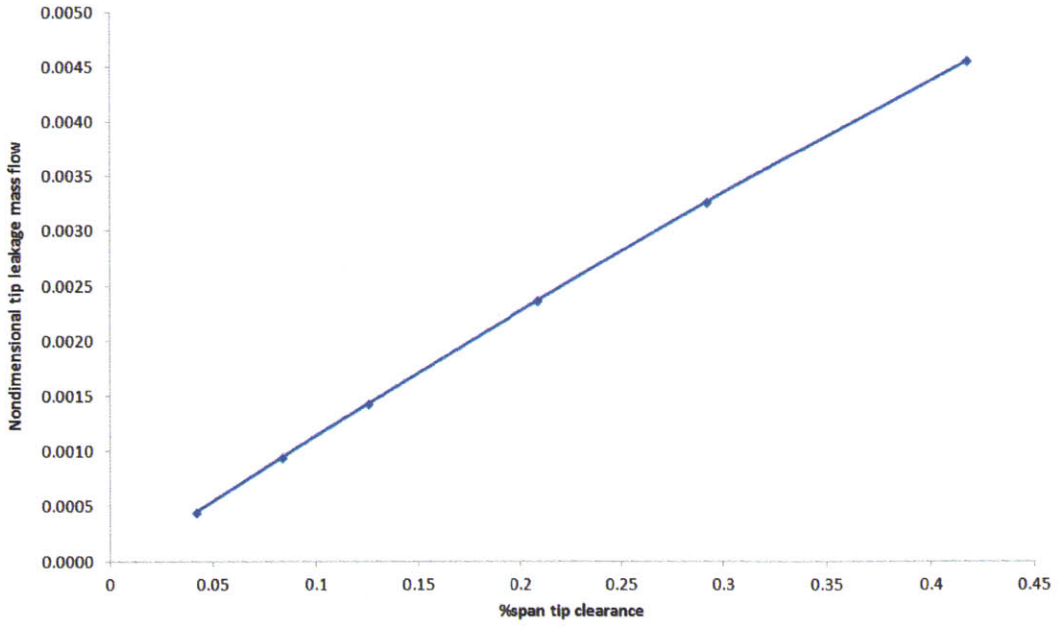

Figure 3-7: Nondimensional net tip leakage mass flow variation with tip clearance.

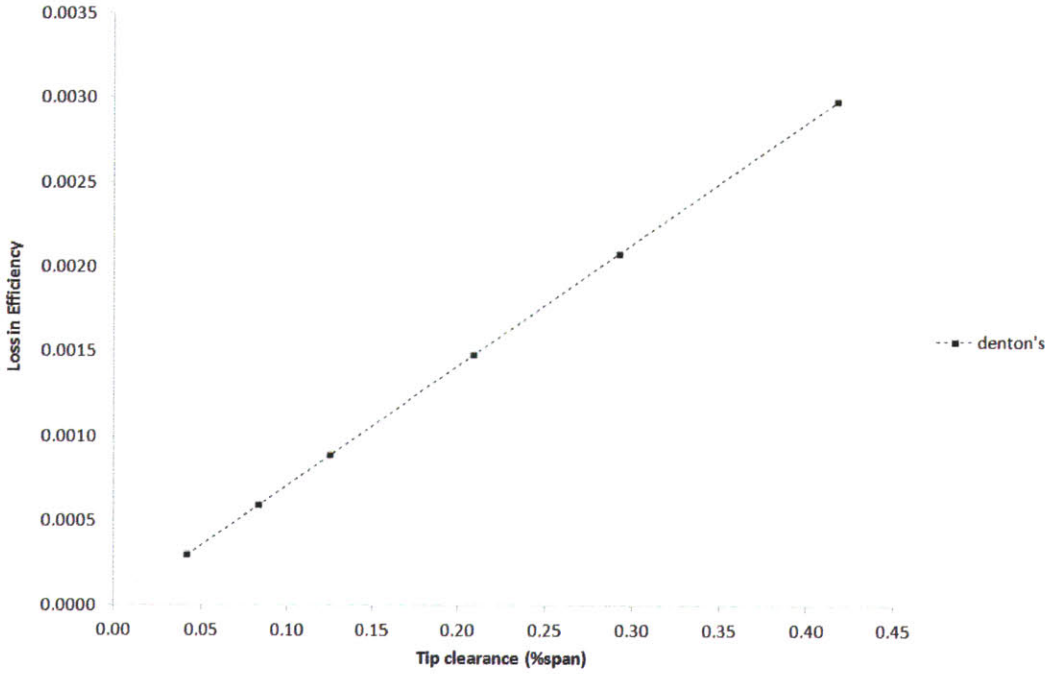

Figure 3-8: Loss in efficiency due to tip leakage flow mixing based on Denton's model.

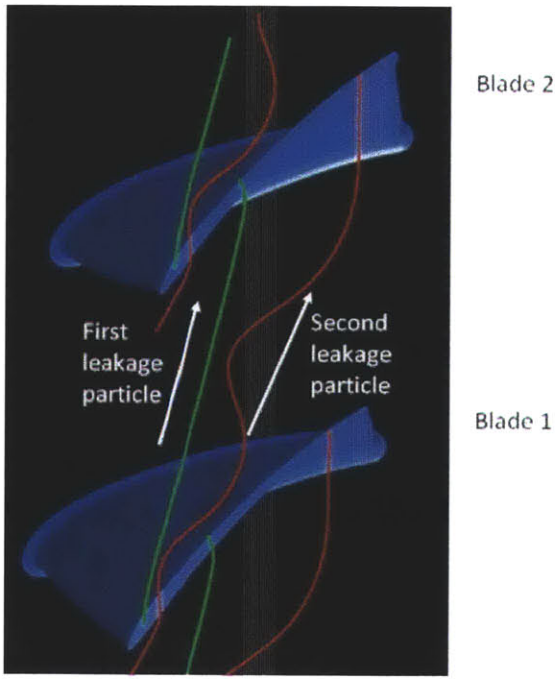

Figure 3-9: Streamlines of two particles released in the tip gap near blade leading edge showing double leakage flow paths.

The flow corner separation at the tip, which forms as tip gap is reduced to vanishing value, is mitigated by the energizing effects of casing relative motion with the blade, i.e. the casing shear work. Figure 3-10 shows a somewhat negligible flow corner separation on the rotor tip suction side on an axial plane at rotor trailing edge for 0.04% span and 0.08% span clearance. The size of the flow separation region is found to remain relatively unchanged for small tip gap in this rotor passage. Hence, this implies that the loss due to flow corner separation at the tip is small compared to tip leakage mixing loss and thus is not a dominant flow process setting up optimum tip clearance in compressor rotor passage.

However, if the casing is rotating with the rotor blade (in other words, stationary relative to rotor blade), flow corner separation on the rotor tip suction side is found to be significant for small tip clearances, as shown in Figure 3-11. The axial velocity contours at the rotor trailing edge with rotating casing demonstrates that when the endwall is stationary relative to the blade, the flow corner separation is significantly affected by the size of the blade clearance: as the blade end gap increases, the size of flow separation region decreases considerably. In other words, for rotor cascade where the endwalls are stationary, the loss due to flow corner separation increases when tip gap decreases. Thus, for rotor cascade flow corner separation at the tip is one of the dominant flow processes setting up optimum tip clearance. However, our interest lies in the optimum tip clearance for compressor rotor, thus we will focus on optimum tip gap with stationary casing where the loss due to flow corner separation at the tip is not a dominant player.

In addition, Figure 3-12 shows that Reynolds number has insignificant effect on flow corner separation at the tip, which is in agreement with the conclusions of Lei et al [16]. This suggests that flow corner separation at the tip is not one of the dominant flow processes setting up optimum tip gap for both high speed and low speed compressor rotor, due to the energizing effect of the casing relative motions to the blade.

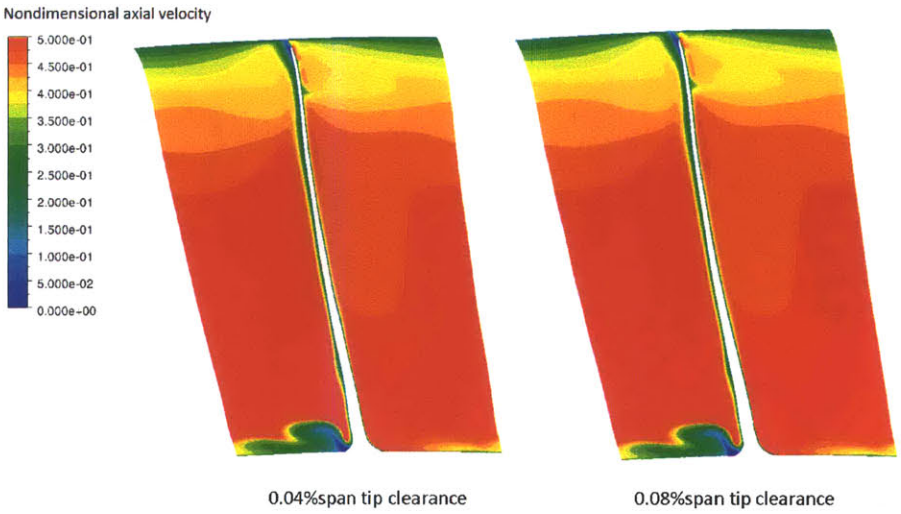

Figure 3-10: Axial Velocity at rotor trailing edge for two small tip clearances. Blue indicates reverse flow, i.e. flow separation.

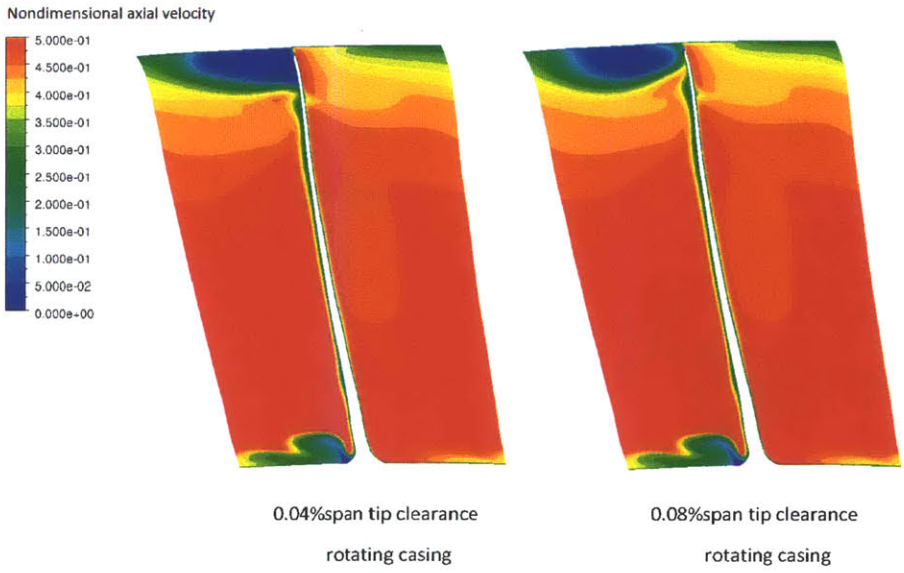

Figure 3-11: Axial Velocity at rotor trailing edge for two small tip clearances with rotating casing, i.e. casing is stationary relative to rotor blade. Blue indicates reverse flow, i.e. flow separation.

We now turn to assessing the contribution of the viscous shear at the casing to loss generation in rotor passage. When tip clearance is small, the viscous effect becomes significant. The motion of the casing relative to the rotor blade results in viscous

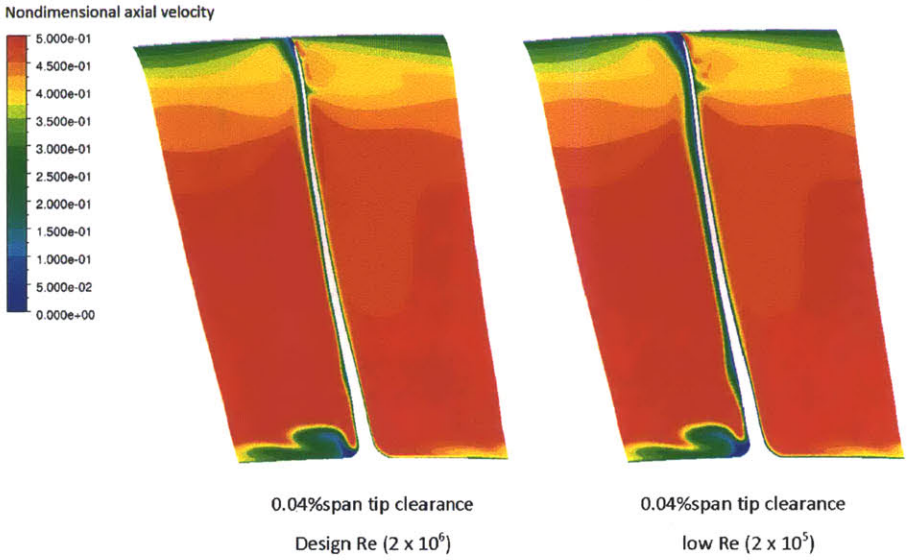

Figure 3-12: Axial Velocity at rotor trailing edge for different Reynolds number. Blue indicates reverse flow, i.e. flow separation.

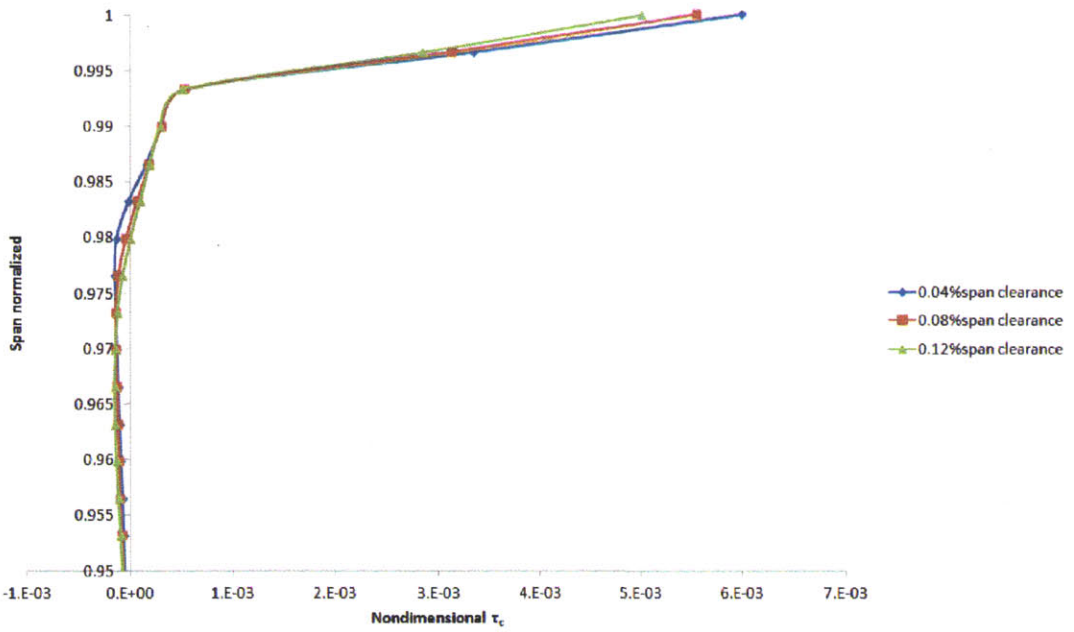

Figure 3-13: Spanwise distrubution of nondimensional shear stress due to radial gradient of circumferential velocity at the casing for small tip clearances.

shear loss at the casing. With reducing tip gap, the length scale for the viscous shear layer due to the casing motion becomes smaller, thus the casing viscous shear

loss increases accordingly as depicted in Figure 3-13. Therefore, there is a tip gap size below which the casing viscous shear induced loss overtakes the tip flow mixing induced loss, hence the high likelihood of an optimum tip gap for maximum efficiency. It is then hypothesized that the competing processes setting up optimum tip gap are tip leakage mixing loss and viscous shear loss at the casing.

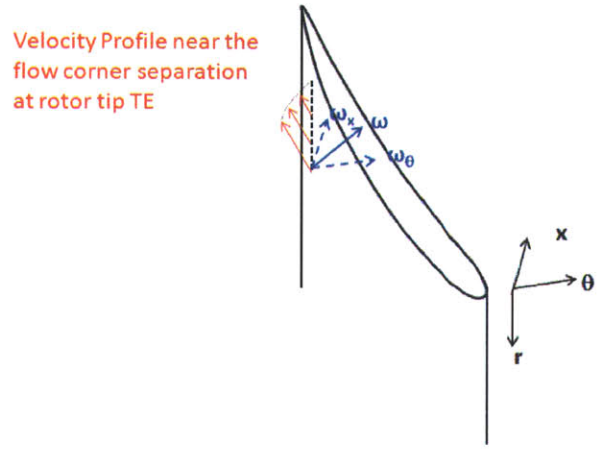

(a) Flow corner separation on blade suction side at rotor tip TE

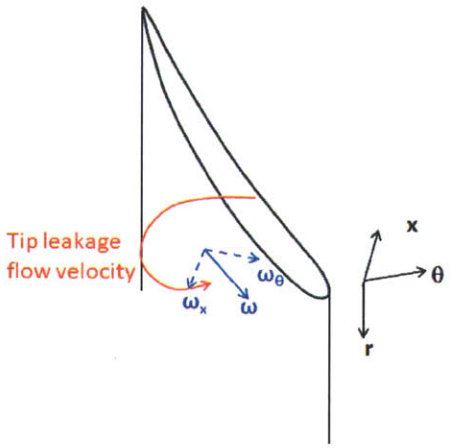

(b) Tip leakage flow

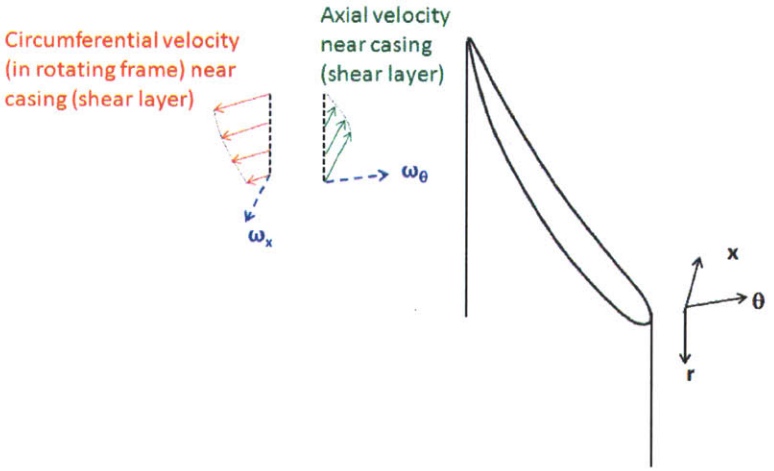

(c) Viscous shear layer at the casing

Figure 3-14: Axial component of vorticity (ω_x) due to different flow processes

To assess this hypothesis, the change in entropy generation due to flow corner separation, tip leakage mixing and viscous shear loss at the casing with small tip gap is assessed. In other words, the following analysis aims to determine if flow corner separation on the blade suction surface at the rotor tip trailing edge is not

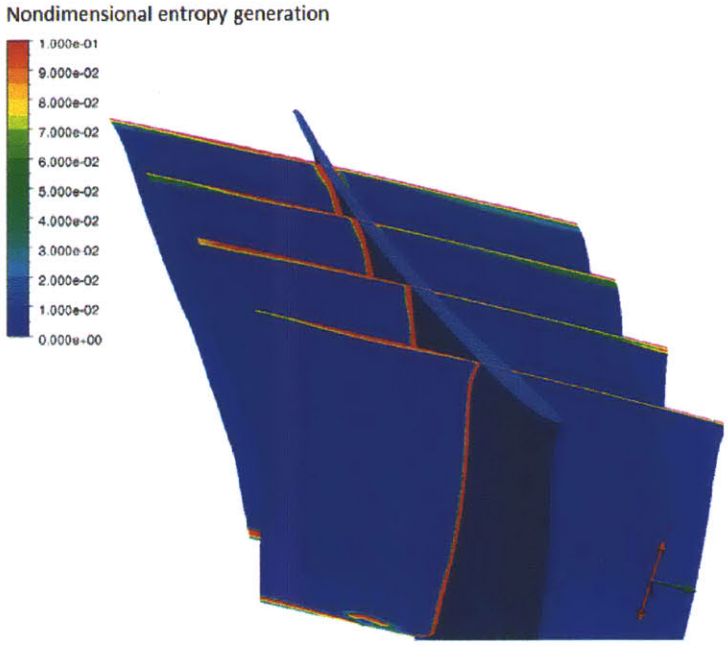

(a) Local entropy generation for rotor with 0.2% span tip gap, showing tip leakage flow

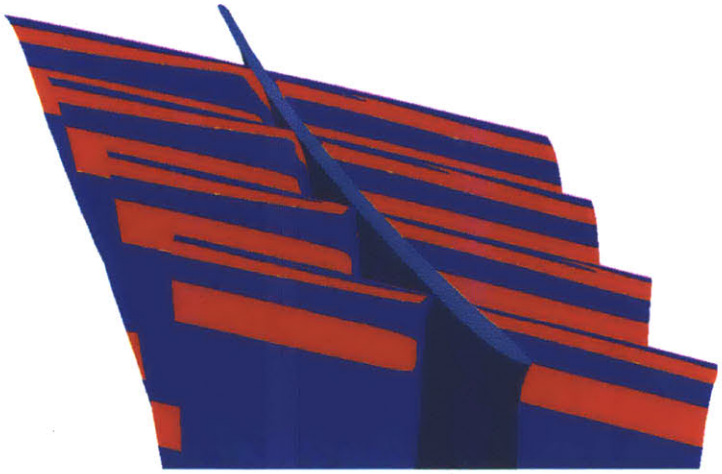

(b) Axial component of vorticity (ω_x) for rotor with 0.2% span tip gap showing negative (ω_x) in tip leakage flow region. Blue is negative (pointing upstream) and red is positive (pointing downstream).

Figure 3-15: The region with negative ω_x next to the casing is referred to as "tip leakage flow region" in the analysis in this section.

a dominant flow process setting up optimum tip gap (as posed in the hypothesis). First, the passage is to be divided into two regions: "inside tip leakage flow region" (a combination of tip leakage flow and viscous shear layer at the casing) and "outside tip

leakage flow region" (the region of flow separation at rotor tip TE and the flow region extending from the edge of tip leakage flow toward the hub), using axial component of vorticity near the casing. Figure 3-14 shows ω_x based on the three flow processes; tip leakage flow and viscous shear layer at the casing has negative ω_x (pointing upstream) but flow corner separation at rotor tip TE SS has positive ω_x (pointing downstream). The region of tip leakage flow (shown in Figure 3-15a) and viscous shear layer is then identified by the blue region with negative ω_x next to the casing as shown in Figure 3-15b. The local entropy generation "inside tip leakage flow region" and "outside tip leakage flow region" is then evaluated for small tip clearances as depicted in Figure 3-16.

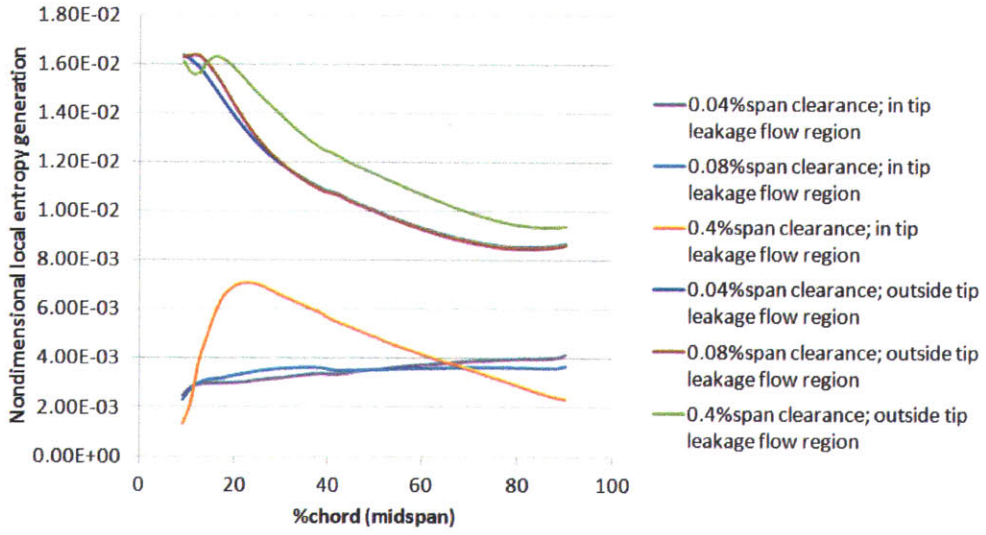

Figure 3-16: Local entropy generation rate inside and outside tip leakage flow region for small tip clearances. (Analysis of optimum tip clearance phenomena)

Inside tip leakage flow region, entropy is locally generated by the mixing of the tip leakage flow and the viscous shear loss at the casing. The mixing loss of the tip leakage flow decreases with decreasing tip gap but the viscous shear loss at the casing increases with decreasing tip gap. Figure 3-16 shows that local entropy generation "inside tip leakage flow region" starts to become higher for smaller tip clearance toward the trailing edge. This implies that near the leading edge, the mixing loss of tip leakage flow (which forms near the blade leading edge for small tip clearance)

with main flow is a dominant source of entropy generation and thus the local entropy generation is lower for small tip clearance. However, near the trailing edge, the viscous shear loss at the casing is the dominant source of loss and the local entropy generation is then higher for small tip clearance. It thus can be inferred from Figure 3-16 that both the mixing out of tip leakage flow and the viscous shear loss at the casing are dominant flow processess setting up the optimum tip gap.

However, outside tip leakage flow region, entropy is locally generated by flow corner separation at rotor tip TE SS, a part of the mixing loss of the tip leakage flow with the main flow, as well as other tip-gap-independent loss (such as blade surface boundary layer, hub corner separation, etc.). The mixing loss of the tip leakage flow with main flow decreases with decreasing tip gap but loss due to flow corner separation at the tip increases with decreasing tip gap. Figure 3-16 shows that local entropy generation "outside tip leakage flow region" is in general lower for smaller tip clearance along the blade chord. In other words, the change in the loss due to flow corner separation with tip gap is small compared to that due to tip leakage mixing loss; hence, the entropy generation does not increase with decreasing tip gap along the whole chord from leading edge to trailing edge. It thus can be inferred from Figure 3-16 that flow corner separation at rotor tip TE SS is not a dominant flow process setting up optimum tip gap. Therefore, it is hypothesized that the competing processes setting up optimum tip gap are tip leakage mixing loss and viscous shear loss at the casing.

The optimum tip gap hypothesis allows one to establish its scaling as follows. First, the casing viscous shear is essentially set by the radial distribution of the circumferential velocity; thus an estimate is

$$\tau_c \approx \mu \frac{\partial u_c}{\partial r} \sim \mu \frac{U_{casing}}{g} \tag{3.1}$$

$$\sim \left(\frac{\mu}{\rho V_1 c}\right)\left(\frac{c}{g}\right)(\rho V_1 U_{casing})$$

$$\sim Re^{-1}\left(\frac{g}{s}\right)^{-1}\left(\frac{c}{s}\right)(\rho V_1 U_{casing}) \tag{3.2}$$

Using the expression given in equation 3.2, an estimate for the change in efficiency $\Delta\eta_{shear}$ arising from entropy generation assoxiated with casing viscous shear effect is given below as:

$$\dot{S}'''_{gen} \sim \frac{\mu}{T}\left(\frac{\partial u_c}{\partial r}\right)^2 \sim \frac{\tau_c^2}{\mu T}$$

Thus,

$$\begin{aligned}\Delta\eta_{shear} &\sim \frac{T\dot{S}'''_{gen} gcp}{\dot{m}\Delta h} \sim \frac{\tau_c^2 gcp}{\mu \dot{m}\Delta h} \\ &\sim \left(\frac{\tau_c}{\rho V_1^2}\right)^2 \left(\frac{V_1^2}{\Delta h}\right)\left(\frac{\rho^2 V_1^2 gcp}{\mu \dot{m}}\right)\end{aligned}$$

,where $\dot{m} \approx \rho V_1 ps \cos\beta_1$ and τ_c given in equation 3.2. Hence,

$$\begin{aligned}\Delta\eta_{shear} &\sim \left(\frac{Re^{-1}\left(\frac{g}{s}\right)^{-1}\left(\frac{c}{s}\right)(\rho V_1 U_{casing})}{\rho V_1^2}\right)^2 \left(\frac{V_1^2}{\Delta h}\right)\left(\frac{\rho^2 V_1^2 gcp}{\mu \rho V_1 ps\cos\beta_1}\right) \\ &\sim Re^{-1}\left(\frac{g}{s}\right)^{-1}\left(\frac{c}{s}\right)^2\left(\frac{U_{casing}}{V_1}\right)^2\left(\frac{V_1^2}{\Delta h}\right)\frac{1}{\cos\beta_1} \\ &\sim Re^{-1}\left(\frac{g}{s}\right)^{-1}\left(\frac{c}{s}\right)^2\left(\frac{U_{casing}}{V_1}\right)^2\frac{\phi^2}{\psi\cos^3\beta_1} \qquad (3.3)\end{aligned}$$

The entropy generation due to casing viscous shear effect is inversely proportional to the Reynolds number Re, clearance-to-span ratio $\frac{g}{s}$, stage loading coefficient ψ, and aspect ratio squared $\left(\frac{s}{c}\right)^2$. As for the loss associated with mixing out of tip clearance flow, it can readily be estimated using Denton's leakage mixing model to yield an expression for the efficiency change as derived in the following:

From Denton's tip leakage mixing model,

$$T\Delta s_{mix} = \frac{C_d}{V_1 \cos\beta_1}\left(\frac{c}{p}\right)\left(\frac{g}{s}\right)\int_0^1 V_s^2\left(1-\frac{V_p}{V_s}\right)\sqrt{V_s^2-V_p^2}\,\mathrm{d}\frac{z}{c}$$

Thus, with the assumption of $V_s \sim V_1$

$$\begin{aligned}\Delta\eta_{mix} = \frac{T\Delta s_{mix}}{\Delta h} &\sim \frac{C_d}{V_1\cos\beta_1\Delta h}\left(\frac{c}{p}\right)\left(\frac{g}{s}\right)V_s^3\left(1-\frac{V_p}{V_s}\right)\sqrt{1-\left(\frac{V_p}{V_s}\right)^2} \\ &\sim C_d\left(\frac{c}{p}\right)\left(\frac{g}{s}\right)\left(1-\frac{V_p}{V_s}\right)\sqrt{1-\left(\frac{V_p}{V_s}\right)^2}\left(\frac{V_1^2}{\Delta h}\right)\frac{1}{\cos\beta_1} \\ &\sim C_d\left(\frac{c}{p}\right)\left(\frac{g}{s}\right)\left(1-\frac{V_p}{V_s}\right)\sqrt{1-\left(\frac{V_p}{V_s}\right)^2}\frac{\phi^2}{\psi\cos^3\beta_1} \qquad (3.4)\end{aligned}$$

The optimum tip gap scaling can now be obtained by seeking the minimum of the total entropy generation from viscous shear loss at the casing and tip leakage mixing loss with respect to gap-to-span ratio, since the former increases and the latter decreases with decreasing gap-to-span ratio $\frac{\partial(\Delta\eta_{shear}+\Delta\eta_{mix})}{\partial(\frac{g}{s})} = 0$. Doing so yields the optimum gap scaling as:

$$\begin{aligned}\left(\frac{g}{s}\right)_{optimum} &\sim \left(\frac{Re^{-1}\left(\frac{c}{s}\right)^2\left(\frac{U_{casing}}{V_1}\right)^2\frac{\phi^2}{\psi\cos^3\beta_1}}{C_d\left(\frac{c}{p}\right)\left(1-\frac{V_p}{V_s}\right)\sqrt{1-\left(\frac{V_p}{V_s}\right)^2}\frac{\phi^2}{\psi\cos^3\beta_1}}\right)^{\frac{1}{2}} \\ &\sim C_d^{-\frac{1}{2}}Re^{-\frac{1}{2}}\left(\frac{c}{s}\right)\left(\frac{c}{p}\right)^{-\frac{1}{2}}\left(\frac{U_{casing}}{V_1}\right)\left(\left(1-\frac{V_p}{V_s}\right)\sqrt{1-\left(\frac{V_p}{V_s}\right)^2}\right)^{-\frac{1}{2}} \qquad (3.5) \\ &\sim C_d^{-\frac{1}{2}}Re^{-\frac{1}{2}}\left(\frac{c}{s}\right)\left(\frac{c}{p}\right)^{-\frac{1}{2}}\left(\frac{\cos\beta_1}{\phi}\frac{2}{1+\frac{R_{hub}}{R_{casing}}}\right)\left(\left(1-\frac{V_p}{V_s}\right)\sqrt{1-\left(\frac{V_p}{V_s}\right)^2}\right)^{-\frac{1}{2}} \qquad (3.6)\end{aligned}$$

For uniform blade loading and small blade thickness, $\frac{V_p}{V_s}$ can be approximated as (Denton [8])

$$\frac{V_p}{V_s} \approx \sqrt{1 - \frac{\psi}{\phi}\left(\frac{p}{c}\right)\left(\frac{V_x}{V_s}\right)^2 \frac{2}{\cos\gamma}} \approx \sqrt{1 - \frac{\psi}{\phi}\left(\frac{p}{c}\right)\cos^2\beta_1 \frac{2}{\cos\gamma}} \tag{3.7}$$

Having established the optimum tip gap scaling for maximum efficiency, we next proceed to assess the scaling against available computational and experimental data. The variation of computed rotor efficiency with tip gap varying from 0.4% span to vanishing value at operating points corresponding to 0.94 (off-design toward stall), 1.0 (design) and 1.16 (off-design toward choke) design flow is shown in Figure 3-17. It was found that for a small change in tip clearance, the entropy dissipation method provides a more accurate trend of efficiency variation than the entropy flux method. Thus, the rotor efficiency shown in Figure 3-17 is computed based on entropy dissipation method.

The variation in optimum tip gap value with operating points can be rationalized based on the established scaling. For off-design point at mass flow lower than the design value (toward stall), the incidence angle is higher and so is the blade loading with relatively higher tip leakage mass flux and tip leakage flow mixing loss. This should thus decrease the relative size of the optimum tip clearance for operating points at mass flow lower than the design value. Conversely, for operating point at mass flow higher than the design value (toward choke), the incidence angle and the blade loading is relatively lower; thus the corresponding tip leakage mass flux and tip leakage mixing loss is lower, yielding a relatively larger optimum tip gap value. This trend is correctly reflected in the computational results of Figure 3-17.

In addition, when Reynolds number decreases, the casing viscous shear effect is enhanced but the change in tip leakage mixing loss is insignificant (as the tip flow is essentially a pressure-driven phenomenon), thus the optimum tip gap becomes larger. This is consistent with the scaling and the computed results for Reynolds number of 2×10^6 versus 2×10^5 indeed reflect this trend. Based on the scaling,

the changes in the optimum tip gap of the rotor with stage design characteristics are also presented in Figure 3-18. The optimum tip gap increases when decreasing Reynolds number, aspect ratio, solidity and stage loading coefficient. However, for high Reynolds number of more than 10^6, it is shown that it would be difficult to design a rotor with an optimum tip gap that is manufacturable (e.g. $\sim$ 1% span).

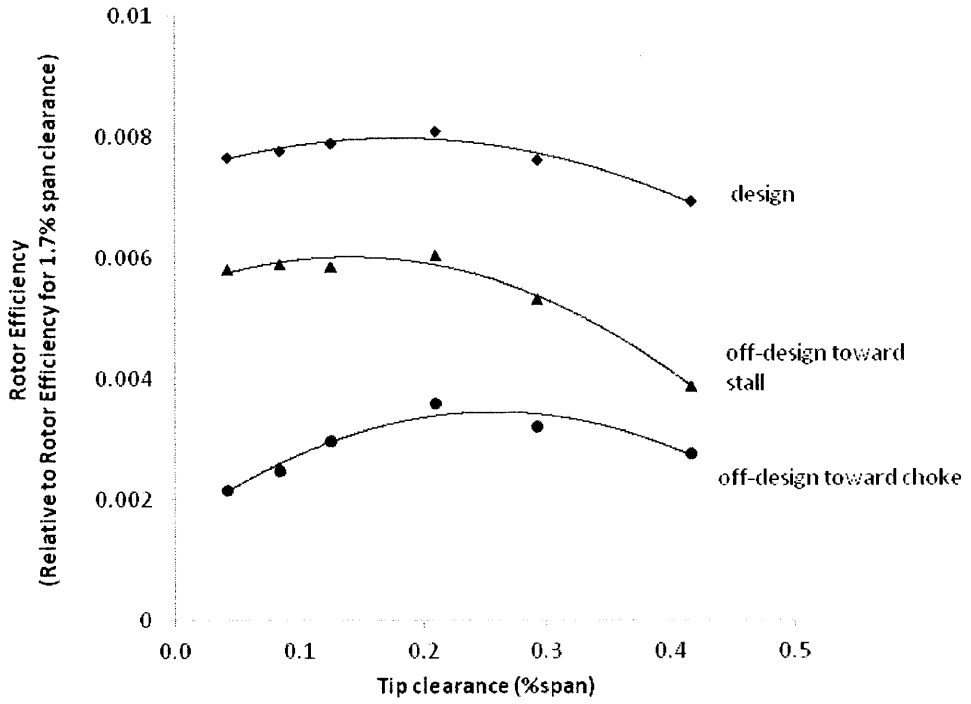

Figure 3-17: Rotor efficiency variation with tip clearance for small tip clearances at 3 different operating points

The scaling given in Equation 3.5 is used to estimate the optimum tip gap for three rotor-stator stage: the compressor stage used here, the Deverson compressor stage described in MacDougall et al. [18] and in Cumpsty [6], and the transonic compressor stage described in Wennerstrom [26]. For the first compressor, the estimated value is assessed against the computed value while for the latter two compressor stage, the estimated tip gap value is assessed against experimental measurements. These comparisons are tabulated in Table 3.1. One can thus infer that the scaling can provide a useful estimation of the optimum tip gap for a fairly broad range of conditions.

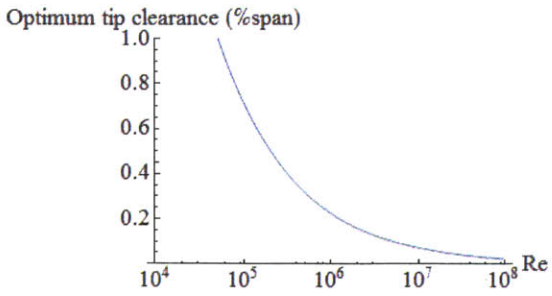

(a) Reynolds number

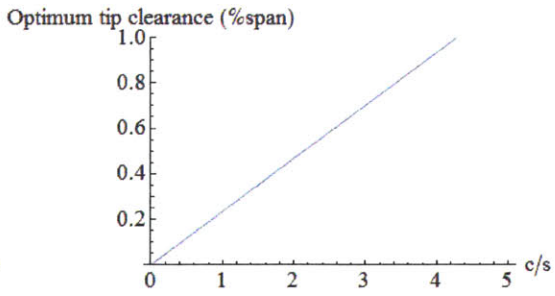

(b) chord-to-span (inverse of aspect ratio)

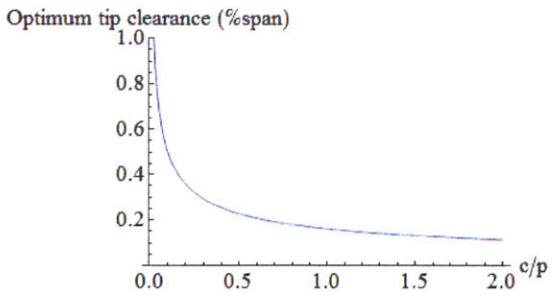

(c) chord-to-pitch (solidity)

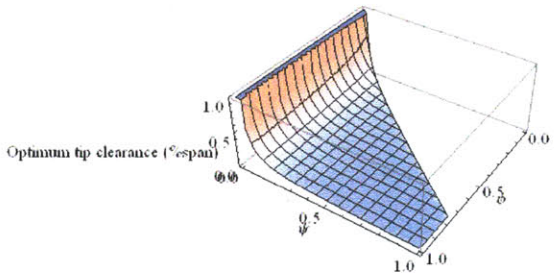

(d) flow coefficient and stage loading coefficient

Figure 3-18: Optimum tip gap variation with various parameters

For the Wennerstrom's transonic compressor stage, the optimum tip gap has been estimated for operating Reynolds number ranging from 3×10^5 to 1×10^6 as the operating Reynolds number based on the data given in Wennerstrom [26] cannot be reliably estimated.

For compressor in a large industrial gas turbine with cantilevered stator, the same conceptual basis for scaling optimum tip gap can be applied for scaling optimum hub gap for minimum loss in the stator passage. With cantilevered stator and rotating hub, the processes setting up optimum hub gap are now hub leakage mixing loss and viscous shear loss at the hub. Therefore, in the scaling shown in equation 3.5, the casing velocity relative to the rotor blade is replaced by the hub velocity relative to the stator blade. From CFD results, the optimum hub clearance is approximately 0.11% span for the compressor stage investigated while the use of scaling estimates the optimum hub clearance to be 0.13% span.

To summarize, there exists an optimum tip/hub gap for maximum efficiency. It

Optimum tip clearance (% span)	Stage 9 at design	Stage 9 toward choke	Stage 9 toward stall	Deverson compressor(Cumpsty, Mcdougall)	Wennerstrom Transonic compressor
From scaling	0.14%	0.21%	0.14%	0.7%	0.4%-0.7%
From CFD or experiment	0.17%	0.25%	0.13%	1%	0.5%

Table 3.1: Assessment of optimum tip gap scaling with computational and experimental data.

is set by the competing effects of the loss generation associated with increasing casing/hub shear and decreasing clearance flow mixing out loss with decreasing gap-to-span ratio. A scaling for optimum tip gap has been established and shown to be able to satisfactorily quantify the value of the optimal gap. The scaling delineates the parameter values (e.g. Reynolds number, operating points, stage aerodynamic and geometrical characteristics) that mark the change in behavior of efficiency variation with gap-to-span ratio and compressor operating points. Because of the high operating Reynolds number encountered in large industrial gas turbine, the optimum blade end gap is relatively small and thus difficult to deploy due to operational, mechanical and manufacturing constraints. However, deploying optimum blade clearance may be viable in compressors with relatively low Reynolds number.

3.3 Effects of large tip clearance on compressor stage performance

For tip gap region larger than approximately 3.4% span, the efficiency variation with gap-to-span ratio is shown in Figure 3-19. The relative rotor efficiency is computed for tip clearance values ranging from 0.8% span to 5% span at two operating points with one at 0.94 design flow and the other at design. There is a distinct change in the behavior of efficiency variation with tip gap greater than 3.4% span. This aspect of efficiency variation with tip gap is elaborated further in the following.

The computed rotor efficiency is clearly less sensitive to tip gap variation for the

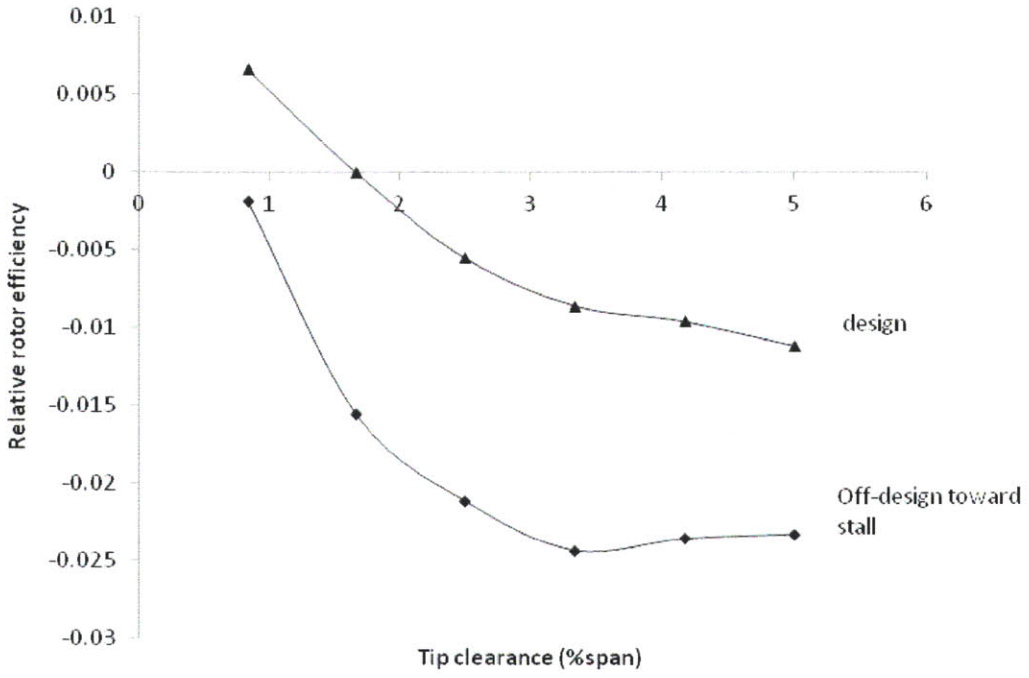

Figure 3-19: Rotor efficiency variation with tip clearance for tip clearance larger than 3.4% span.

range of tip gap larger than 3.4% span. As shown in Figure 3-19, the slope of the efficiency curve drop to a lower value relative to that for tip gap ranging from 0.8% to 3.4% span. In fact, the efficiency curve at 0.94 design mass flow (off-design toward stall) is approximately flat for gap-to-span ranging from 3.4% to 5% indicating only a marginal drop in efficiency for any increase in tip clearance; this is despite the fact that the slope is relatively steeper than that at design for gap-to-span less than 3.4%.

Application of Denton's leakage mixing model to this range of tip gap shows no change whatsoever in the efficiency slope as shown in Figure 3-4, which depicts a comparison of the loss estimated from Denton's leakage mixing model and the computed loss. The reason that Denton's model does not capture this distinct change in the slope of the efficiency curve is that the model inherently assumes instantaneous mixing of tip leakage flow with main flow. If the mixing out of tip leakage flow is completed within the rotor passage, then there should not be any change in the efficiency slope at all. The implication then is that the mixing out of tip clearance flow

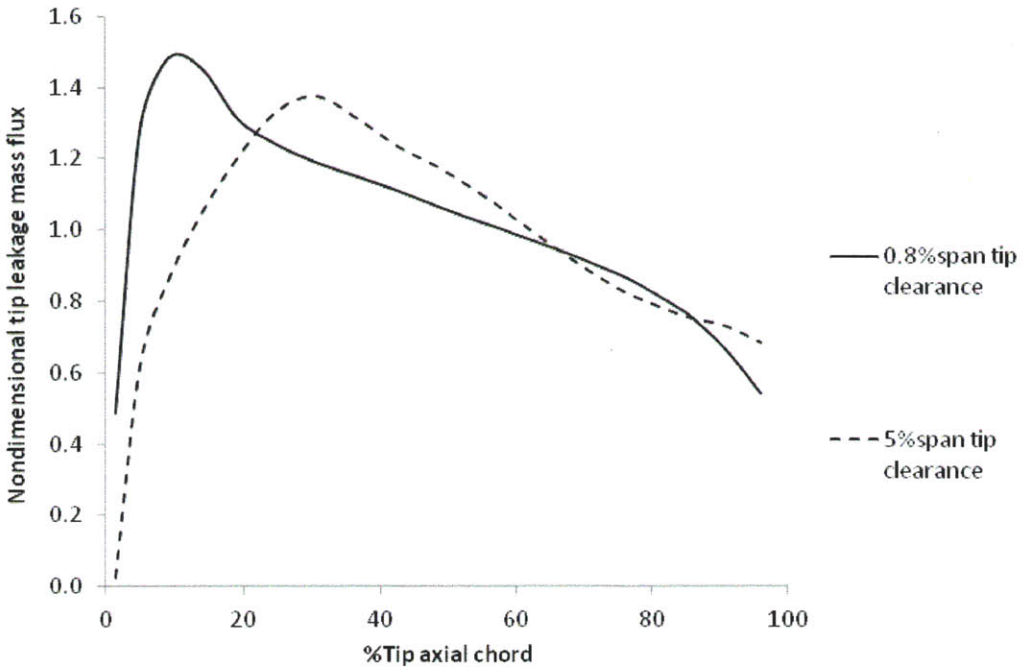

Figure 3-20: Tip leakage mass flow per unit area.

is incomplete in the rotor passage especially for tip gap larger than 3.4% span while fortuitously it is nearly complete for values that are smaller (see previous sections). Next we proceed to propose a rationale as to why the mixing out of tip flow is incomplete and as to when the near complete mixing out of tip flow is a good approximation so that Denton's leakage mixing model is applicable.

Computed results in Figure 3-20 show that the peak of the tip leakage mass flux (i.e. tip leakage flow per unit gap area) is shifted toward the rotor trailing edge and likewise those in Figure 3-21 show that the blade tip peak loading is also shifted downstream toward the trailing edge. The computed flow also shows that the tip leakage flow formation is shifted downstream toward the rotor trailing edge when tip clearance size is increased. Such a trend of the loading aft-shift with relative large tip gap has also been observed by Williams et al. [27], Storer and Cumpsty [23], and Intaratep [11]. Storer and Cumpsty found that the tip clearance flow rolls up into a tip leakage vortex and starts to move away from the suction surface of the blade at the point which is usually at the maximum blade loading of the blade. They also

concluded that the axial location of the peak in blade loading varies with tip gap size, i.e. when tip gap increases, the peak loading location moves downstream and the roll up of the tip clearance vortex is delayed. The present computed results on the aft-shifting of blade tip peak loading and tip leakage flow formation toward the rotor trailing edge are thus in accord with those of Storer and Cumpsty [23].

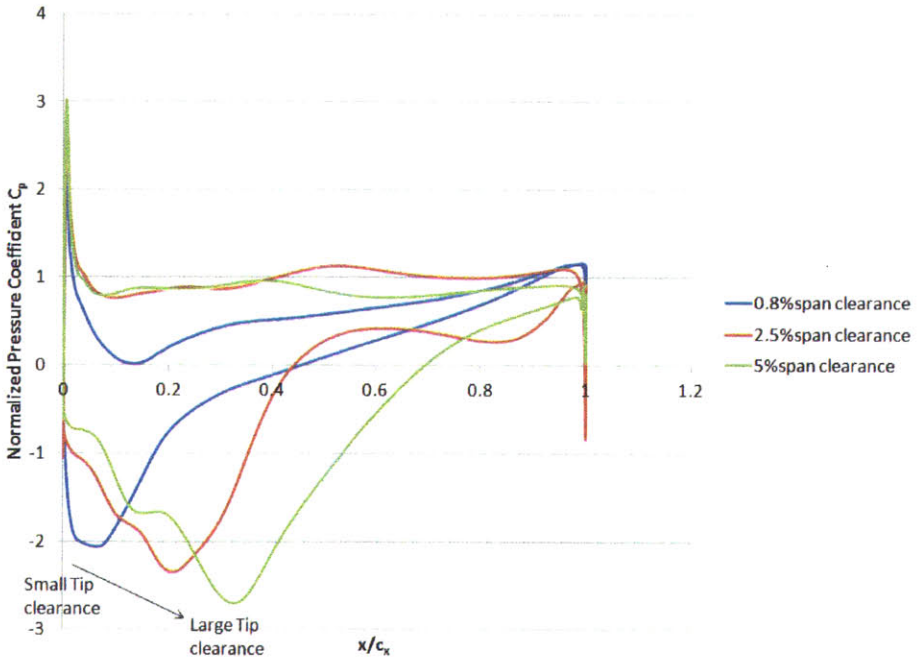

Figure 3-21: blade loading at the tip for different tip clearances.

A consequence of the aft-shift in the blade tip peak loading is that the tip leakage formation is delayed toward the trailing edge. This reduces the opportunity for the mixing out of the tip flow in rotor passage (and the tip flow induced flow blockage production as well) so that the tip leakage flow can remain relatively unmixed at the rotor exit. This is indeed the case as can be seen in the computed results shown in Figure 3-22 that elucidates the development of entropy profile in the tip region from rotor leading edge to rotor exit for a gap-to-span ratio less than 3.4% and for a value greater than 3.4%. At a gap-to-span ratio of 1.7%, the tip flow appears to have realized nearly all its loss generation potential; this certainly is not the case at a gap-to-span ratio of 5% where the tip flow is relatively unmixed at rotor trailing

edge (An elaboration on this figure is presented in Appendix A). As such the rotor efficiency would become less sensitive to tip clearance variation beyond the critical gap value (of 3.4% span for the compressor stage here). This critical value is set by two competing effects in loss generation: an increase in tip leakage mass flow rate associated with increasing tip gap and a decrease in tip flow mixing loss due to blade tip peak loading being aft-shifted as the tip gap increases. The fact that the tip flow induced loss generation is less sensitive to tip gap variation is also brought out in the computed results for local entropy generation rate shown in Figure 3-23 for gap-to-span ratio of 3.4% and 4.2%. We infer from the results presented here that for rotor design with its tip peak loading located in the immediate blade leading edge region, the assumption that the mixing-out of tip flow is complete within the rotor passage is a good approximation. For this situation Denton's leakage mixing model is applicable. However for rotor design with aft-loaded tip, there is less opportunity for the tip flow to realize its mixing-out loss generation potential so that Denton's model is not applicable here because of its inherent assumption of instantaneous mixing of tip leakage flow with main flow.

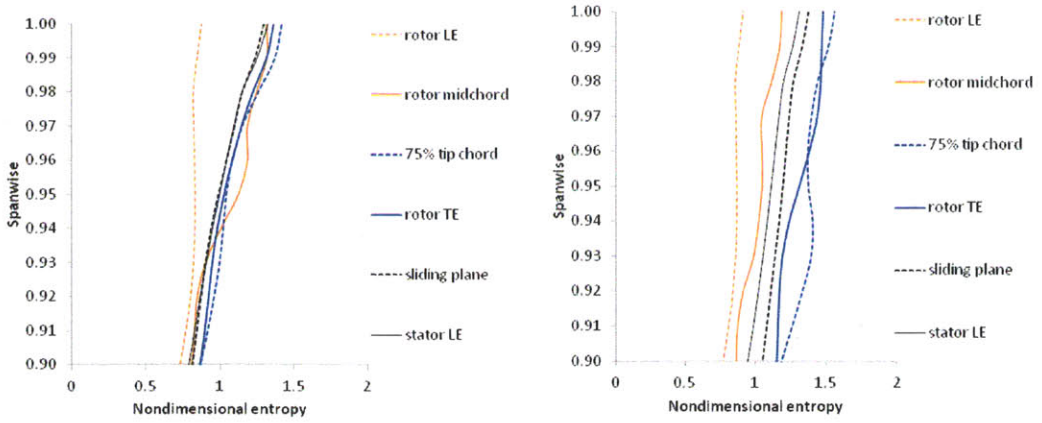

(a) 1.7% span tip clearance

(b) 5% span tip clearance

Figure 3-22: Entropy profile near the casing.

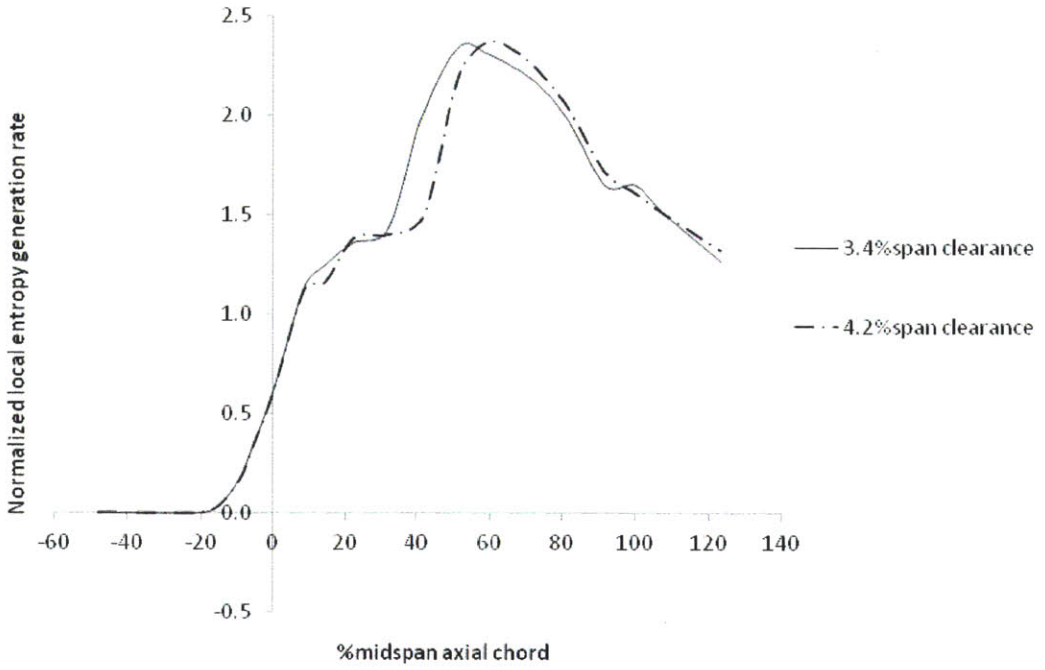

Figure 3-23: Local entropy generation rate.

3.4 Effects of rotor tip clearance on flow blockage generation and pressure rise

In general, an increase in tip leakage mass flow due to the enlargement of the tip gap size increases flow blockage generation in rotor passage. In Figure 3-24, when tip clearance increases, computed flow blockage at the rotor exit based upon Khalid's flow blockage definition increases and correspondingly the stage pressure rise decreases. However, even though the flow blockage at the rotor exit increases with tip clearance, the axial variation in flow blockage generation within the rotor passage can be non-monotonic. We also infer from Figure 3-25 that the flow blockage associated with the formation of tip leakage flow is generated mostly in the leading edge region for medium tip clearance. Subsequently, the passage of the wake-like tip leakage flow (Khalid et al. [12], Valkov and Tan [24, 25]) through the rotor passage with a diffusing flow induces additional flow blockage generation. However, the mixing out of tip leakage flow in the

passage decreases the flow blockage so that when its mixing out becomes dominant toward the rotor trailing edge region, the flow blockage can begin to decrease. This is indeed reflected in the results shown in Figure 3-24.

The effect of the non-monotonic flow blockage generation in rotor passage is reflected in the pressure rise distribution as shown in Figure 3-26. Near the leading edge, where flow blockage generation is large due to the formation of tip leakage flow, the slope of pressure rise starts to drop when flow blockage is large enough (i.e. for large tip gap). However, downstream of approximately mid-chord, the slope of pressure begins to increase again as flow blockage generation decreases due to the mixing out of the tip leakage flow.

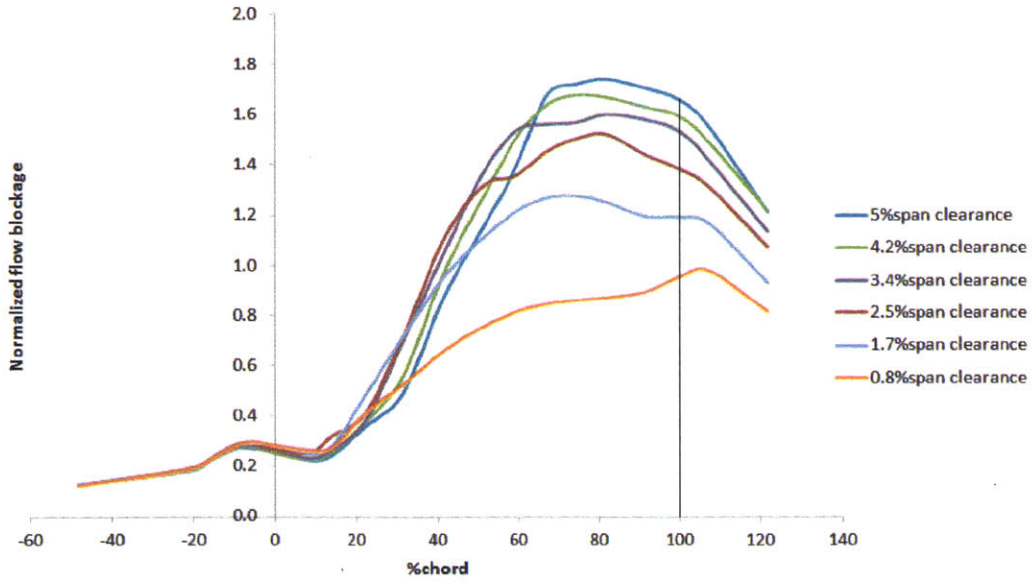

Figure 3-24: Flow blockage variation along axial chord for different tip clearances. (Midspan LE: 0% midspan chord (y-axis) and Midspan TE: 100% midspan chord (red dashed line))

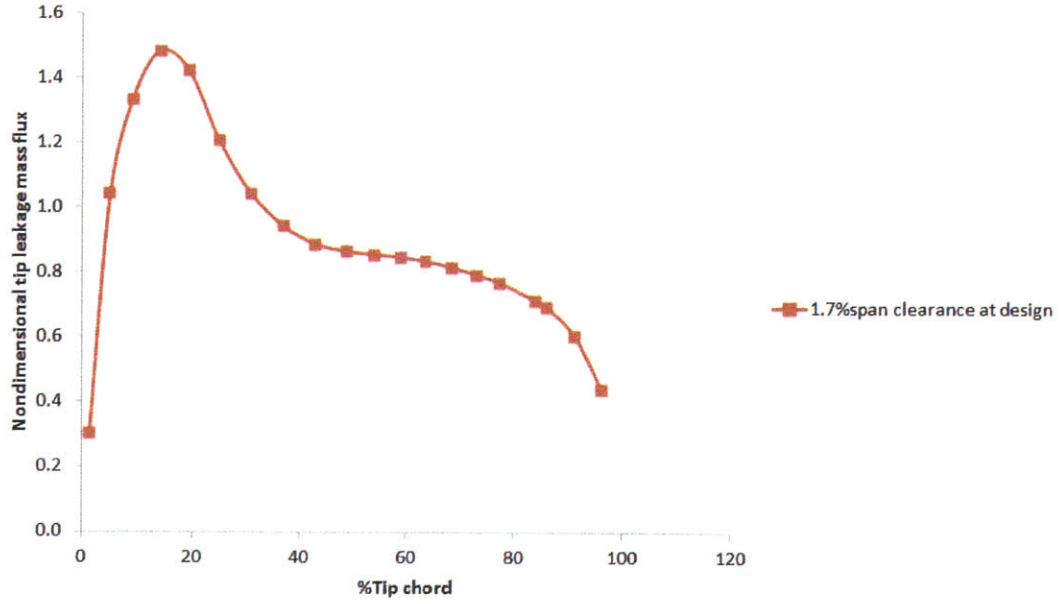

Figure 3-25: Nondimensional tip leakage mass flux variation with tip chord (0% at tip LE and 100% at tip TE) for 1.7% span tip clearance at design.

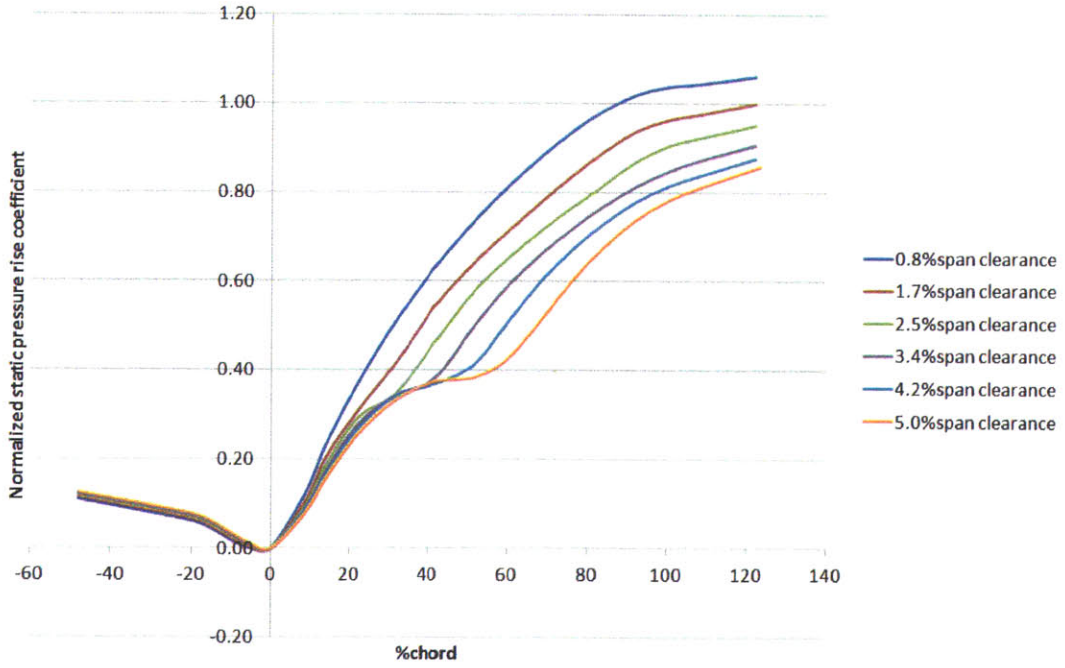

Figure 3-26: Pressure rise in rotor passage for different tip clearances.

3.5 Effects of operating point on efficiency sensitivity to tip gap

For tip gap larger than the optimum tip clearance and smaller than the threshold value, the sensitivity of the efficiency to tip gap (i.e. the slope of the efficiency-gap curve) depends on operating point. When the rotor is operating at lower mass flow (i.e. toward stall), the pressure difference across the blade gap increases and drives more tip leakage flow through the gap. As a results, the loss arising from the mixing out of the tip leakage flow increases as the mass flow decreases. In addition, as we move toward stall, the rotor becomes more fore-loaded (Figure 3-27 and 3-28), thus tip leakage flow is formed further upstream near leading edge as shown in Figure 3-29 (The low-pressure region at the rotor tip (tip leakage core) is formed further upstream with lower mass flow.). Thus, toward stall tip leakage mixing out process starts earlier upstream for medium tip gap and hence at the exit of the rotor, tip leakage flow would have more opportunity to mix out.

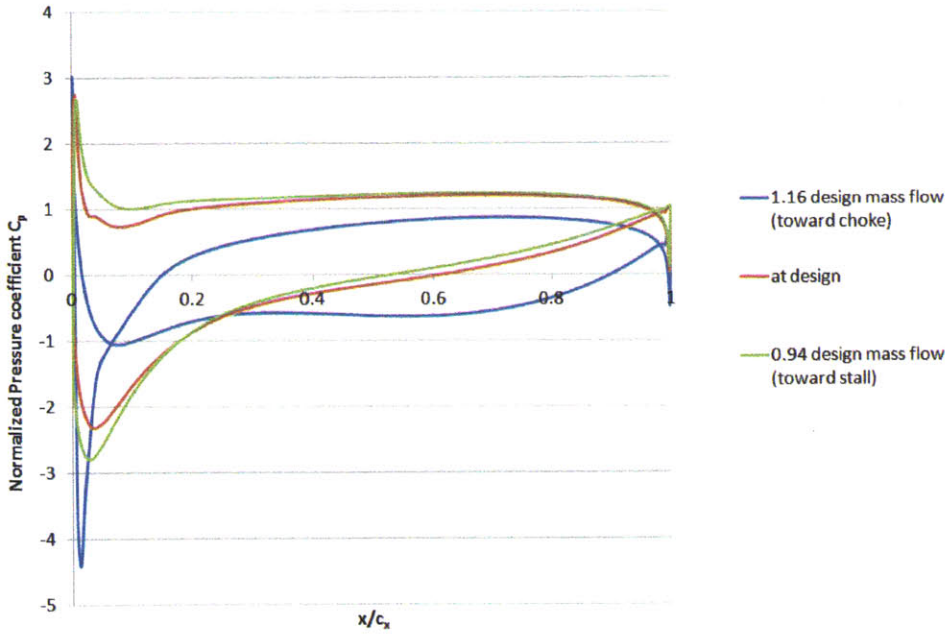

Figure 3-27: Blade loading of rotor with 2.5% tip clearance at midspan for 3 operating points.

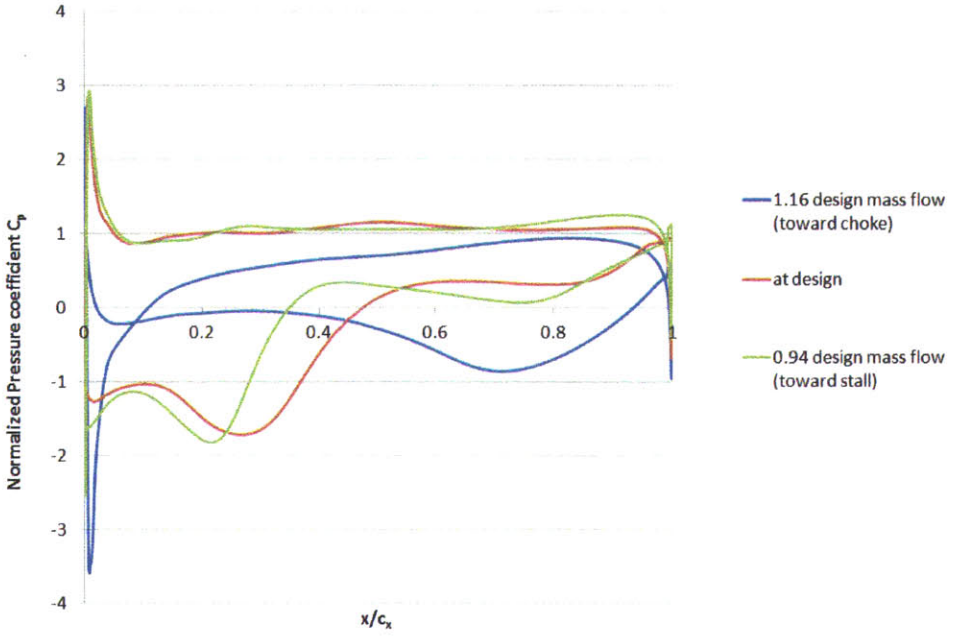

Figure 3-28: Blade loading of rotor with 2.5% tip clearance at 3%span from blade tip for 3 operating points.

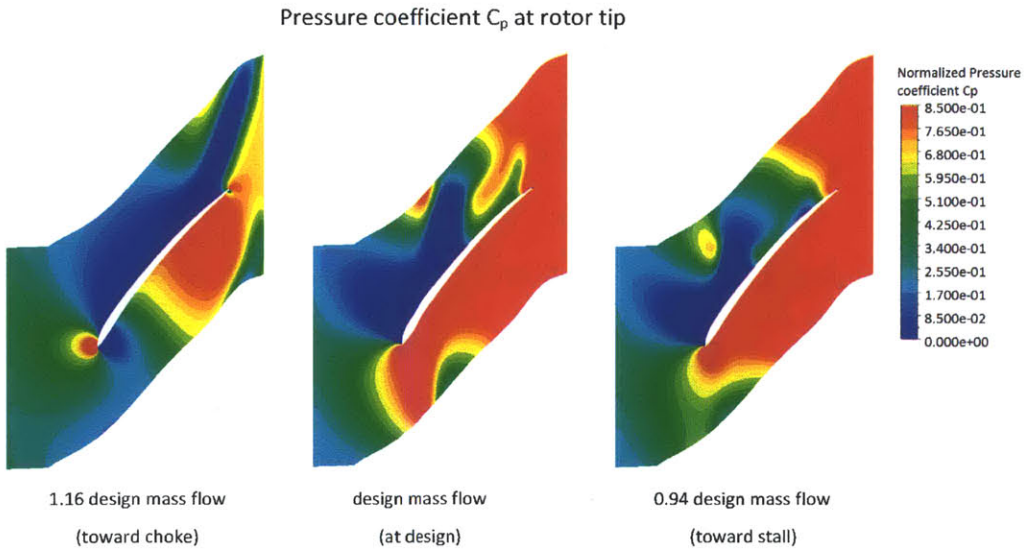

Figure 3-29: Static pressure at the blade tip. Blue indicates low pressure and red indicates high pressure. (Range of 0.3 between minimum C_p (blue) and maximum C_p (red))

In summary, for lower mass flow with tip gap smaller than the threshold value, tip leakage flow increases due to higher pressure difference and the mixing out of this

leakage flow begins right at the leading edge proximity. The tip leakage mixing loss in the rotor passage is thus higher and the efficiency is therefore more sensitive to rotor tip gap. This is shown in Figure 3-19 where the efficiency curve below a threshold tip gap value is steeper toward stall.

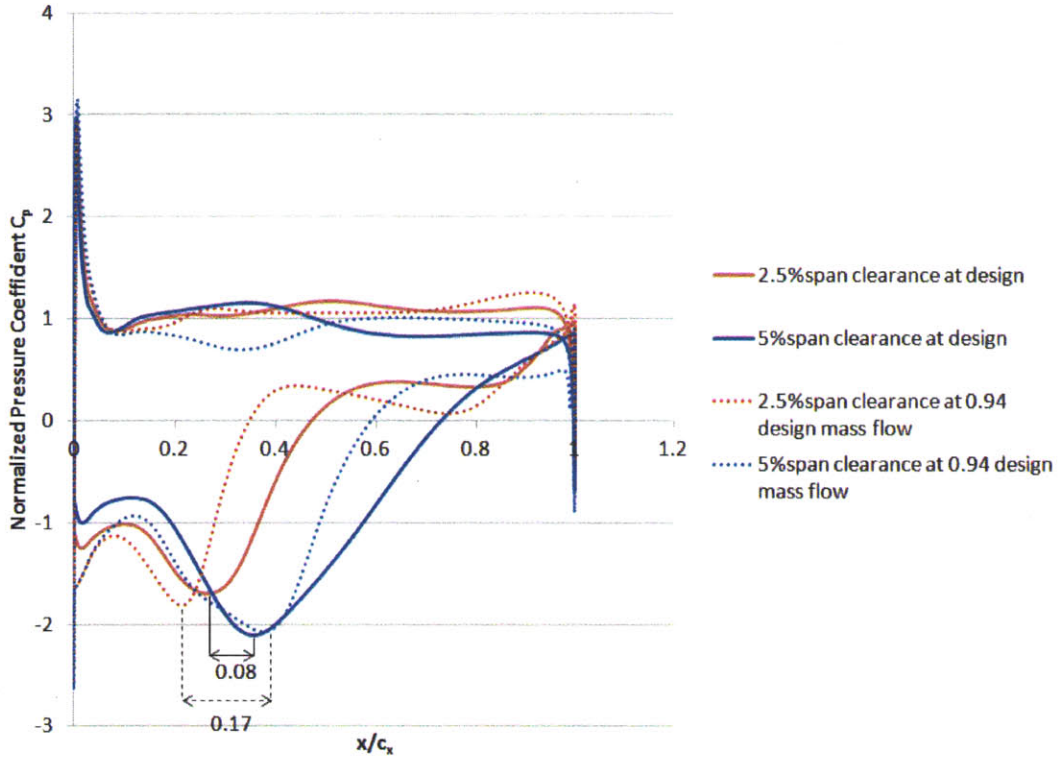

Figure 3-30: A comparison of the aft-shifting of blade loading at rotor tip with tip gap at two operating points.

For large tip gap (more than 3.4% span), Figure 3-19 shows that the efficiency becomes more desensitized to tip gap variation with decreasing mass flow (i.e. flat efficiency curve for tip gap beyond the threshold value). This is due to the further aft-shifting of the blade tip peak loading (with increasing tip gap) at decreasing mass flow. As rotor tip gap increases from 2.5% span to 5% span, the peak loading at the tip is moved aft by 8% chord at design mass flow but by as much as 17% chord at 0.94 design mass flow. In other words, with decreasing mass flow toward stalling value, tip leakage flow increases and thus the mixing loss increases for the same tip gap size (i.e. lower efficiency for the"same tip clearance" with decreasing mass flow

as shown in Figure 3-19). However, beyond a critical tip gap value, the attendant mitigation in mixing loss from further aft-loading the blade tip (with increasing tip gap) at decreasing mass flow more than compensates for the mixing loss arising from the increase in tip leakage flow. Thus, the rotor efficiency can be less sensitive to tip gap variation toward stall with the efficiency curve flattening out more at 0.94 design mass flow than at design mass flow beyond 3.4% span tip gap.

3.6 Summary

Computational experiments have been designed and carried out to assess efficiency sensitivity to tip clearance over a wide range of tip gap-to-span ratio, from vanishing value up to 5% for an embedded compressor stage at Reynolds number $\sim 2 \times 10^6$. The results have shown that there are three distinct regimes of efficiency variation with tip gap size as summarized below:

1. For tip clearance smaller than approximately 0.8% span, there exists an optimum tip gap for maximum efficiency and it is set by the competing effects in loss generation associated with casing/hub shear (which increases with decreasing gap-to-span ratio) and mixing out of clearance flow (which decreases with decreasing gap-to-span ratio). A scaling for optimum tip gap has been established and shown to be able to satisfactorily quantify the value of the optimal gap. The scaling delineates the parameter values (e.g. Reynolds number, operating points, stage aerodynamic and geometrical characteristics) that mark the change in behavior of efficiency variation with gap-to-span ratio and compressor operating points

2. For tip gap-to-span ratio ranging from about 0.8% to 3.4%, the efficiency variation with tip clearance is found to be in accord with Denton's tip leakage mixing model. The efficiency increases approximately on a linear basis when tip clearance decreases and the dominant flow process responsible for the change in efficiency in this tip gap range is the mixing out of tip leakage flow. For the em-

bedded compressor stage assessed here, there is approximately 1 point efficiency benefit for every 1% span decrease in tip gap size.

3. For tip clearance larger than 3.4% span, the efficiency sensitivity to tip gap is reduced. When tip clearance increases, the blade tip peak loading and thus the tip leakage flow formation are aft-shifted toward trailing edge. This reduces the opportunity for the mixing out of the tip flow in rotor passage (and the tip flow induced flow blockage and loss production as well) so that the tip leakage flow can remain relatively unmixed at the rotor exit. As such the rotor efficiency would become less sensitive to tip clearance variation beyond a critical gap value set by two competing effects in loss generation: an increase in tip leakage mass flow rate associated with increasing tip gap and a decrease in tip flow mixing loss due to blade tip being aft-loaded as tip gap increases.

Based on the findings, we can also deduce an additional useful inference for the application of Denton's tip leakage mixing model. For rotor design with its tip peak loading located in the immediate blade leading edge region, the assumption that the mixing-out of tip flow is complete within the rotor passage is a good approximation. For this situation Denton's tip leakage mixing model is applicable. However, for rotor design with aft-loaded tip, there is less opportunity for the tip flow to realize its mixing-out loss generation potential. Therefore, Denton's model is not applicable here because of its inherent assumption of instantaneous mixing of tip leakage flow with main flow.

Chapter 4

Effects of tip clearance on compressor performance in unsteady flow

In chapter 3, we have asesssed and quantified the effects of tip clearance on an embedded compressor stage performance using a mixing plane steady flow approximation. The mixing plane, appropriately located at an axial location within the intra rotor-stator gap, eliminates the circumferential non-uniformity of the inlet flow to the downstream stator (CFX-Solver modeling guide [2]). Hence, the solution does not take into account the effects of the flow unsteadiness associated with the relative motion of the rotor and stator blades.

However, the effects of the flow unsteadiness due to upstream wake and leakage flow on loss in compressor stage can be rather significant (Smith [21], Valkov and Tan[24, 25]). Thus, this chapter aims at assessing the effects of tip clearance on compressor performance in unsteady flow. This is accomplished by replacing the mixing plane approximation with a sliding plane in the intra rotor-stator gap, thus changing steady flow computation to time-accurate unsteady flow computation in the compressor stage. As described in chapter 2, phase-lag sliding plane option is not available in CFX 12.0, thus unsteady calculation in CFX is performed with an assumption of a unity rotor-stator blade ratio, despite the non-unity blade ratio of

the stage. Therefore, the unsteady results presented here will provide correct trend for unsteady flow effects in compressor stage but the numerical values will be different from those expected in the actual ninth stage.

Three-dimensional unsteady flow fields in the stage are simulated for 2 different tip clearances, 1.7% span and 5% span. The computed results are post-processed to identify and quantify the time-averaged impact of flow unsteadiness associated with rotor-stator interaction involving rotor tip clearance flow and wake. The effect of the rotor tip peak loading design, i.e. that with aft-loaded rotor tip compared to the original design, will then be assessed on a preliminary basis in the next chapter.

4.1 Past research work

There has been reseach work carried out in the past several decades that was directed at understanding the effects of flow unsteadiness on compressor performance. Here we only confine the review to the work by Smith and Valkov, whose researches present the effects of the upstream flow non-uniformity (i.e. wake and clearance flow) on the unsteady flow in the downstream blade row.

The arguments presented by both authors are cast in terms of flow circulation in an inviscid incompressible flow. First, Smith [21] has presented a model on evolution of an upstream wake in a downstream blade row. He explains that as the wake can be represented as a region of velocity defect (i.e. negative axial velocity disturbance). The disturbance flow is defined as the difference between the time-averaged flow field and the instantaneous flow field. Thus, the wake region has negative axial velocity disturbance and the main flow region has a positive axial velocity disturbance. The wake defect region is then passed through downstream blade row in the an unsteady manner as shown in Figure 4-1. The blue region represents the wake and the orange region represents the main flow. Based on the difference in the axial velocity disturbance of the wake and the main flow, the disturbance vorticity associated with the wake is in a radial direction as shown in Figure 4-1. The evolution of the fluid contour (defined by the black contour line) through the stator is as depicted in Figure

4-1.

Through the downstream blade row, the wake (as well as the fluid contour) is stretched due to the higher velocity on the suction side of the blade. Thus, at the exit of the blade row, the length of the wake increases and the width of the wake decreases. However, assuming inviscid incompressible flow, vorticity is constant with time in a planar two-dimensional flow (i.e. velocity components which depends on two coordinates x and θ) and the flow circulation also remains constant (Kelvin's theorem). Consequently, the velocity disturbance (which is due to the difference in the velocity of the wake and the main stream) is proportional to to the wake width. Hence, passing a wake through a downstream blade row reduces the velocity disturbance (as the wake width decreases) and thus decreases the potential for mixing loss (i.e. yielding reversible work recovery).

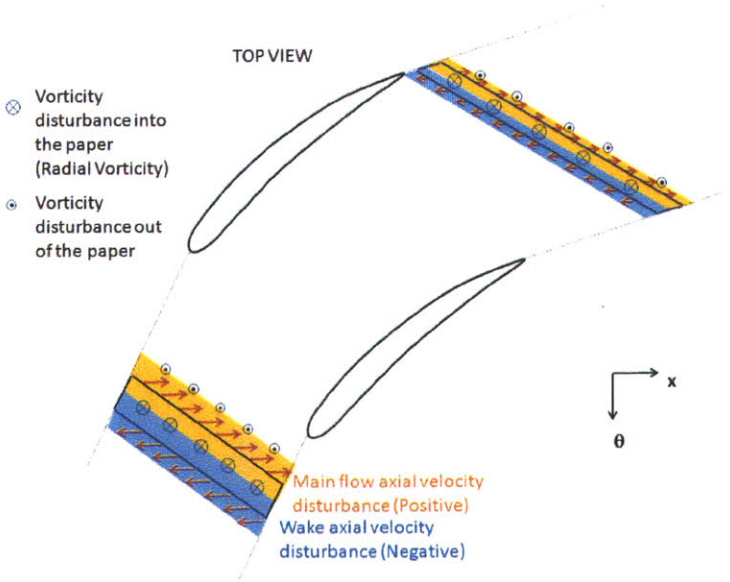

Figure 4-1: Evolution of wake velocity disturbance through a stator passage. The red arrows represent axial velocity disturbance.

Valkov and Tan [24, 25] determined the loss generation associated with the unsteady interaction of upstream tip leakage flow with stator and its impact on time-average compressor stage performance. He found that at the inlet of the stator, tip leakage flow appears as a jet with excess tangential velocity (tangential velocity disturbance) and axial velocity defect (negative axial velocity disturbance). There are

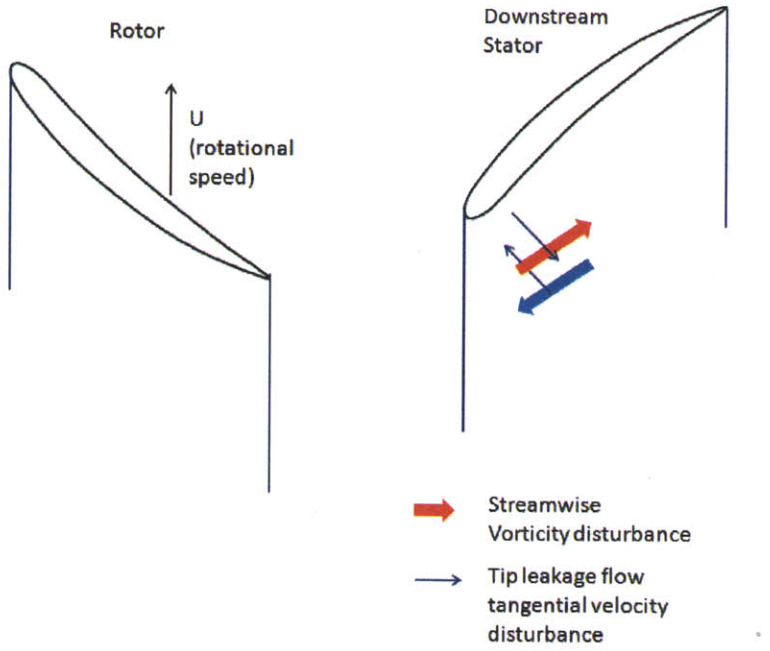

Figure 4-2: Streamwise vorticity disturbance of tip leakage flow

thus streamwise vorticity disturbance (associated with tangential velocity disturbance as shown in Figure 4-2) and normal vorticity disturbance (associated with axial velocity defect, similar to the wake in Figure 4-1). As a result, the axial velocity defect in rotor tip leakage flow is attenuated though the downstream stator in the same manner as the wake (Smith [21]). In other words, the stretching of the wake-like part of the tip flow is accompanied by an attenuation of the associated axial flow non-uniformity of the tip leakage flow without an entropy increase and thus decreasing potential for mixing loss.

As for the tangential velocity disturbance, Valkov explains that its associated streamwise vorticity disturbance is attenuated through the stator in an analogy to the change in streamwise vorticy through a diffuser. The flow through a diffuser is decelerated, accompanying by a static pressure rise. Thus, a fluid contour will be shortened and widened as shown in Figure 4-3 (red dashed line). Assuming inviscid incompressible flow, a vortex line moves with the fluid (i.e. it moves as a material line.). Thus, the shortening of the material line in the diffuser leads to a decrease in

the streamwise vorticity through a diffuser. Similarly, the streamwise vorticity and thus the tangential velocity disturbance decreases through a stator.

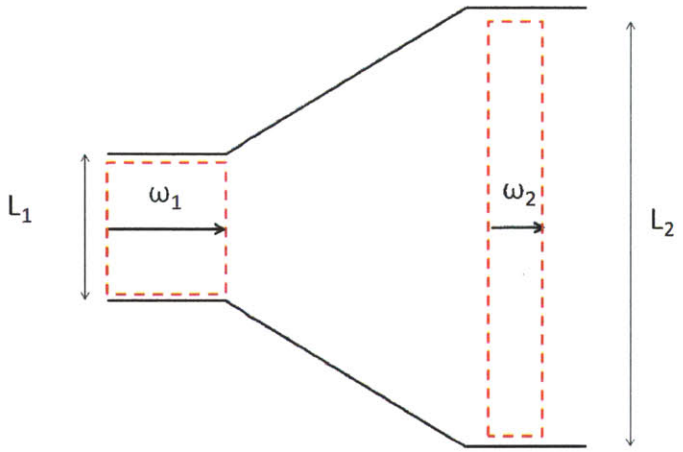

Figure 4-3: Evolution of wake and tip leakage flow streamwise vorticity disturbance through a diffuser, which is an anaologous to a stator passage.

To summarize, the attenuation of the tangential velocity excess and axial velocity defect in tip leakage flow through downstream blade row implies that: (1) processing of tip vortices in a stator passage is beneficial; and (2) most of the kinetic energy of the vortex is recovered in the stator without any attendant increase in entropy. As noted by Valkov and Tan [24, 25], the attenuation in tip leakage flow can be significantly higher than that in wake. We will use the results from the work of Smith and Valkov described in this section to interpret the computed unsteady flow in the embedded compressor stage presented in the next section.

4.2 Results from unsteady simulations of the rotor-stator stage

Computed results from unsteady rotor-stator stage calculations with rotor tip clearance of 1.7% span and 5% span were assessed against the corresponding steady flow results (note the mixing plane approximation inherently implies mixing out of tip flow in the circumferential direction). Relative to the steady flow value, the time-average

stage efficiency increases by 0.45% for 1.7% span tip clearance and by 0.7% for 5% span tip clearance. The increase in efficiency when taking into account of the effects of the flow unsteadiness can be explained using the work of Smith and Valkov: the efficiency benefit arises from the attenutation of tip leakage flow in the downstream stator row.

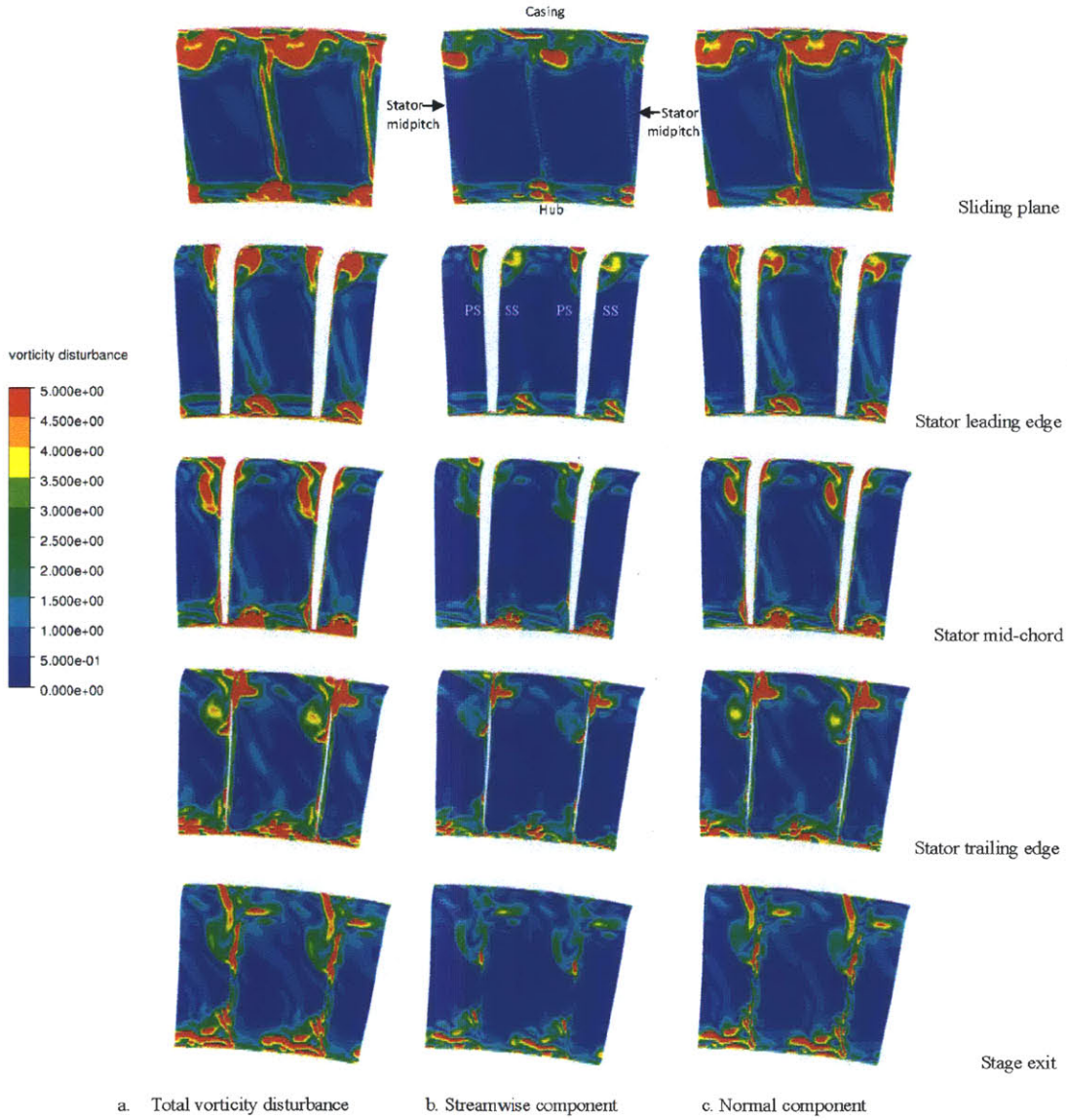

Figure 4-4: Evolution of tip leakage flow vorticity disturbance through a stator passage. The axial planes shown move with tip leakage flow.

Computed results elucidating the evolution of vorticity disturbance, normal vor-

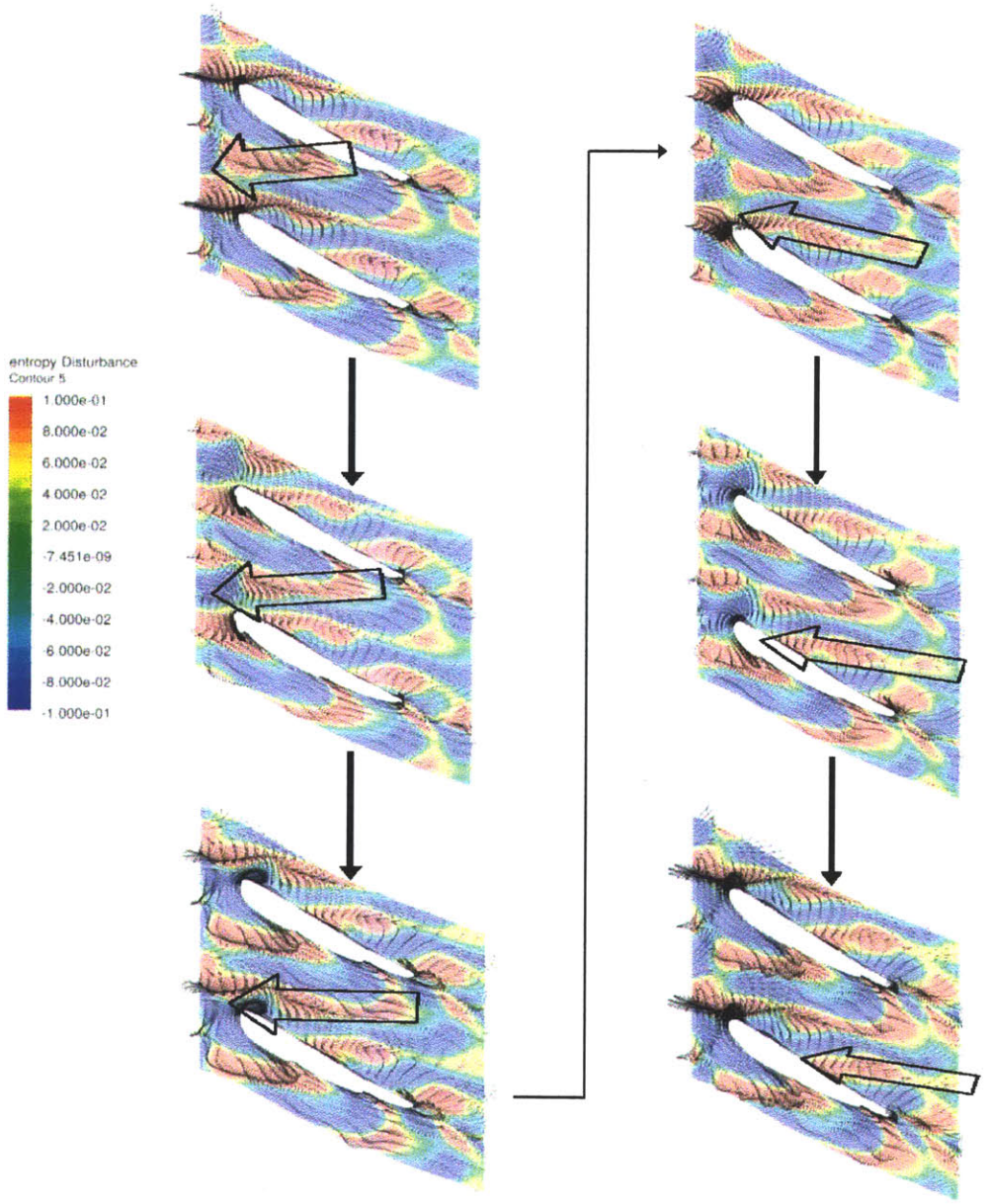

Figure 4-5: Evolution of tip leakage flow entropy disturbance (contour) and velocity disturbance (vector) through a stator passage at 95% span. (Figure is not to scale.)

ticity disturbance and streamwise vorticity disturbance of the tip leakage flow on axial plane from a location upstream of the stator leading edge to one at the stator outlet is shown in Figure 4-4. The contours (looking downstream from stator LE to TE) span two stator passages (such that the contours span from the left midpitch of one stator

toward the right mid-pitch of the adjacent stator). The white regions on the contour represents the two stator blades. The vorticity disturbance has been derived from a disturbance flow obtained by subtracting the time-average flow from the instantaneous unsteady flow. Similarly, the velocity disturbance and the entropy disturbance on the spanwise plane at 95 % span (near the casing) are plotted in Figure 4-5.

As can be inferred from Figure 4-4, the streamwise component of the vorticity disturbance in the tip leakage flow decreases through the stator. This has been explained by Valkov, using an analogy of a streamwise vorticity evolution in a diffuser. As shown in Figure 4-3, assuming inviscid incompressible flow, vortex lines follows a material line. However, the material line is shortened through a diffuser due to the deceleration of the flow, thus the streamwise vorticity also decreases. As a result, the streamwise vorticity disturbance and thus the associated tangential velocity disturbance of tip leakage flow is attenuated through pressure rise in downstream stator. This is in agreement with the result shown in Figure 4-4.

In addition, Valkov argues that the axial velocity disturbance defect in the tip leakage flow is also attenuated through the downstream stator in the same manner as the wake. The tip leakage flow region associated with the axial velocity disturbance defect and the associated normal vorticity (Figure 4-1) is stretched through a stator due to the velocity difference on the blade pressure side and suction side. The unsteady results of the investigated stage are in agreement with Valkov's argument as depicted in the stretching of the tip leakage flow shown in Figure 4-5. In two-dimensional planar flow, the normal vorticity and the circulation remain constant. Therefore, the axial velocity disturbance decreases with the width of the tip leakage flow. Finally, it is noted that the evolution of tip leakage flow in downstream stator can be significantly three-dimensional. Thus, the normal vorticity disturbance of tip leakage flow can be tilted and distorted through the stator passage so that we can expect to see a change in the magnitude of the normal vorticity component as shown in Figure 4-4.

In summary, the change in the time-average performance of the embedded compressor stage computed based on unsteady three-dimensional flow is in agreement

with the results presented by Smith and Valkov. The tangential velocity disturbance as well as the axial velocity disturbance associated with tip leakage flow are attenuated in the downstream blade row. In addition, streamwise vorticity disturbance is attenuated through the stator passage. For three-dimensional flow, the normal vorticity disturbance associated with tip leakage flow could decrease through the stator passage. There is thus a performance benefit associated with tip leakage flow attenuation in the downstream stator.

4.3 A hypothesis on compressor stage design guideline

We learnt from the results of chapter 3 that by aft-loading the rotor tip as much as it is feasible, we can reduce the potential of generating mixing-out loss by the tip leakage flow inside rotor passage. The consequence of this is that there is a reduced sensitivity in efficiency variation with tip gap. We have also learnt from the work by Valkov and Tan [24, 25] as well as the result presented in this chapter that unsteady rotor-stator interaction results in significant attenuation of rotor tip leakage flow in the following stator (analogous to wake attenuation noted by Smith [21]) and, as a result, decreases the loss generation potential in downstream stator passage. Thus there is an additional benefit to having the tip flow being relatively unmixed at rotor exit through aft-loading the rotor tip. This unmixed tip leakage flow, which is essentially wake-like, can then be advantageously attenuated in the following stator to further reduce the opportunity for tip-induced loss and flow blockage generation. We can apply the same conceptual framework of thinking to addressing the stator hub clearance flow to maximize compressor performance by its prudent management through design.

Thus to desensitize compressor performance variation with clearance gap, rotor should be tip aft-loaded and hub fore-loaded while stator should be tip fore-loaded and hub aft-loaded as much as it is feasible so as to reduce the opportunity for blade

clearance flow induced loss and flow blockage generation. This would also create environment for maximizing the benefits of reversible work from unsteady effects through the downstream blade-row in attenuating the wake-like clearance flow. A preliminary assessment of the hypothesis will be presented in the next chapter.

Chapter 5

Hypothesis on compressor stage design guideline for performance enhancement: a preliminary assessment

In this Chapter we implement a preliminary assessment of the hypothesis formulated in Chapter 4. The hypothesis is restated here for ease of reference: For large industrial gas turbine compressor with Reynolds number 2×10^6 to 7×10^6, the blade surface boundary layer is relatively thin and robust. So, the dominant source of flow blockage and loss generation is the leakage flow. Therefore, to reduce compressor performance sensitivity to clearance gap variation, the compressor stage design should be such that rotor is tip aft-loaded and hub fore-loaded while stator is tip fore-loaded and hub aft-loaded as much as it is feasible so as to reduce the opportunity for blade clearance flow induced loss and flow blockage generation. This creates an environment for maximizing the benefits of reversible work from unsteady effects through the downstream blade-row in attenuating the wake-like clearance flow. It is hypothesized that the overall performance benefit can include compressor performance enhancement as measured in terms of efficiency, pressure ratio, broadening of useful operating range

and of island of peak efficiency.

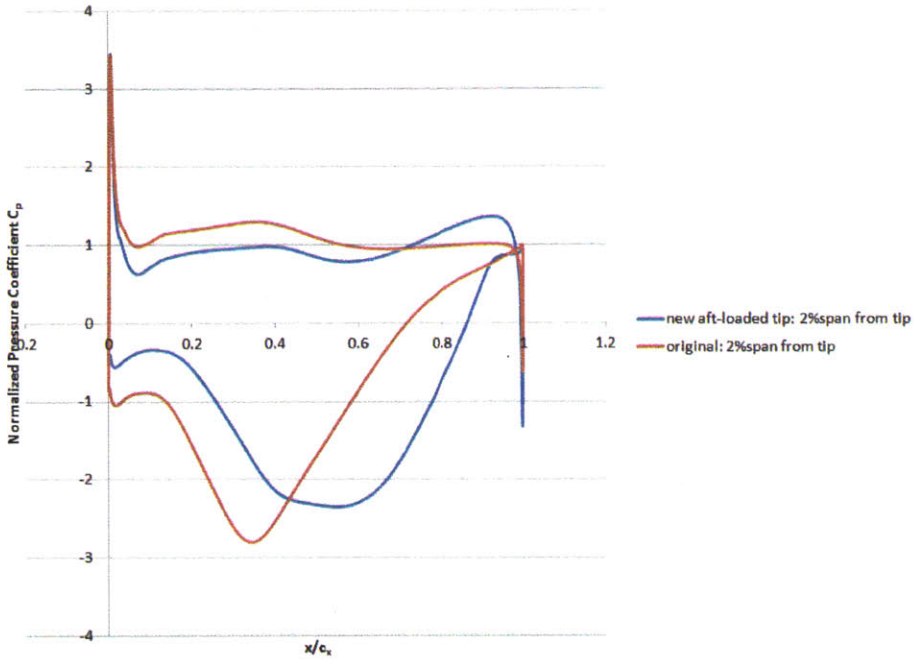

Figure 5-1: Comparison of blade loading between the original and the 20% chord tip aft-loaded blade design at 2% span from rotor tip

Only one specifc aspect of the hypothesis is assessed: namely the improvement in compressor stage efficiency at design by aft-shifting the rotor tip blade peak loading. To this end, new rotor blade redesigns for 2 different tip clearances have been implemented: (1) a new design for 1.7% span tip clearance in which the tip is aft-loaded by 4% chord with an aft-loaded span extending approximately 5% span from blade tip; (2) a new design for 5% span tip clearance for which the tip is aft-loaded by 20% chord with an aft-loaded span extending over approximately 15% span from blade tip. Figure 5-1 shows that the peak loading at the rotor tip is shifted by approximately 20 % chord from leading edge with the new design for 5% span tip clearance. In addition, Figure 5-2 shows that at 15% span from the rotor blade tip, the peak loading is still significantly aft-loaded with this new design, thus the redesign has an aft-loaded span extending over 15% span from the blade tip. Steady simulations at design have been done for both clearances and unsteady simulation at design has been done for the new design of 1.7% span tip clearance. The results and the preliminary assessment

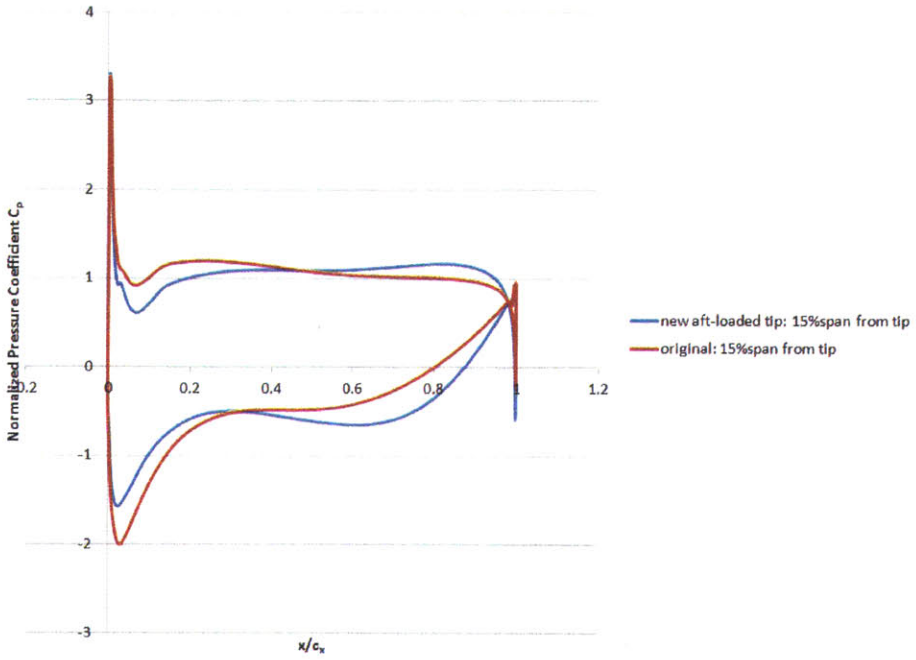

Figure 5-2: Comparison of blade loading between the original and the 20% chord tip aft-loaded blade design at 15% span from rotor tip

of the hypothesis are presented in this Chapter.

5.1 Effects of blade aft-loading in steady flow

It is found that the comparison of the steady flow fields between original design and new tip aft-loaded design gives the same trend for both tip clearances. The figures shown in this chapter are taken from flow fields of 5% span tip clearance rotor designs but they are representative of the trend for both tip gaps.

As the blade tip peak loading is aft-shifted, the tip leakage flow formation is delayed. Figure 5-3 shows that for the new design, tip leakage is formed further downstream compared to the original design. This is also shown in the local entropy generation rate contours at different axial location in rotor passage depicted in Figure 5-4 and Figure 5-5.

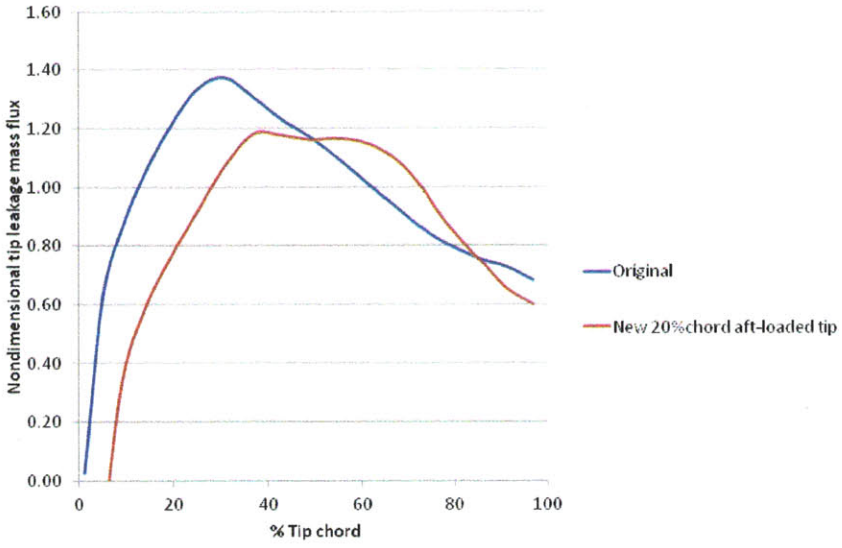

Figure 5-3: Comparison of tip leakage mass flux (i.e. tip leakage formation) between the original and the 20% chord tip aft-loaded blade design

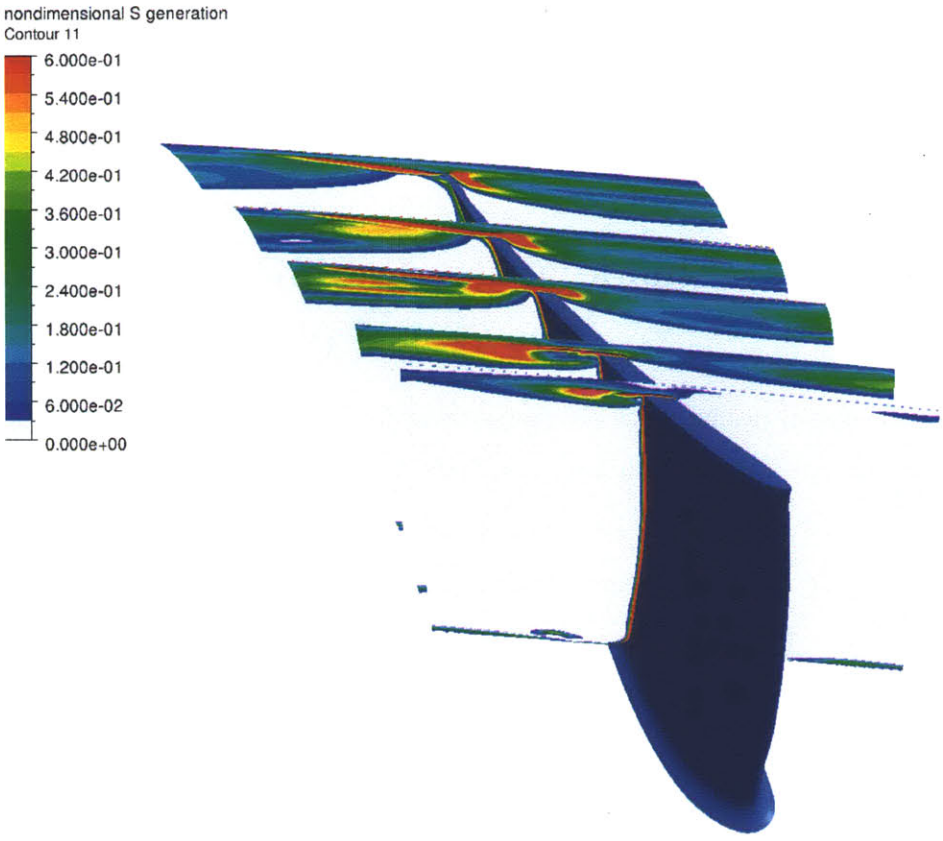

Figure 5-4: Local entropy generation near the casing, showing the formation and mixing out of tip leakage flow for the original design with 5% span tip clearance

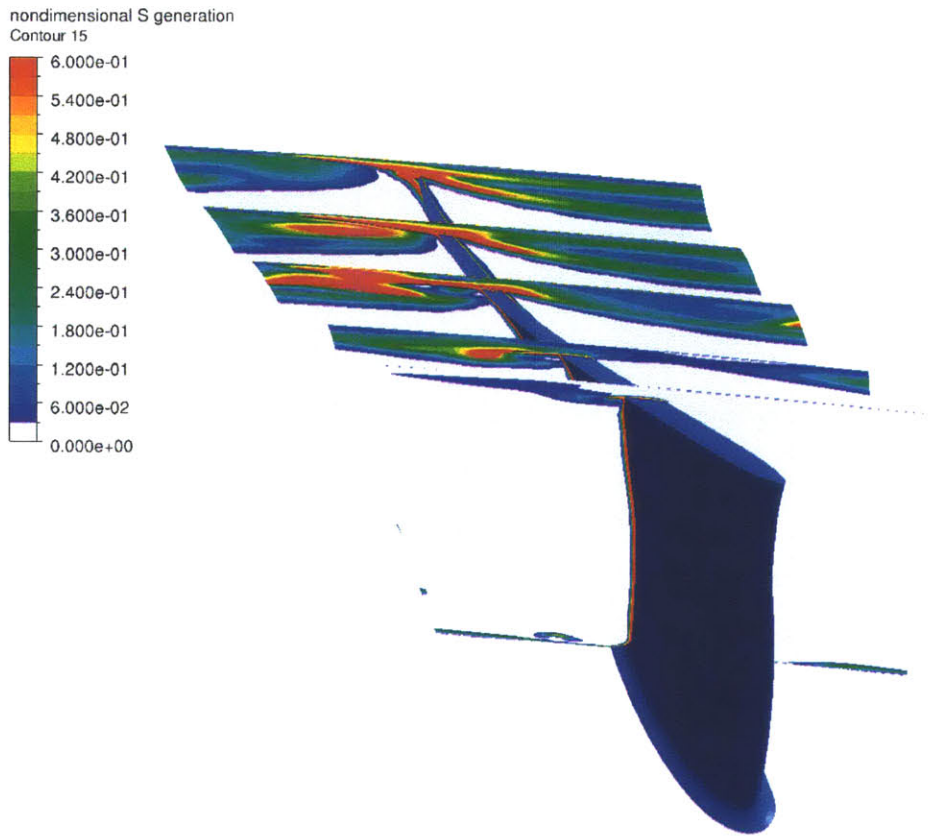

Figure 5-5: Local entropy generation near the casing, showing the formation and mixing out of tip leakage flow for the redesign with 5% span tip clearance

The tip leakage flow is clearly formed further downstream with the new design; the tip leakage flow region (shown as a region with high local entropy generation) is significantly smaller on the first axial plane close to the leading edge with the new design (Figure 5-4 vs Figure 5-5). The second axial plane from leading edge shows significantly higher local entropy generation with the original design; this implies that mixing out of the tip leakage flow starts earlier upstream for the original design.

For the original design, the local entropy generation rate inside the tip leakage flow region (i.e. the mixing out of tip leakage flow) starts to decrease downstream of the second axial plane. However, for the new design, the local entropy generation rate inside the tip leakage flow region starts to decrease downstream of the third axial plane. In addition,the local entropy generation in the tip leakage flow on the last axial plane at the rotor trailing edge is lower with the original design. These

imply that the mixing out of tip leakage flow in rotor passage is less complete with the tip aft-loaded design. Thus, the new tip aft-loaded rotor design has lower loss generated in the rotor passage associated with the mixing out of tip leakage flow.

However, the steady state computed flow fields also show that with aft-loaded rotor tip, the likelihood of flow separation on the blade suction surface in the rotor tip trailing edge is increased. This can be attributed to the increase in adverse pressure gradient in the rotor tip trailing edge region with blade tip peak loading being aft-shifted. Figure 5-6 shows the presence of a substantial region of flow separation (indicated as red region in the figure) on the tip trailing edge blade suction surface (in the figure trailing edge is at the left while leading edge is on the right) for the new design of 5% span tip gap. Similarly, the contours of the axial velocity on the trailing edge axial plane also show a distinct region of reverse flow on blade suction side in the tip trailing edge region with the new design (Figure 5-7).

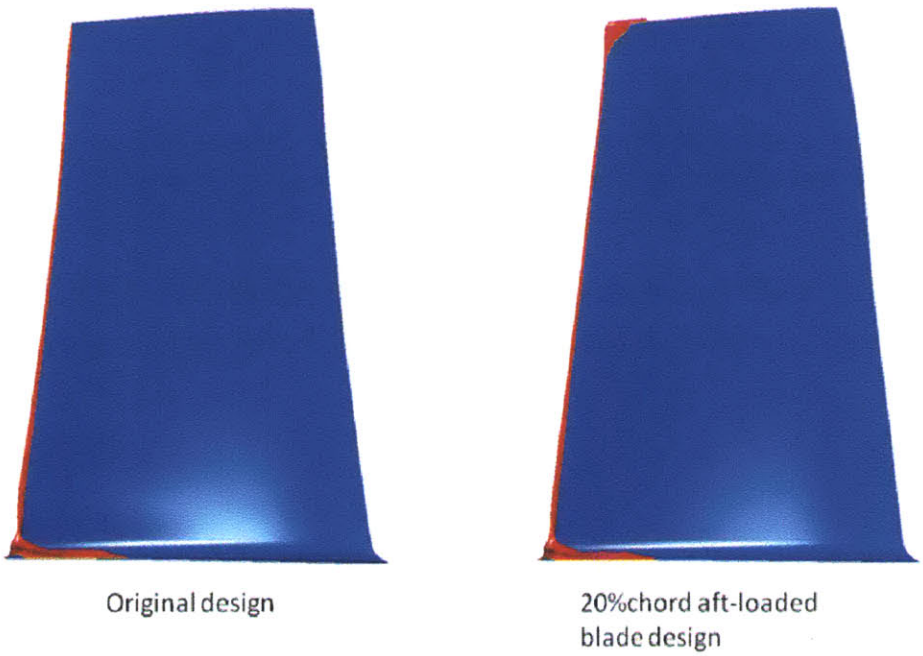

Figure 5-6: Comparison of flow separation on rotor blade suction side between the original and the 20% chord tip aft-loaded blade design

The presence of a substantial region of flow separation would increase the loss generated in the rotor passage. Figure 5-8 shows that in the blade passage from

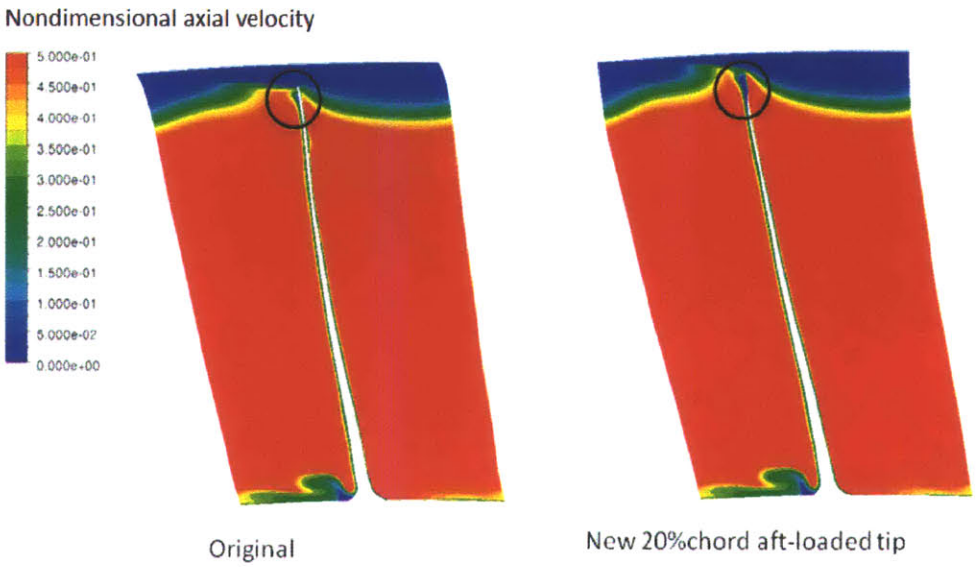

Figure 5-7: Comparison of axial velocity at rotor trailing edge between the original and the 20% chord tip aft-loaded blade design

leading edge to 70% chord, the accumulative entropy generation is lower with the new design; however, toward trailing edge, the mixing out of the tip leakage flow of the new design (which starts further downstream) and the additional loss arising from flow separation are more dominant compared to the original. For the new 5% span tip clearance design, the additional loss due to flow separation is higher than the decrease in loss inside the rotor passage due to the delayed tip leakage flow formation. As a result, the total entropy generation (thus loss) inside the rotor domain increases.

The steady flow fields for the original and new designs with 5% span tip clearance are also computed at another operating point toward stall with the mass flow reduced by 5%. From the computed steady flow results, both stage efficiency and pressure ratio decreases when aft-shifting the rotor blade tip loading (Figure 5-9); this is principally due to the absence of tip leakage and separated flow attenuation process in the assumed steady flow environment (see Chapter 4). However, in Figure 5-10 even though the rotor efficiency evaluated downstream of mixing plane (where tip leakage flow is mixed out circumferentially) is lower for the aft-loaded design, the rotor efficiency evaluated upstream of mixing plane is higher for the aft-loaded design

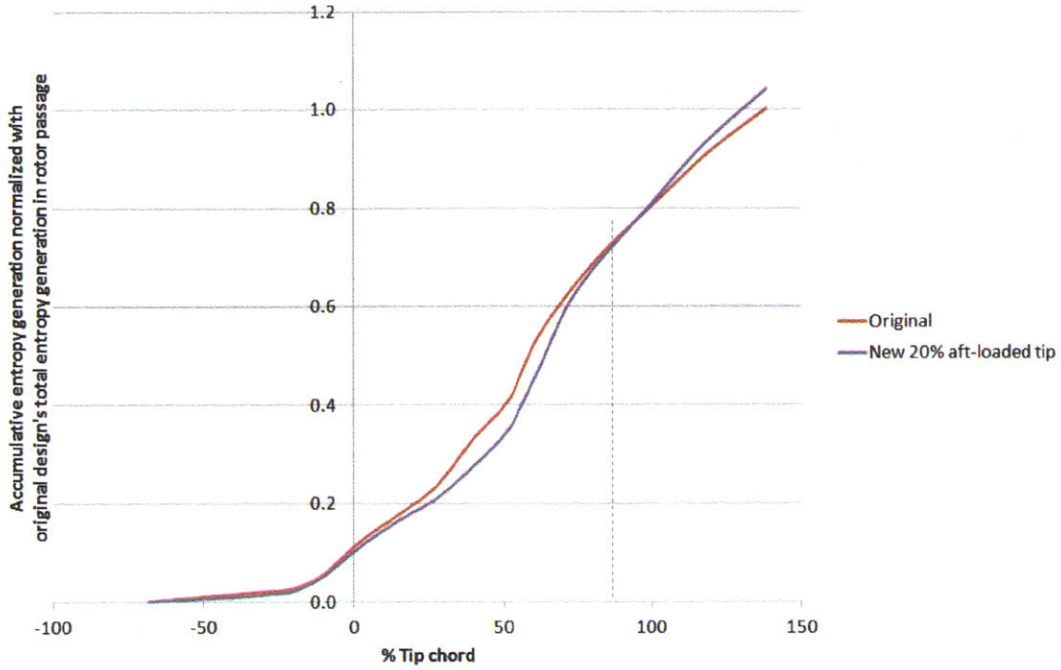

Figure 5-8: Comparison of accumulative entropy generation in rotor domain between the original and the 20% chord tip aft-loaded blade design

at 0.95 design mass flow operating point. This can be rationalized as follows.

Toward stall (decreasing mass flow), tip leakage flow increases because of higher pressure difference across the blade and thus the loss due to tip leakage mixing becomes more dominant compared to the loss due to flow separation. As a result, moving toward stall, the decrease in mixing loss generated inside rotor passage (upstream of mixing plane) due to the delay in tip leakage flow formation outweighs the increase in loss arising from flow separation. This could then implies that the benefit of reverible work recovery from tip leakage (as well as the separated) flow attenuation process in unsteady flow will increase with decreasing mass flow. The implication is that despite the observed flow separation accompanying aft-loading the blade tip, there would be an overall performance benefit.

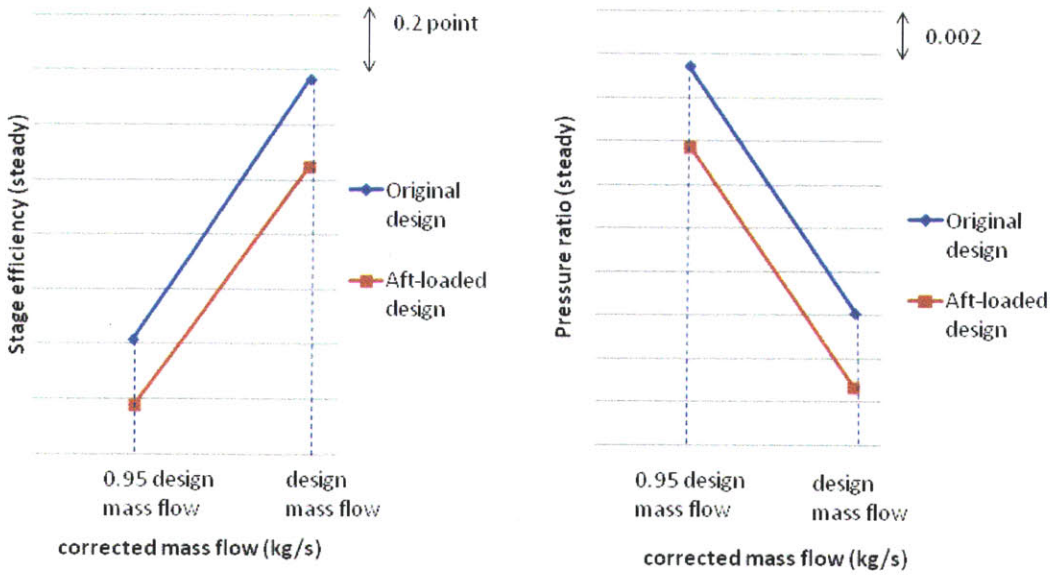

Figure 5-9: Comparison of stage efficiency (left) and pressure ratio (right) between the original and the 20% chord tip aft-loaded blade design at two different operating points

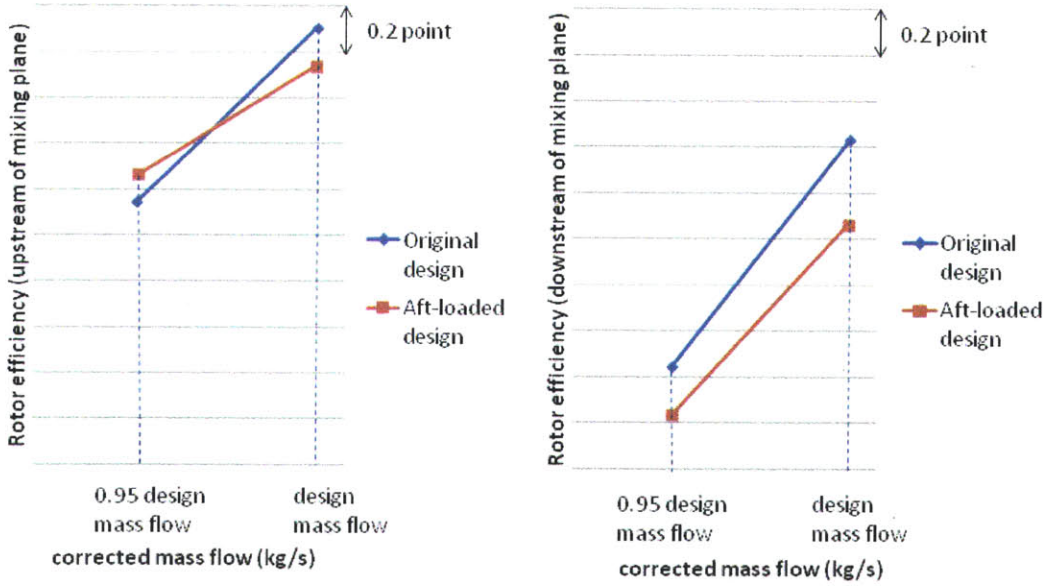

Figure 5-10: Comparison of rotor efficiency evaluated upstream of the mixing plane (left) and downstream of the mixing plane (right) between the original and the 20% chord tip aft-loaded blade design at two different operating points

5.2 Effects of blade aft-loading in unsteady flow

Unsteady flow fields have been simulated for the new design of 1.7% span tip clearance with its tip peak loading aft-shifted by 4% chord. The time-averaged result based on unsteady computations of this modified design stage shows that it has a 0.2 % efficiency improvement over that based on the time-averaged result for the stage with rotor tip fore-loaded. However, increasing flow separation on the rotor tip trailing edge suction side is observed.

It is then suggested that a larger improvement in efficiency (could be up to 0.5%) is possible if the rotor tip peak loading can be more aft-shifted. A difficulty is achieving this is that aft-loading the rotor blade tip is often accompanied by flow separation on the tip suction surface toward the trailing edge. It then implies that there should be an optimum blade loading design that minimizes the total loss from the mixing out of leakage flow (which decreases when aft-load rotor tip/stator hub) and flow separation on the suction side of the rotor tip/stator hub trailing edge (which increases when aft-load rotor tip/stator hub). In other words, it is suggested that rotor tip should be aft-loaded as much as possible (up to the optimum peak blade loading location when there is flow separation at rotor tip suction side). All these propositions and suggestions will need to be quantified and assessed.

5.3 Summary

Preliminary assessment of the proposed blade design shows that with tip aft-loaded rotor blade design, the tip leakage flow formation and mixing out process are delayed; however, flow can begin to separate on the rotor trailing edge suction side. Thus, by aft-loading rotor tip, there is a benefit from unsteady tip leakage attenuation in stator passage. However there is a need to manage the additional loss arising from increasing flow separation at the rotor tip suction side; this additional loss can be somewhat mitigated in the rotor-stator unsteady flow environment in a manner analogous to wake rectification (i.e. wake attenuation with attendant reversible work

recovery) (see Chapter 4). We can then inferred that there should be an optimum blade loading design that minimizes the total loss from the mixing out of leakage flow (which decreases when aft-load rotor tip/stator hub) and flow separation on the suction side of the rotor tip/stator hub trailing edge (which increases when aft-load rotor tip/stator hub). Based on preliminary unsteady embedded rotor-stator computed flow, there can be a more than 0.2 point efficiency benefit when aft-load the rotor blade tip by 4% chord for the rotor with 1.7% span tip

Chapter 6

Summary and future work

This chapter provides a concise summary of the thesis followed by delineating the key research findings. It then concludes with a section on recommendations for future work.

6.1 Summary

Computations were carried out to define rotor efficiency variation with tip clearance ranging from 0.04% to 5% span. This aspect is of engineering relevance to axial compressor in large industrial gas turbine where the rotor tip and stator hub clearance can be less than 0.5% span in the front stages and as large as more than 5% span in the rear stages. The rotor efficiency variation over this wide range of tip clearance is established for an embedded compressor stage; the compressor stage used is representative of that in high-performance large industrial gas turbine where the operational Reynolds number ranges from 2×10^6 to 7×10^6. Based upon the results from the steady calculations, a hypothesis on compressor stage design guideline for overall compressor performance enhancement is then formulated. Subsequently, additional embedded stage computations, steady (based on mixing plane approximation) and unsteady, are carried out for a preliminary assessment of the formulated hypothesis.

6.2 Key findings

The key findings of this research includes new understandings of the flow physics underlying the efficiency response to the change in blade end gap as well as a hypothesis on a design strategy to improve compressor performance. These are delineated in the following:

1. There are three distinct regimes of rotor efficiency variation with tip gap size: small tip gap (less than 0.8% span for the stage analyzed), medium tip gap (0.8% to 3.4% span) and large tip gap (larger than 3.4% span). The distinguishing features of each region are as follows:

   (a) For small tip gap, there exists an optimum tip gap for maximum efficiency, which is set by the competing effects for loss generation associated with casing/hub shear (which increases with decreasing gap-to-span ratio) and mixing out of clearance flow (which decreases with decreasing gap-to-span ratio). A scaling for optimum tip gap has been established and shown to be able to satisfactorily quantify the value of the optimal gap. The scaling delineates the parameter values (e.g. Reynolds number, operating points, stage aerodynamic and geometrical characteristics) that mark the change in behavior of efficiency variation with gap-to-span ratio and compressor operating points.

   (b) For medium tip gap, the efficiency variation with tip clearance is found to be in accord with Denton's tip leakage mixing model. The efficiency increases approximately on a linear basis when tip clearance decreases and the dominant flow process responsible for the change in efficiency in this tip gap range is the mixing out of tip leakage flow. For the embedded compressor stage assessed here, there is approximately 1 point efficiency benefit for every 1% span decrease in tip gap size.

   (c) For large tip gap, the efficiency sensitivity to tip gap is reduced. When tip clearance increases, the blade tip peak loading and thus the tip leak-

age flow formation are aft-shifted toward trailing edge. This reduces the opportunity for the mixing out of the tip flow in rotor passage (and the tip flow induced flow blockage and loss production as well) so that the tip leakage flow can remain relatively unmixed at the rotor exit. As such the rotor efficiency would become less sensitive to tip clearance variation beyond a critical gap value set by two competing effects in loss generation: an increase in tip leakage mass flow rate associated with increasing tip gap and a decrease in tip flow mixing loss due to blade tip being aft-loaded as tip gap increases.

2. For rotor design with its tip peak loading located in the immediate blade leading edge region, the assumption that the mixing-out of tip flow is complete within the rotor passage is a good approximation; for this situation Denton's tip leakage mixing model is applicable. However, for rotor design with aft-loaded tip, there is less opportunity for the tip flow to realize its mixing-out loss generation potential, therefore Denton's model is not applicable here because of its inherent assumption of instantaneous mixing of tip leakage flow with main flow.

3. For large industrial gas turbine compressor with Reynolds number 2×10^6 to 7×10^6, the blade surface boundary layer is relatively thin and robust. So, the dominant source of flow blockage and loss generation is the leakage flow. Therefore, to reduce compressor performance sensitivity to clearance gap variation, the compressor stage design should be such that rotor is tip aft-loaded and hub fore-loaded while stator is tip fore-loaded and hub aft-loaded as much as it is feasible so as to reduce the opportunity for blade clearance flow induced loss and flow blockage generation. This would also create an environment for maximizing the benefits of reversible work from unsteady effects through the downstream blade-row in attenuating the wake-like clearance flow. It is hypothesized that the overall performance benefit can include compressor performance enhancement as measured in terms of efficiency, pressure rise capability, broadening of useful operating range and of island of peak efficiency.

4. Preliminary assessment of the proposed design strategy shows that with tip aft-loaded rotor blade design, the tip leakage flow formation and mixing out process are delayed; however, it has been observed that flow begins to separate on the rotor trailing edge suction side.

   (a) It can thus be inferred that there should be an optimum blade loading design that minimizes the total loss from mixing-out of leakage flow (which decreases when aft-load rotor tip/stator hub) and from flow separation on the suction side of the rotor tip/stator hub trailing edge (which increases when aft-load rotor tip/stator hub). The former benefits from reduced mixing out of tip leakage flow in the rotor passage as well as subsequent tip flow attenuation in the downstream stator. The latter loss penalty can be mitigated through an unsteady process analogous to wake attenuation.

   (b) There is a 0.2 point efficiency benefit when the rotor blade tip peak loading is aft-shifted by 4% chord for 1.7% span tip clearance.

6.3 Future work

The work presented in this thesis is based upon a single-stage calculation. However, the proposed design guideline is best exploited in unsteady multi-blade-row environment for a high-performance multi-stage compressor representative of next generation design. Thus, it is recommended that for future work, the effects of the proposed design strategy in multi-stage environment should be assessed (e.g. rotor-stator-rotor or 2-stage unsteady flow computation).

Based upon the results presented in Chapter 3 and 4, a hypothesis on compressor stage design guideline (for an overall compressor performance enhancement in terms of efficiency, pressure rise capability, robustness to end gap variation and potentially useful operable range broadening) has been formulated. Chapter 5 presents the preliminary assessment of the hypothesis in terms of the benefit of the proposed redesign on compressor efficiency improvement at design point. In other words, only one as-

pect of the hypothesis has been assessed. The next follow-on research should thus consist of the following assessments of the proposed compressor design strategy: (1) assess the extent of performance robustness (i.e. efficiency retention) to blade end gap variation, (2) determine and quantify the achievable broadening of the useful operable range, (3) determine and quantify the extent of operating range over which the retention of near design point efficiency is achievable (i.e. nearly flat efficiency trend with corrected mass flow) , (4) use (1) to (3) to establish the criteria for the optimum blade loading design (i.e. the location of the blade tip peak loading and the spanwise-extent of the aft-loaded region), and (5) synthesize results in (1) to (4) to delineate the attributes of multistage compressor design to enable retention of efficiency with blade end gap variations and operating point as well as maximizing useful operable range and island of peak efficiency.

Appendix A

The change in the circumferential averaged entropy profile between rotor trailing edge and stator leading edge.

Figure 3-19 shows a decrease in circumferential-averaged local entropy near the casing from rotor trailing edge to stator leading edge. This may seem at first counter-intuitive as global entropy actually increases from rotor trailing to stator leading edge due to the mixing loss. In this appendix a simple model is shown to rationalize the possible drop in local averaged entropy with an increase in global entropy.

Tip leakage flow region consists of low-pressure, low-axial velocity and high-entropy fluid, while the main flow consists of high-pressure, high-axial velocity and relatively low-entropy fluid. However, due to entrainment, a part of the fluid from the main flow will move into the tip leakage flow region similar to a simple model depicted in figure 1.

Assuming that the entropy generation (i.e. that from the mixing of two streams) is confined within section 1, the specific entropy remains constant throughout section

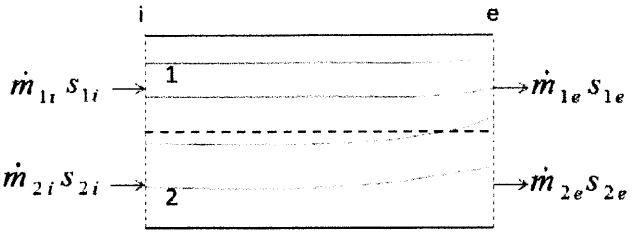

Figure A-1: Model of an evolution of the local averaged entropy in a passage.

2 ($s_{2i} = s_{2e}$) and the balance of entropy flux yields

$$\dot{m}_{1i}s_{1i} + \dot{m}_{2i}s_2 + \dot{m}_{1e}s_{gen} = \dot{m}_{1e}s_{1e} + \dot{m}_{2e}s_2 \tag{A.1}$$

Note that in this appendix, m represents mass flow rate (i.e. $\dot{m}$).

Let $\dot{m}_c$ be the mass flow from section 2 to section 1 due to the pressure gradient. Thus, by continuity

$$\dot{m}_{1e} = \dot{m}_{1i} + \dot{m}_c \tag{A.2}$$

$$\dot{m}_{2e} = \dot{m}_{2i} - \dot{m}_c \tag{A.3}$$

Equation A.1 then becomes

$$\begin{aligned}
\dot{m}_{1i}s_{1i} + \dot{m}_{1e}s_{gen} &= \dot{m}_{1e}s_{1e} - \dot{m}_c s_2 \\
\frac{\dot{m}_{1i}}{\dot{m}_{1e}} + \frac{s_{gen}}{s_{1i}} &= \frac{s_{1e}}{s_{1i}} - \frac{\dot{m}_c}{\dot{m}_{1e}}\frac{s_2}{s_{1i}} \\
\frac{s_{1e}}{s_{1i}} &= 1 - \frac{\dot{m}_c}{\dot{m}_{1e}} + \frac{s_{gen}}{s_{1i}} + \frac{\dot{m}_c}{\dot{m}_{1e}}\frac{s_2}{s_{1i}} \\
\frac{s_{1e}}{s_{1i}} &= 1 + \frac{s_{gen}}{s_{1i}} + \frac{\dot{m}_c}{\dot{m}_{1e}}\left(\frac{s_2}{s_{1i}} - 1\right)
\end{aligned} \tag{A.4}$$

Therefore, the circumferential averaged of the entropy in section 1 can decrease (i.e. $\frac{s_{1e}}{s_{1i}} < 1$) if and only if

	V_1	$\dot{m}_1$	s_1	V_2	$\dot{m}_2$	s_2	$\dot{m}_c$
Case 1	1	1	3	2	2	1	0.1
Case 2	1	1	3	2	2	1	0.5
Case 3	50	50	3	150	150	1	25

Table A.1: Case examples.

$$\frac{s_{gen}}{s_{1i}} + \frac{\dot{m}_c}{\dot{m}_{1e}}(\frac{s_2}{s_{1i}} - 1) < 0$$

$$\frac{s_{gen}}{s_{1i}} < \frac{\dot{m}_c}{\dot{m}_{1e}}(1 - \frac{s_2}{s_{1i}}) \tag{A.5}$$

In other words, if the contribution of the entropy generation or the loss due to the mixing between the two streams is small enough (or approaching zero for streamline deviation assuming no mixing), then the local averaged entropy of section 1 with high-entropy inflow can decrease while the local averaged entropy of section 2 remains constant. A simple example is shown in Table A.1.

Now, assuming that the injected mass flow m_c is small compared to the main stream m_1 and the stagnation temperature of the main stream and the injected stream are the same, the maximum entropy generation due to the mixing of the two streams can be approximated using equation 22 in Denton [8]:

$$s_{gen} = \frac{\dot{m}_c}{\dot{m}_{1e}T}(V_1^2 - V_1 V_2 \cos\alpha) \tag{A.6}$$

For maximum mixing loss, let α be 90 degree, then the left hand side of equation A.5 becomes

$$\frac{s_{gen}}{s_{1i}} = \frac{\frac{\dot{m}_c}{\dot{m}_{1e}T}V_1^2}{s_{1i}} \tag{A.7}$$

Let the temperature be 300 K and assume that all the mixing loss is realized (i.e.

	$\dot{m}_{1e}$	$\frac{s_{gen}}{s_{1i}}$	$\frac{\dot{m}_c}{\dot{m}_{1e}}(1-\frac{s_2}{s_{1i}})$
Case 1	1.1	1×10^{-4}	0.06
Case 2	1.5	3.7×10^{-4}	0.22
Case 3	75	0.93	0.22

Table A.2: Examples on the change of the local averaged entropy in a passage.

the mixing of the flow in section 1 is completed), then the values of the left hand side and the right hand side of equation A.5 are shown in table A.2. Because in Case 1 and 2 the right hand side is larger than the left hand side, the drop in the local averaged entropy in section 1 due to streamline deviation is greater than the entropy generation in section 1 due to the mixing of two streams. Thus, the local averaged entropy in section 1 will decrease toward downstream. On the other hand, in case 3, the increase in entropy from the mixing process is higher than the decrease in the local averaged entropy due to streamline deviation. This implies that the right hand side of equation A.5 can be greater or smaller than the left hand side, depending on the inlet flow conditions as well as the completeness of the mixing out of the two streams. In other words, even with additional loss due to mixing (and entropy increases globally), local averaged entropy can either increase or decrease.

In the entropy profiles for 1.7% span and 5% span tip gap shown in Figure 3-19, the circumferential-averaged local entropy decreases from rotor trailing edge to stator leading edge. There is no additional loss from tip leakage flow formation, as opposed to inside the rotor passage. The entropy generation due to the mixing of the tip leakage flow with the main flow in the space between the rotor blade and the stator blade in this stage is smaller than the drop in the local circumferential averaged entropy due to streamline deviation (driven by the pressure difference between the high-pressure main flow and low-pressure leakage flow region). Thus, even though the global entropy increases from rotor trailing edge to stator leading edge due to the mixing, the local averaged entropy near the tip can drop.

However, it should be stated that the main purpose of Figure 3-19 is rather to show that the mixing out of the tip leakage flow of 1.7% span tip clearance is more completed within the rotor passage than that of 5% span tip clearance. As shown in

Figure 3-19, the entropy profile near the casing no longer signigicantly changes from rotor exit (sliding plane) to stator leading edge for 1.7% span tip clearance, compared to 5% span tip clearance. This indicates that the mixing out process of the tip leakage flow is still significantly carried out downstream of the rotor for large tip gap.

Bibliography

[1] J. Adamczyk. Aerodynamic Analysis of Multistage Turbomachinery Flows in Support of Aerodynamic Design. *ASME Journal of Turbomachinery*, 122(2):189–217, 2000.

[2] ANSYS, Inc. *ANSYS CFX-Solver Modeling Guide*, 12.0 edition, 2009.

[3] J. Bae, K. S. Breuer, and C. S. Tan. Active Control of Tip Clearance Flow in Axial Compressors. *ASME Journal of Turbomachinery*, 127(2):352–362, 2005.

[4] T. Belamri, P. Galpin, A. Braune, and C. Cornelius. CFD Analysis of a 15 Stage Axial Compressor: Part I — Methods. *Proceedings of ASME Turbo Expo 2005 (GT2005-68261).*

[5] T. Belamri, P. Galpin, A. Braune, and C. Cornelius. CFD Analysis of a 15 Stage Axial Compressor: Part II — Results. *Proceedings of ASME Turbo Expo 2005 (GT2005-68262).*

[6] N. A. Cumpsty. *Compressor Aerodynamics.* Longman Scientific & Technical, 1989.

[7] N. A. Cumpsty and J. H. Horlock. Averaging Nonuniform Flow for a Purpose. *ASME Journal of Turbomachinery*, 128(1):120–129, 2006.

[8] J. D. Denton. The 1993 IGTI Scholar Lecture: Loss Mechanisms in Turbomachines. *ASME Journal of Turbomachinery*, 115(4):621–656, 1993.

[9] F. Eulitz, B. Kuesters, F. Mildner, M. Mittelbach, A. Peters, B. van den Toorn, U. Waltke, P. Rimmington, and D. Wasdell. Design and Validation of a Compressor for a New Generation of Heavy-Duty Gas Turbines. *Proceedings of ASME Power 2007 (GT2007-22100).*

[10] C. Freeman. Effect of Tip Clearance Flow on Compresor Stability and Engine Performance. *Von Karman Institute for Fluid Dynamics, Lecture series 1985*, 05, 1985.

[11] N. Intaratep. *Formation and Development of the Tip Leakage Vortex in a Simulated Axial Compressor with Unsteady Inflow.* PhD thesis, Virginia Polytechnic Institute and State University, Department of Aerospace and Ocean Engineering, 2006.

[12] S. A. Khalid, A. S. Khalsa, I. A. Waitz, C. S. Tan, E. M. Greitzer, N. A. Cumpsty, J. J. Adamczyk, and F. E. Marble. Endwall Blockage in Axial Compressors. *ASME Journal of Turbomachinery*, 121(3):499–509, 1999.

[13] C. C. Koch and L. H. Smith. Loss Sources and Magnitudes in Axial-Flow Compressors. *ASME Journal of Engineering for Power*, 98(3):411–424, 1976.

[14] S. Kulkarni. Development of a Methodology to Estimate Aero-Performance of a Multistage Axial Compressor, Including Aero-Operbility Limits. Master's thesis, Case Western Reserve University, Department of Mechanical and Aerospace Engineering, 2011.

[15] R. B. Langtry, F. R. Menter, S. R. Likki, Y. B. Suzen, P. G. Huang, and S. Völker. A Correlation-Based Transition Model Using Local Variables—Part II: Test Cases and Industrial Applications. *ASME Journal of Turbomachinery*, 128(3):423–434, 2006.

[16] V. M. Lei, Z. S. Spakovszky, and E. M. Greitzer. A Criterion for Axial Compressor Hub-Corner Stall. *ASME Journal of Turbomachinery*, 130(3), 2008.

[17] John P. Longley. Calculating Stall and Surge Transients. *Proceedings of ASME Turbo Expo 2007 (GT2007-27378).*

[18] N. M. McDougall, N. A. Cumpsty, and T. P. Hynes. Stall Inception in Axial Compressors. *ASME Journal of Turbomachinery*, 112(1):116–123, 1990.

[19] F. R. Menter, R. B. Langtry, S. R. Likki, Y. B. Suzen, P. G. Huang, and S. Völker. A Correlation-Based Transition Model Using Local Variables—Part I: Model Formulation. *ASME Journal of Turbomachinery*, 128(3):413–422, 2006.

[20] B. T. Sirakov and C. S. Tan. Effect of Unsteady Stator Wake—Rotor Double-Leakage Tip Clearance Flow Interaction on Time-Average Compressor Performance. *ASME Journal of Turbomachinery*, 125(3):465–474, 2003.

[21] L. H. Smith. Wake Dispersion in Turbomachines. *ASME Journal of Basic Engineering*, 88(3):688–690, 1966.

[22] L. H. Smith. Casing Boundary Layers in Multistage Axial-Flow Compressors. *ASME Proceedings of the Symposium on Flow Research on Blading*, 1969.

[23] J. A. Storer and N. A. Cumpsty. Tip Leakage Flow in Axial Compressors. *ASME Journal of Turbomachinery*, 113(2):252–259, 1991.

[24] T. V. Valkov and C. S. Tan. Effect of Upstream Rotor Vortical Disturbances on the Time-Averaged Performance of Axial Compressor Stators: Part 1—Framework of Technical Approach and Wake–Stator Blade Interactions. *ASME Journal of Turbomachinery*, 121(3):377–386, 1999.

[25] T. V. Valkov and C. S. Tan. Effect of Upstream Rotor Vortical Disturbances on the Time-Averaged Performance of Axial Compressor Stators: Part 2—Rotor Tip Vortex/Streamwise Vortex–Stator Blade Interactions. *ASME Journal of Turbomachinery*, 121(3):387–397, 1999.

[26] A. J. Wennerstrom. Experimental Study of a High-Throughflow Transonic Axial Compressor Stage. *ASME Journal of Engineering for Gas Turbines and Power*, 106(3):552–560, 1984.

[27] R. Williams, D. Gregory-Smith, L. He, and G. Ingram. Experiments and Computations on Large Tip Clearance Effects in a Linear Cascade. *ASME Journal of Turbomachinery*, 132(2), 2010.

[28] D. C. Wisler. Loss Reduction in Axial-Flow Compressors Through Low-Speed Model Testing. *ASME Journal of Engineering for Gas Turbines and Power*, 107(2):354–363, 1985.

[29] T. Wong. Effects of Asymmetric Tip Clearance on Compressor Performance and Stability. Master's thesis, Massachusetts Institute of Technology, Department of Aeronautics and Astronautics, 1996.

[30] M. Zlatinov, C. S. Tan, M. Montgomery, T. Islam, and M. Seco-Soley. Turbine Hub and Shroud Sealing Flow Loss Mechanisms. *Proceedings of ASME Turbo Expo 2011 (GT2011-46718).*